# POWER REACTOR TECHNOLOGY

*A Quarterly Technical Progress Review*

Prepared for DIVISION OF TECHNICAL INFORMATION, USAEC, by
W. H. ZINN and J. R. DIETRICH, GENERAL NUCLEAR ENGINEERING CORPORATION

*March 1963*

● VOLUME 6

● NUMBER 2

# TECHNICAL PROGRESS REVIEWS

To meet the needs of industry for concise summaries of current atomic developments, the Atomic Energy Commission is publishing this series, Technical Progress Reviews. Issued quarterly, each of the reviews digests and evaluates the latest findings in a specific area of nuclear technology and science.

The four journals published in this series are:

*Nuclear Safety*, Wm. B. Cottrell, W. H. Jordan, and associates, Oak Ridge National Laboratory

*Power Reactor Technology*, W. H. Zinn and J. R. Dietrich, General Nuclear Engineering Corporation

*Reactor Materials*, R. W. Dayton, E. M. Simons, and associates, Battelle Memorial Institute

*Reactor Fuel Processing*, Stephen Lawroski and associates, Chemical Engineering Division, Argonne National Laboratory

Each journal may be purchased ($2.00 per year for subscription and individual issues $0.55) from the Superintendent of Documents, U. S. Government Printing Office, Washington 25, D. C. See back cover for remittance instructions and foreign postage requirements.



## Availability of Reports Cited in This Review

*Unclassified AEC reports* are available for inspection at AEC depository libraries and are sold by the Office of Technical Services, Department of Commerce, Washington 25, D. C. Some of the reports cited are not available owing to their preliminary nature; however, the information contained in them will eventually be made available in formal progress or topical reports.

*Unclassified reports issued by other Government agencies or private organizations* should be requested from the originator.

*Unclassified British and Canadian reports* may be inspected at AEC depository libraries. British reports are sold by the British Information Service, 45 Rockefeller Plaza, New York, N. Y.; Canadian reports (AECL series) are sold by the Scientific Document Distribution Office, Atomic Energy of Canada, Ltd., Chalk River, Ontario, Canada.

*Classified U. S. and foreign reports* identified in this journal as Classified may be purchased by properly cleared Access Permit Holders from the Division of Technical Information Extension, U. S. Atomic Energy Commission, P. O. Box 1001, Oak Ridge, Tenn. Such reports may be inspected at classified AEC depository libraries.

# POWER REACTOR TECHNOLOGY

## A REVIEW OF RECENT DEVELOPMENTS

Prepared for DIVISION OF TECHNICAL INFORMATION, USAEC,
by W. H. ZINN and J. R. DIETRICH,
GENERAL NUCLEAR ENGINEERING CORPORATION

● MARCH 1963
● VOLUME 6
● NUMBER 2

# Foreword

This quarterly review of reactor development has been prepared at the request of the Division of Technical Information of the U. S. Atomic Energy Commission. Its purpose is to assist interested organizations in the task of keeping abreast of new results in reactor technology for civilian application.

*Power Reactor Technology* contains reviews of selected recently published reports that are judged noteworthy, in the fields of power-reactor research and development, power-reactor applications, design practice, and operating experience. It is not meant to be a comprehensive abstract of all material published during the quarter, nor is it meant to be a treatise on any part of the subject. However, related articles are often treated together to yield reviews having some breadth of scope, and from time to time background material is added to place recent developments in perspective.

The intention is to cover the various areas of reactor development from the general viewpoint of the reactor designer rather than from the more detailed points of view of specialists in the individual areas. To whatever extent the coverage of *Power Reactor Technology* may occasionally overlap the fields of the other Technical Progress Reviews, the overlaps will be motivated by this objective of viewing current progress through the eyes of the reactor designer.

A degree of critical appraisal and some interpretation of results are often necessary to define the significance of reported work. Any such appraisals or interpretations represent only the opinions of the reviewers and the editor of *Power Reactor Technology* who are General Nuclear Engineering Corporation personnel. Readers are urged to consult the original references in order to obtain all the background of the work reported and to obtain the interpretation of the results given by the original authors.

W. H. ZINN, President
J. R. DIETRICH, Vice President and Editor
*General Nuclear Engineering Corporation*

# Contents




Issued quarterly by the U. S. Atomic Energy Commission. Funds for printing this publication approved by the Director of the Bureau of the Budget on November 1, 1960.

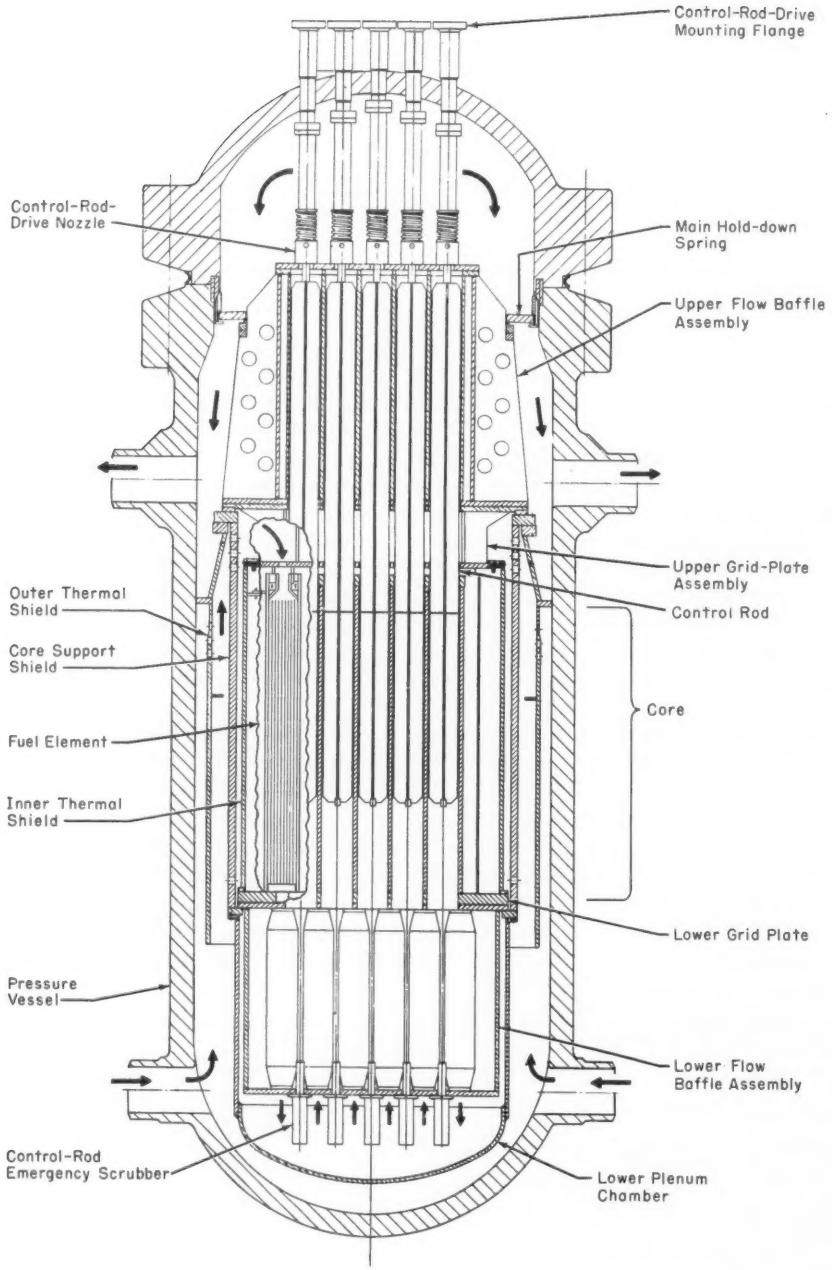


Fig. VI-1 Vertical cross section through the N.S. *Savannah* reactor.

**Note: Incorrect flow paths were shown in this figure in *Power Reactor Technology*, 6(1): 44. The correct flow paths are shown here.**

Section

I

Power Reactor Technology

# The AEC Report to the President

On Nov. 20, 1962, the Atomic Energy Commission submitted formally the Report on Civilian Nuclear Power[1] which the President had requested in March. Since the Report is generally available and since it has been summarized and commented upon in several publications, it will not be treated here at great length. It is, however, a significant document that appears to lay out the AEC recommendations for government activities in the civilian nuclear power field for some years to come.

The major points made by the Report may be summarized as follows:

1. There is a real long-term need for nuclear electric power, based on the foreseeable depletion of fossil-fuel resources. The estimates quoted predict that, if no additional forms of energy were utilized, we would exhaust our readily available, low-cost fossil fuels in a century or less and our presently visualized total supplies in about another century. Early development of nuclear power for producing electricity and for other straightforward applications is needed because other components of the fossil-fuel consumption may not be easily satisfied by the alternate of nuclear power.

2. Nuclear electric power also holds important near-term possibilities: (a) as a means of significantly reducing power generation costs, especially in areas where fossil-fuel costs are high; (b) as an important contributor to new industrial technology and to our technological world leadership; (c) as a significant positive element in our foreign trade; and (d) potentially as a means of strengthening our national defense.

3. An early objective of the nuclear power program should be to reach the point where, with appropriate encouragement and support, industry can provide nuclear power installations of economic attractiveness sufficient to induce utilities to install them at their own expense. Once this is achieved, the government can shift emphasis to advanced research and development design to meet long-range objectives.

4. Certain classes of power reactors (e.g., water-cooled converters producing saturated steam) are now on the threshold of economic competitiveness with conventional power in large installations in high-fossil-fuel-cost areas of the country. Foreseeable improvements will substantially increase the areas of competitiveness.

5. The water-cooled saturated-steam reactors have certain inherent limitations: (a) they provide relatively poor steam conditions and (b) they achieve relatively low utilization of the basic nuclear fuel. Improvements in thermal converters are needed to improve the economics and the fuel utilization; reactors of types other than the saturated-steam water-cooled converters may eventually show the best performance in these respects.

6. In the long term, nuclear fuels will not be significant sources of energy unless breeders are developed which will utilize a large fraction of the energy contained in $U^{238}$ and/or thorium. Converters must be used until economic breeders are developed, and there will probably be a transition stage, lasting for many decades, in which fast breeders that burn as well as make plutonium will be augmented by thermal converters which burn $U^{235}$ and which produce plutonium for fast-breeder inventory buildup. It is important that eventually the combination of breeders and converters reach an overall net breeding capability, or very nearly so, while relatively cheap nuclear fuel supplies are still available.

7. The nuclear power program should continue on an expeditious basis. Commission support should continue with added emphasis on stimulating industrial participation. The program should include: (a) early construction of plants of the presently most competitive reactor types; (b) development, construction, and demonstration of advanced converters to improve the economics and the use of nuclear fuels; (c) intensive development and, later, demonstration of breeder reactors to fill the long-range needs of utilizing fertile as well as fissile fuels.

8. Specifically, a construction program for the next 12 years, to implement the above program, might entail the following: (a) the construction and placing into operation of seven or eight electric-power-producing prototype reactors, approximately half of which would be advanced converters and the rest breeders; most of their cost would probably be borne by the AEC; (b) assistance, as necessary, to industry in the con-

struction of 10 to 12 full-scale power plants of improving design as time goes on; hopefully, industry will concurrently bear full costs of many more of well-proved design.

9. Continuation of the Commission's effort, along lines indicated in 7 and 8 above, should (a) provide industry with the needed stimulus to build a significant number of large reactors in the near future, (b) bring nuclear power to a competitive status with conventional power throughout most of the country during the 1970's, and (c) make breeder reactors economically attractive by the 1980's. Under these conditions it is estimated that, by the end of the century, nuclear power would be assuming the total increase in national electric-energy requirements and would be providing half the electric energy generated.

10. The private ownership of special nuclear materials should be authorized at an early date, but such ownership should not be made mandatory for a decade or so. Toll enrichment should be made available within the United States and to friendly foreign users subject to proper safeguards against diversion for military use.

11. Before and during the period of transition to private ownership, the charges set by the Commission on enriched uranium should, as at present, be based on full cost recovery; prices for the purchase of plutonium should be in accordance with its "near term" value as a reactor fuel and should take into account the content of fissionable isotopes.

12. Careful planning is necessary to guide the procurement of uranium so that the industry will be kept viable during any slack period before civilian power creates another large demand. The Commission is planning to offer the industry a "stretch out" program under which an AEC commitment to purchase additional material after the present contracts expire (at the end of 1966) would be used as an incentive to induce industry to delay until after that date the delivery of part of the uranium presently under contract.

13. The Commission intends to continue to extend encouragement to the industrial activities, such as fuel processing, which are ancillary to the major nuclear equipment industry. As rapidly as a private capability comes into being, the Commission should withdraw from all such work deriving from industry and should utilize private plants to fill its own requirements except, perhaps, for those related to materials for weapons.

14. The simplifying and streamlining of licensing and regulatory procedures can be a major help in encouraging the utility industry to adopt nuclear power. Steps have been taken in this direction, and the Commission is studying means of further improvement.

From the technical point of view, the major new step that has been taken in the Report is the recognition of the problem of nuclear fuel utilization. The significance of this problem can be stated very simply. With good fuel utilization (i.e., with the utilization of a large fraction of the available $U^{238}$ and/or thorium) the usable energy content of available nuclear fuel is, for practical purposes, almost infinite. With poor utilization (i.e., with the nuclear fuel utilization restricted to something like the fuel value of the contained $U^{235}$) the effective energy content of the nuclear fuel resource is too small to be of long-term consequence. These questions of fuel utilization have been recognized for a long time, and have, in fact, been discussed at some length in previous issues of *Power Reactor Technology* (e.g., 2(3): 1-12; 3(2): 21-29; and 4(2): 1-3). Indeed, the ultimate need for breeding has never been seriously questioned, but opinions have differed as to (1) the schedule on which breeder development should proceed, (2) the place of the high-conversion-ratio converter in the interim and in the long term, and (3) whether the gap between the present poor utilization of fuel and the high utilization, which must be attained in the future, can be bridged without encountering any important shortage of nuclear fuel. Although the breeder reactor and its fuel cycle have been significant parts of the AEC program for a long time, the Report to the President appears to be the first instance in which the Commission has acknowledged the necessity of examining in some detail the time schedule for the breeder requirement and the question of what the transition to breeder reactors might be like. Apparently these detailed examinations remain to be made — and no doubt they must involve a very substantial program of analysis and evaluation — for the relevant statement in the Report is only a rather general one. The statement is presented briefly below.

To evaluate fuel supplies one must first have some estimate of the energy consumption over a period of years. Figure I-1 shows the curves used for this and other purposes in the Report to the President. For the total and electric consumptions, the curves are derived by extrapolating (beyond the year 2000) the estimates of the Federal Power Commission; for the nuclear power fraction, the curve given is consistent with the estimate that by the year 2000 nuclear electric power will be assuming the total increase in electric-power production. For convenience, the difference between curves A and C of Fig. I-1 gives the annual production of nuclear electric energy and is plotted in Fig. I-2.

The Report contains the following comments regarding the effects, on fossil-fuel and nuclear

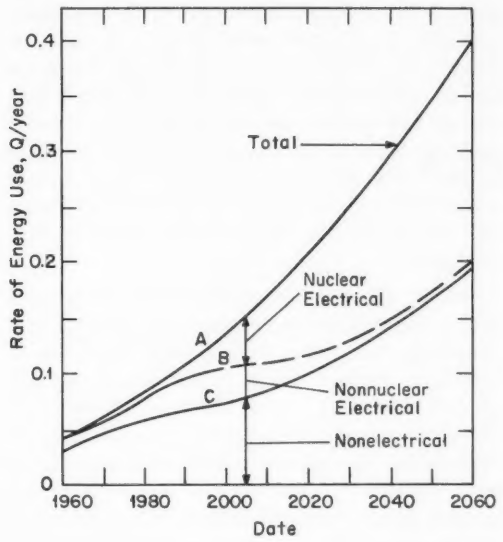


Fig. I-1 Projected annual energy consumption in the United States for electric-power generation and other uses.[1] (One $Q$ unit = $10^{18}$ Btu.)

fuel supplies, of the estimated rate of progress of nuclear power generation (as indicated in Fig. I-2):

For conservation of our fossil fuels, this rate of progress would appear to be sufficient, if by mid-century nuclear energy were also contributing appreciably to filling other needs, either directly or through the use of electric power for tasks not now performed by it. Any appreciably slower rate of growth could result, however, in undue short-term consumption of our fossil fuels, especially if the more conservative views of their availability and ultimate recovery costs should turn out to be correct. Fortunately, provided the nuclear technology is developed in a timely manner, the economic pressures of a coming scarcity of fossil fuel would tend to accelerate its use.

Provided our assumptions regarding breeders are reasonably accurate, the estimated growth of nuclear power described above would raise no problem with respect to the supply of nuclear fuels. By the year 2000, approximately the amount of uranium listed in the 0–10 dollars per pound category of Table I[*] would have been mined. Of the 0.4$Q$ of energy originally contained in the uranium-235, approximately half would still exist in reactor inventories and in stockpiles of depleted uranium. By that time the ratio of breeders and converters would be such that a major fraction of the energy produced would be coming from what was originally uranium-238 and thorium, so that somewhat higher ore prices would have no appreciable effect on the cost of power. On the other hand, should breeders be seriously delayed, for example by as much as a few decades, the high grade uranium ore might be exhausted while large amounts of uranium-235 were still required. Hence, it is important that the breeder technology be developed expeditiously.

On the basis of Fig. I-2 or a similar curve, it is easy to demonstrate that, if nothing were done to improve the level of fuel utilization currently achieved in our reactors, nuclear fuel shortages would be felt soon after nuclear plants were built in quantity.

Figure I-3 shows approximately the amount of nuclear fuel (in $Q$ units) which would be committed to nuclear reactors, as a function of time, if the nuclear-power-generating capacity indicated by Fig. I-2 were provided by water-moderated reactors of current types without plutonium recycle. The reactors are assumed to extract, from each ton of virgin natural uranium that is mined, 5700 Mwd(t). This is just equal to the energy that would be produced if all the $U^{235}$ were destroyed, and it happens to be approximately a typical figure for current water-moderated reactors. For estimating the fuel inventory, it is assumed that (1) the reactors are fueled with uranium of 2.2% enrichment, (2) they operate at a specific power of

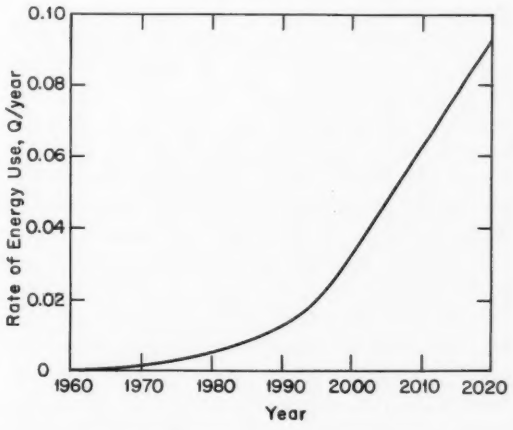


Fig. I-2 Projected annual nuclear energy use for electric-power production in the United States. (From Fig. I-1.)

*Table I is not included here; however, the $U^{235}$ content of the estimated total U. S. resource in the low-cost range (0 to $10 per pound of $U_3O_8$) is given as 0.4$Q$. See also Fig. I-3.

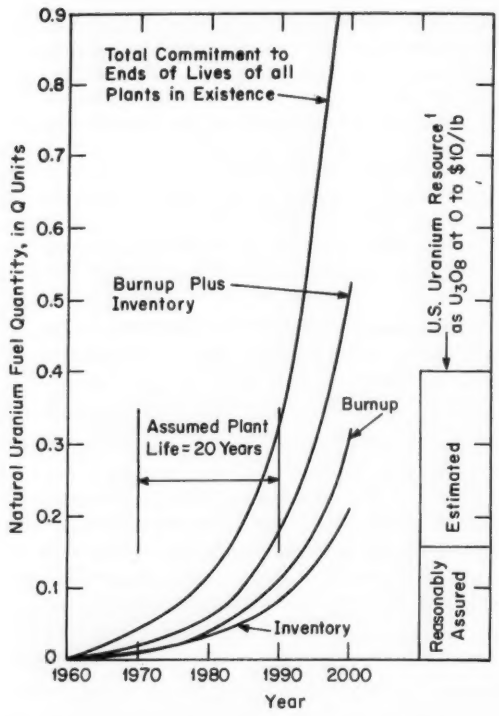


Fig. I-3 Estimated nuclear fuel commitment if the nuclear energy use of Fig. I-2 were provided by water reactors with present characteristics without plutonium recycle.

20 Mw(t) per metric ton of uranium, and (3) this value is reduced to an effective specific power of 10 Mw(t) per metric ton of uranium by the effects of plant factor and out-of-pile inventory.

At any given time the amount of nuclear fuel committed to each reactor is considered to be the fuel in inventory plus that burned since the beginning of operation plus that which will be burned up to the end of the assumed 20-year life of the plant. These components are shown separately in Fig. I-3. Also shown in the figure is the estimated U. S. reserve of cheap uranium (0 to $10 per pound of $U_3O_8$), expressed in terms of the energy value ($Q$ units) of the contained $U^{235}$. It is evident that, if the installed capacity were to grow as rapidly as has been assumed and if improvements were not made in the fuel utilization, the low-cost reserves could be quickly committed. A substantial improvement would, of course, result simply from the recycling of plutonium. The questions of (1) how much this improvement would be, (2) how much the basic neutron economy of current reactors can be improved, (3) how much improvement may be expected from alternate converter types, and (4) how rapidly the breeders will be developed and what their characteristics will be are the ones that determine whether a large-scale nuclear power industry can, indeed, be brought into being without encountering nuclear fuel shortages.

One of the striking characteristics brought out by Fig. I-3 is the very rapid rate of growth of nuclear fuel commitment when that rate of growth is expressed in terms of a time unit equal to an average plant lifetime. Although the estimated rate of commitment depends upon an estimate of the rate of growth of installed nuclear generating capacity and is therefore uncertain, there does not appear to be any basis for assuming that the growth rates indicated by Fig. I-2 are unreasonable. Since a large fraction of the present electric-power-generating capacity in the United States utilizes fossil fuel within a relatively narrow price range, it is reasonable to expect that, once nuclear power becomes competitive within that range, its use will expand rapidly.

The disturbing feature of the rapid growth rate, with respect to nuclear fuel supplies, comes about because each new plant built represents a 20- to 30-year commitment of nuclear fuel, probably at a fixed value of fuel utilization representative of the state of the technology at the time the reactor was designed. This emphasizes the need for early development of reactors and fuel cycles which will utilize the nuclear fuel effectively. If economic pressures are expected to provide the incentive for the improvement of fuel utilization as fuel supplies become depleted and fuel becomes more expensive, then it must be recognized that the plant life will represent something like a 20- to 30-year lag-time constant in the economic feedback circuit. It is important that the effects of this lag be anticipated and counteracted by the foresight of those who plan and carry out the development of nuclear plants.

## Reference

1. Civilian Nuclear Power, a Report to the President—1962, Nov. 20, 1962.

Section

II

Power Reactor Technology

# Reactor Physics

## Control Rods

### Theory

One of the principal functions of reactor physics is the prediction of the reactivity and power-distribution characteristics of a reactor when control elements are present. The highly absorptive nature of most control rods and the strong perturbation of the neutron-flux and -energy distribution near the rods pose severe problems in the accurate treatment of the control-rod effects. The direct application of transport theory, although correct in principle, is far too complex to be useful in most practical applications. For this reason a variety of useful approximations and empirical recipes has been developed to provide an estimate of control-rod performance. A brief survey of control-rod calculation methods was previously presented in *Power Reactor Technology*, 1(3): 9-12, and a discussion of control-rod effectiveness was given in 3(3): 26-37. A more detailed survey of control-rod theory, including an extensive bibliography, is given in Ref. 1. The reference also includes a review of the theoretical treatment of burnable poison, both distributed and lumped, as well as a compilation of effective cross-section values for a number of control-rod materials.

The usual methods of control-rod analysis utilize diffusion theory in one way or another, but they supplement it by imposing a boundary condition at the surface of the control rod which, in effect, will force diffusion theory to yield nearly the same values as an exact transport analysis for the reactivity, the neutron current into the rod, and the neutron flux at some distance from the rod surface. The transport boundary condition is usually imposed by the concept of the linear extrapolation distance ($d$), which requires that the ratio of neutron flux at the surface of the rod to the total neutron current into the rod from the surrounding diffusion medium be that required by transport theory within the control rod, i.e.,

$$\left(\frac{D\nabla\phi}{\phi}\right)_{\text{rod surface}} = \frac{D}{d} \qquad (1)$$

where $D$ is the diffusion coefficient of the surrounding medium and $d$ is the linear extrapolation distance obtained by transport theory.

The quantity $D/d$ may be introduced into a multigroup calculation as a boundary condition where possible; or alternatively, equivalent diffusion constants may be generated, and the control rod may be treated as an equivalent diffusion region. The PDQ code, for example, permits the boundary condition $D/d$ to be specified as part of the input.

In general, the linear extrapolation distance $d$ can be obtained from the relation[2,3]

$$d = 0.7104\lambda_{tr}\frac{1+p_1}{1-p_0} \qquad (2)$$

which is given by normalizing to the known transport extrapolation distance ($0.7104\lambda_{tr}$) for a black absorber ($p_0$ and $p_1$ equal zero). Here $p_0$ and $p_1$ are the probabilities of a neutron escaping from the rod without being captured, for the isotropic and anisotropic components of the flux, respectively, and $\lambda_{tr}$ is the transport mean free path of the surrounding diffusion medium. In his work on neutron diffusion, Placzek[4] derived an expression for the escape probability for monoenergetic neutrons in both slab and cylindrical geometry, considering only the isotropic ($p_0$) component of the flux. In a recent publication by Kear,[2] this has been extended, in slab and cylindrical geometry, to include both the isotropic ($p_0$) and the anisotropic ($p_1$) components of the flux. The slab-

geometry case with anisotropy has also been previously reported by Henry.[3] The following equations were obtained for the $p_0$ and $p_1$ escape probabilities:

Slab of thickness $t$ and cross section $\Sigma$:

$$p_0(\Sigma t) = 2\int_0^1 e^{-\Sigma t/x} x\,dx = 2E_3(\Sigma t) \tag{3}$$

$$p_1(\Sigma t) = 3\int_0^1 e^{-\Sigma t/x} x^2\,dx = 3E_4(\Sigma t) \tag{4}$$

Cylinder of radius $r$ and cross section $\Sigma$:

$$\begin{aligned} p_0(\Sigma r) = 1 - \frac{4}{3}(\Sigma r)^2 \Big\{ & 2\left[\Sigma r I_0(\Sigma r) K_0(\Sigma r) \right. \\ & \left. + \Sigma r\, I_1(\Sigma r)\, K_1(\Sigma r) - 1\right] \\ & + K_1(\Sigma r)\, I_0(\Sigma r) \\ & - I_1(\Sigma r)\, K_0(\Sigma r) + \frac{I_1(\Sigma r)\, K_1(\Sigma r)}{\Sigma r}\Big\} \end{aligned} \tag{5}$$

$$\begin{aligned} p_1(\Sigma r) = 1 - \Big\{ & \left[\frac{32}{15}(\Sigma r)^4 + 2(\Sigma r)^2\right] \\ & \times \left[I_0(\Sigma r) - I_1(\Sigma r)\right]\left[K_1(\Sigma r) - K_0(\Sigma r)\right] \\ & + \frac{4}{5}(\Sigma r)^2 I_0(\Sigma r) K_0(\Sigma r) \\ & + \frac{4}{15}\left[11 - (\Sigma r)^2\right] I_1(\Sigma r) K_1(\Sigma r) \\ & + \frac{2}{15}\left[3\ \Sigma r + 8\,(\Sigma r)^3\right]\left[I_1(\Sigma r) K_0(\Sigma r)\right. \\ & \left. - I_0(\Sigma r) K_1(\Sigma r)\right] \\ & + 2\,\Sigma r\, I_1(\Sigma r) K_0(\Sigma r)\Big\} \end{aligned} \tag{6}$$

An expression that is similar to Eq. 2 has been reported by Pomraning[5] for the calculation of $d$. Effective albedo or reflection functions were used to replace the $p_0$ and $p_1$ escape probabilities. More important is the use of two multiplicative correction terms, $C$ and $\Gamma$, to correct the transport extrapolation distance of a black absorber. The factor $C$ accounts for the curvature of the rod ($C = 1.000$ for a slab) and $\Gamma$ corrects for the nonzero absorption in the diffusion medium surrounding the rod. The factor $\Gamma$ is necessary since the black-slab extrapolation distance ($0.7104\lambda_{tr}$) was obtained on the assumption of zero absorption in the medium. The factor $C$ is the usual geometrical correction, which may be obtained from either Ref. 6 or Ref. 7. The following approximate expressions for $C$ and $\Gamma$ have been given by Pomraning:[5]

$$C = \frac{1 + [0.7603795/(R/\lambda_{tr})]}{0.40515635/(R/\lambda_{tr})} \tag{7}$$

and

$$\Gamma = 1 + 0.495\left(\frac{\Sigma_a}{\Sigma_s + \Sigma_a}\right) - 0.131\left(\frac{\Sigma_a}{\Sigma_s + \Sigma_a}\right)^2 \tag{8}$$

where $R$ is the rod radius, $\lambda_{tr}$ is the transport mean free path of the surrounding medium, and $\Sigma_s$ and $\Sigma_a$ are the macroscopic scattering and absorption cross sections of the surrounding medium in which diffusion theory is assumed to be applicable.

In the use of the two correction terms, $C$ and $\Gamma$, as multiplicative factors, it is assumed that the effects of rod curvature and medium absorption are separable.

The usual approximation for the linear extrapolation distance ($d$) of a cylinder, which has frequently been used in connection with the absorption-area approximation, is as follows:

$$d = \lambda_{tr}\left(0.7104C + \frac{p_0}{1 - p_0}\right) \tag{9}$$

Here the second-order terms, which distinguish between $p_0$ and $p_1$, are ignored. Equation 9, in the limit for large radius ($C = 1.00$), does not approach the expression for a slab. Deutsch[8] has normalized the equation in the large-radius limit to the diffusion-theory result ($d$ for a black slab of $\frac{2}{3}\lambda_{tr}$) and has obtained the following equation:

$$d = \lambda_{tr}\left(0.7104C + \frac{4}{3}\frac{p_0}{1 - p_0}\right) \tag{10}$$

Alternatively, Eq. 9 can be normalized to the transport-theory extrapolation distance (0.7104 for a black slab), and the following equation[9] (including the $\Gamma$ term) has been obtained:

$$d = \Gamma\lambda_{tr}\left(0.7104C + 1.4208\,\frac{p_0}{1-p_0}\right)$$
$$\rightarrow 0.7104\lambda_{tr}\left(\frac{1+p_0}{1-p_0}\right) \quad \text{for } C = 1 \text{ and } \Gamma = 1 \quad (11)$$

In the limit of a black control rod, Eqs. 2 and 9 to 11 are identical except for the two correction factors, $C$ and $\Gamma$.

### Comparison with Experiment

In a number of cases the theoretical treatment has been verified against a particular set of critical experiments. Reference 3 (using Eq. 2 in slab geometry) indicates that the $k_{eff}$ for water-moderated rodded cores can be predicted with the same degree of accuracy ($\pm 1\%$) as that for the unrodded cores. Similarly, Ref. 9 reports differences of less than 1% between experimental and calculated reactivity effects for cylindrical control rods (using Eq. 11) in water-moderated cores. Reference 9 also indicates $\pm 5\%$ agreement between the calculated and experimental power distributions in the vicinity of the control rod.

A detailed systematic study of the effect of control slabs of various widths and cylinders of various diameters in water-, $D_2O$-, graphite-, and organic-moderated lattices has been completed.[10] A pulsed-neutron technique was used to measure directly the rate of decay of the thermal-neutron population following a burst of neutrons. The decay constant ($\alpha$) for the fundamental mode can be obtained from these data and can then be used as a sensitive measure of the strength of a control rod or blade inserted in a critical assembly. Analyses of the systems[2] were performed with the PDQ code; each control rod was described explicitly in the thermal group by a boundary condition and in the epithermal group (with a few exceptions) as a diffusion medium. The control rods were assumed to be thermally black, and a linear extrapolation distance of $0.71\lambda_{tr}$ was used for both cylindrical and slab cases. No geometric correction factor was applied for the curvature of the cylindrical control rods. In most cases the calculated values of the control-rod worth ranged from a few percent to as much as 40% higher than the experimental values. Better agreement with experiment would be expected if (1) the linear extrapolation distance had been corrected for the curvature of the cylindrical rods and (2) the control rods had been described in the epithermal group by a transport-theory boundary condition. A check of the latter correction in two cases reduced, but did not eliminate, the discrepancy between theory and experiment. Although a considerable amount of experimental information is available, a significant amount of further work is needed before existing control-rod theory can be used to predict reactor performance reliably in all cases.

### Hafnium Resonance Integral

The experimentally derived values for the resonance integral of hafnium, which are reported in the literature, range from 1270 barns to as high as 3400 barns. A calculated value of about 1950 barns is obtained from the published values of the resonance parameters for natural hafnium. Reference 11 is a recent review of (1) the available experimental data for the hafnium resonance integral and (2) the possible sources of the apparent discrepancies. The recommendations given in Ref. 11 are (1) an effective resonance integral of $2000\,^{+200}_{-300}$ barns in a $1/E$ spectrum and (2) a capture cross section of $105 \pm 5$ barns (at 2200 m/sec). Also in Ref. 11 is a compilation of the resonance parameters for the several isotopes of hafnium.

## Calculation Methods for Heterogeneous Reactors

The usual approach in calculating the physics characteristics of heterogeneous reactors is to transform the physical heterogeneous lattice into a homogeneous "equivalent" that, if infinite in extent, would possess the same mean neutron parameters as the infinite heterogeneous lattice. An alternate approach is to make a direct heterogeneous calculation of the finite configuration. This approach offers the possibility of increasing the accuracy of reactivity and power-distribution calculations, particularly when the scale of the heterogeneity is not small relative to the dimensions of the reactor. This method, in principle, permits the determination of the relative neutron-absorption rate in each individual fuel rod in the lattice. In addition, the explicit consideration of the individual fuel rods (utilizing kernels to describe the interactions between the rods) admits the straightforward solution of some problems which are difficult to solve by the usual techniques and which result from com-

plex and multicomponent lattices, buildup of lattices to criticality, power flattening in spiked cores, and cores containing control rods.

Physics calculations for heterogeneous reactors were first considered by Feinberg,[12] Galinin,[13] and others in the USSR and by Horning[14] in the United States. Klahr et al. at the Technical Research Group, Inc.,[15] have improved, extended, and applied the calculation methods to practical core configurations of loosely packed lattices. The practical feasibility of digital computer calculations using two IBM-704 codes, HEterogeneous REactor SYstem Programs I and II (HERESY I and II), developed for heterogeneous-reactor calculations is demonstrated in Ref. 15.

## Principles of the Heterogeneous Method

In the calculation model used for heterogeneous calculations, the lattice is considered to be composed of a series of uranium rods of infinite length which are situated in a moderating medium. The rods are sources of fast neutrons and sinks of resonance and thermal neutrons.

In the small-source approximation, it is assumed that each fuel element may be represented as a combination axial line source and line sink of zero thickness. In the calculation of source and sink kernels, no account is taken of the presence of neighboring fuel elements, and it is assumed that elementary diffusion theory is adequate in describing the thermal diffusion between the fuel elements.* The finite size of the fuel element is taken into account by the evaluation of the sink kernel on the surface of the fuel element. The assumptions of the small-source approximation are valid if (1) the dimensions of the rods and the moderator diffusion length are considerably smaller than the distance between the rods (loosely packed lattices) and (2) the moderator absorption is small. It is evident that the neutron density around a fuel rod must possess axial symmetry to satisfy exactly the source and sink conditions. Since a symmetrical lattice arrangement tends toward producing a symmetrical neutron-density distribution around the rods, the theory is applicable even for fairly large rods if the lattice is reasonably symmetrical.

*A transport kernel function is described in Ref. 15, although it is not used in the calculations.

## Criticality Equation

In the absence of epithermal fissions and resonance absorptions, the heterogeneous-reactor equation for a reactor containing $N$ rods is:

$$\gamma_n i_n = \sum_{m=1}^{N} \left( \frac{\eta_m}{k} F_{nm} - f_{nm} \right) i_m \quad n = 1,2,\ldots N \quad (12)$$

The definitions of the terms, as given by Klahr et al.,[15] are

$i_n$ = number of thermal absorptions per unit length per second in the $n$th rod.

$\eta_m$ = number of fission neutrons produced per absorption in the $m$th rod.

$\gamma_n$ = ratio of the asymptotic flux (flux that would be calculated at the rod location using the infinite-medium kernels with the rod removed and the moderator substituted) to absorptions per unit length per second in the rod at thermal energies. The gamma values are independent of core configuration and depend only on the rod type and the moderator properties.

$F_{nm}$ = fission-to-thermal-source kernel (in the absence of resonances) which gives the thermal flux due to an infinite line source in an infinite moderator (without absorbing rods) at a distance from the source which corresponds to the center-to-center separation distance of the $m$th and $n$th rods due to a source intensity of one fission neutron per second per unit length of the $m$th rod.

$f_{nm}$ = thermal-sink kernel, which gives the thermal-flux depression due to an infinite line sink in an infinite moderator at a distance from the sink which corresponds to the center-to-center separation distance of the $m$th and $n$th rods due to a sink intensity of one thermal neutron per second per unit length of the $m$th rod.

$k$ = the static reactivity.

These definitions of the kernel functions and $\gamma$ are considerably different from those given by the earlier investigations,[12–14] in which the kernel functions were defined in terms of the real flux at the rod surface instead of the asymptotic flux and $\gamma$ was defined as the ratio of the surface flux at the rod to absorptions.

After observing that the earlier definitions would require inclusion of the boundary conditions on the rod surface in the calculation of the kernel contributions, Klahr and his coworkers are of the opinion that the previous definitions are difficult to apply. In the present definitions the asymptotic flux contributions are determined by the moderator properties alone and not by the fuel elements. Although the real flux depends upon the geometry and materials of the fuel rods, Ref. 15 indicates that there is no special difficulty in evaluating $\gamma$ from experimental data.

The interpretation of Eq. 12 is that the asymptotic flux at the $n$th rod is made up of the source contributions of all the rods (including itself) $i_m \frac{\eta_m}{k}$, minus the sink contributions of all the rods $i_m f_{nm}$, with $\gamma_n$ relating the asymptotic flux to the real absorptions in the $n$th rod.

The fast-fission factor $\epsilon$ can be included in $\eta$ for loosely packed lattices in which the effect of the interaction between rods on the fast-fission factor is not important.

Resonance absorption is taken into account by modifying the source kernel in Eq. 12. Equation 12 becomes

$$\gamma_n i_n = \sum_{m=1}^{N} \left( \frac{\eta_m}{k} F_{nm\bullet} - f_{nm} \right) i_m \quad n = 1,2,\ldots N \quad (13)$$

where the resonance effects are included in the $F_{nm\bullet}$ kernel

$$F_{nm\bullet} = F_{nm} - \sum_{P=1}^{R} \sum_{t=1}^{N} A_t^{(P)} \, g_{tm}^{(P-1)} F_{nt}^{(P)} \quad (14)$$

where $A_t^{(P)}$ = ratio of resonance absorptions per unit rod length at the $P$th resonance to the asymptotic slowing-down density averaged over rod $t$ at this energy

$g_{tm}^{(P-1)}$ = number of neutrons per cubic centimeter per second slowing down past the $P$-1 resonance energy at rod $t$ due to an infinite line source at rod $m$ having a source strength of one fission neutron per second per unit length

$F_{nt}^{(P)}$ = thermal-neutron flux at rod $n$ due to an infinite line source at rod $t$ with source strength of one neutron per second per unit length emitted at the energy of the $P$th resonance

$R$ = number of discrete resonances

$N$ = number of rods

All other quantities preserve their previous definition. It is noted that $g_{tm}^{(P-1)}$ is defined for an infinite medium, and it represents the contribution of rod $m$ to the slowing-down density calculated using infinite-medium slowing-down kernels with no rod properties included. This is not a real restriction for well-reflected reactors such as the graphite-moderated types.

## HERESY-I Code

HERESY I is an IBM-704 code used to calculate the reactivity and representative rod absorptions in heterogeneous reactors having two spatial dimensions. The small-source assumptions of infinitely long line sources and sinks, no displacement of moderator by fuel, independence of the rod parameters on the interrod separation, and a moderator of infinite extent, which are discussed above, are implicit in the code. In addition, the HERESY-I code ignores fission at nonthermal energy and assumes that all resonances are lumped into one equivalent resonance. These latter effects are, however, explicitly treated in an advanced version, HERESY II.

The HERESY-I code solves the following matrix equation:

$$\underline{\underline{\gamma}}\,\underline{i} = \frac{1}{k}\underline{\underline{G}}\,\underline{i} - \underline{\underline{Z}}\,\underline{i} \quad (15)$$

where $\underline{i}$ is the vector whose components are the relative absorptions in each rod type and $\underline{\underline{G}}$, $\underline{\underline{Z}}$, and $\underline{\underline{\gamma}}$ are matrices relating these absorptions to each other. The HERESY code solves for the reactivity, $k$, and for the vector $i$.

All rods of identical composition, geometry, and spatial symmetry constitute a specific rod type. The order of the matrices and the vector is equal to the number of rod types. All rods of the same type are physically identical at all times during burnup, and they experience the same absorption and fission rates.

## Age-Diffusion Kernels

The kernel functions listed below, expressed in terms of $d$, the interrod distance, were used in the analysis of heterogeneous lattices.

The thermal-diffusion kernel is

$$f(d) = \frac{1}{2\pi L^2 \Sigma_a} K_0 \frac{d}{L}$$

and

$$f(R_0) = \frac{1}{2\pi L^2 \Sigma_a} K_0 \frac{R_0}{L}$$

where $R_0$ is the radius of the rod.

Empirical or age theory slowing-down kernels to resonance energy:

$$g^r(d) = \sum_{i=1}^{3} \frac{A_i}{4\pi\tau_i^r} e^{-d^2/4\tau_i^r}$$

In general, this kernel is taken as a linear superposition of three Gaussian kernels to permit the use of either the age-theory kernel ($A_1$ and $A_2 = 0$) or the empirical slowing-down distributions, which can be fitted by two or three Gaussians. In practice, only one Gaussian was used.

The slowing-down diffusion kernel from fast energies is

$$F(d) = \sum_{i=1}^{3} A_i \frac{e^{\tau_i/L^2}}{2\pi L^2 \Sigma_a} \left[ K_0 \frac{d}{L} + \frac{\tau_i}{2L^2} e^{d^2/4\tau_i} - \frac{1}{2}\left(1 + \frac{d^2}{4L^2}\right) E_1 \frac{d^2}{4\tau_i} \right]$$

The slowing-down diffusion kernel to the resonance energy, $F^r(d)$, was obtained by replacing $\tau_i$ by $\tau_i - \tau_i^r$ in the above equation.

In the above relations, the meanings of the symbols are as follows:

$L$ = diffusion length of thermal neutrons in the moderator

$\Sigma_a$ = macroscopic thermal-absorption cross section

$\tau_i$ = perimeter in empirical Gaussian fit to slowing-down density to thermal energies

$\tau_i^r$ = perimeter in empirical Gaussian fit to slowing-down density to resonance energy

$A_i$ = linear weighting coefficients, usually obtained by an empirical fit to the slowing-down density

## Evaluation of Gamma

The ratio of the asymptotic flux to the absorptions per unit length at the receiver rod, denoted by the parameter $\gamma$, is defined to be dependent on the receiver rod and on the moderator in which it is immersed. In a loosely packed lattice, it is independent of the rod spacing and of the number of rods present. The value of $\gamma$ can thus be calculated by considering an infinite uniform one-rod type lattice of any arrangement in the moderator in question. Alternatively, it can be experimentally determined by measurements made centrally in a large lattice. It is proved[15] for an infinite square lattice that:

$$\gamma = \frac{1}{f} \sum_{n=1}^{\infty} F_{mn} - \sum_{n=1}^{\infty} f_{mn} \qquad (16)$$

where $f$ is the thermal utilization and the other symbols preserve their previous definition.

Thus $f$ can either be measured or determined from a homogeneous type calculation on the infinite lattice. The sums in Eq. 16 can be evaluated by the Poisson summation formula.

An important consequence of evaluating $\gamma$ in this manner is that the error in $\gamma$, which is obtained when incorrect kernels are used in Eq. 16, tends to balance out the error in $k$, which results when these kernels are also used in the criticality relation (Eq. 12 or 13). It is demonstrated in Ref. 15 that the reactivity is independent of the form of the thermal-diffusion kernels $F_{mn}$ and $f_{mn}$ (for an infinite one-rod type lattice) when $\gamma$ is calculated using Eq. 16. Calculations[15] for finite cases and complex cases have shown, in analogy to the infinite-lattice case, that, when this procedure was used to evaluate $\gamma$, the eigenvalue obtained is relatively independent of the kernel function even for extreme variations of kernel. This method was found to be the most reliable for the calculation of $\gamma$.

Other methods for evaluating $\gamma$ require knowledge of the receiver-rod disadvantage factor and of the ratio of the asymptotic to average

flux for the unit cell of the receiver rod, or they employ a simple diffusion-theory approach.

### Lumped Resonance Absorption Parameter A

For an infinite one-rod type lattice, the one equivalent lumped resonance $A$ factor (implicit in HERESY I) is related to the resonance escape probability $p$ by

$$p = 1 - \frac{A}{\sigma}$$

where $\sigma$ is the lattice area per rod. Fermi age theory and a rectangular lattice configuration were used in the derivation, although neither limitation seems essential.

### Applications and Extensions of the Method

Reference 15 presents the results of a number of calculations with the HERESY-I code which illustrate the areas of usefulness of the heterogeneous calculation method. A number of reactivity calculations were made on uranium-graphite lattices containing from 25 to 256 natural-uranium fuel rods. Some of these represented exponential lattices that had been measured at Brookhaven. In general, the heterogeneous calculation predicted reactivities lower than those predicted by the homogeneous method, the difference being in the direction to agree with measurement. As would be expected, the two calculation methods tended to come into agreement for large lattices, the difference in predicted reactivity being quite small for assemblies containing more than 100 rods. The heterogeneous calculation was also applied to spiked cores which were moderated by graphite and $D_2O$ and which contained approximately 100 rods; 10 to 20 rods were spikes of higher enrichment. The differences that were found in calculated reactivity were judged to demonstrate an important advantage of the heterogeneous calculation for this application. Another set of calculations treated cores containing arrays of 16 to 20 control rods. It was found that the heterogeneous theory was very useful in finding the patterns of control-rod location which would give an optimum combination of total rod worth and spatial distribution of power.

Reference 15 also contains a discussion of cases in which the fuel elements are large enough that they must be considered to have a finite size in the calculation, and a "large source" model must be used. In large-source theory, more realistic functions involving adjoint flux distributions and the distribution of thermal absorptions must be considered.

Although the heterogeneous formalism takes into account interference effects between rods due to neutron absorptions, it ignores effects due to dissimilarities in the slowing-down properties of the rods and moderator. The kernels may properly neglect the effects of scattering and slowing down as long as neutron absorptions are the only interactions of importance. However, in many problems these effects must be considered. One manner in which the slowing down and scattering may be included is to calculate the kernels in a fictitious homogenized moderator that includes the effects of the scattering and the slowing down of the rods.

## Differential Scattering Cross Sections

The slow-neutron scattering-law experiments currently in progress at the Canadian NRU reactor (Chalk River) and at the Materials Testing Reactor (National Reactor Testing Station) were reviewed in *Power Reactor Technology*, 6(1): 6-9. Additional data have since been published and are briefly described below.

Compilations of differential scattering cross sections for slow neutrons in Be and BeO (Ref. 16) and graphite (Ref. 17) at 293°K and in $UO_2$ (Ref. 18) at 293 and 698°K have been published. The tables list differential cross sections (barns per electron volt per steradian) in order of increasing incident energy (electron volts) and temperature for angular positions of the detectors in degrees. The cross-section tables for a given incident energy and temperature are followed by the scattering-law tables.

Scattering kernels calculated by the ROBESPIERRE Program[19] for light water at 23, 42, 61, and 82°C using the Nelkin[20] formulation have become available.[21] The kernels are given at each temperature in the form of the first four Legendre components:

$$S^k = \int_{-1}^{+1} P_k(\mu)\, S(E \rightarrow E', \mu)\, d\mu \quad k = 0,1$$

$$S^k = 2 \int_{-1}^{+1} P_k(\mu)\, S(E \rightarrow E', \mu)\, d\mu \quad k = 2,3$$

where $S^k$ is related to the microscopic scattering cross section by a single hydrogen nucleus in water

$$S^k = \frac{\sigma_k(E \rightarrow E')}{20.36}$$

The results are listed as sequential rows of the square matrix

$$\left[S_{ij}^k\right] \; i = 1,2 \ldots 49, j = 1,2 \ldots 49$$

where $S_{ij}^k = S^k(E_j \leftarrow E_i)$

The energy range is covered in 49 steps, with the maximum energy being 1 ev for water at 23°C, 1.06 ev at 42°C, 1.13 ev at 61°C, and 1.20 ev at 82°C.

# Critical and Exponential Results

Reference 22 is a topical report on critical experiments carried out under the USAEC Nuclear Superheat Program. Experimental measurements of critical size, reactivity change resulting from incremental changes in water height, void and temperature coefficients, flux distributions, thermal utilization, and conversion ratio, were made in clean, uniformly spaced arrays of single annular superheat fuel elements. The typical fuel element consisted of an annular column of high-density $UO_2$ pellets (inside diameter, 0.3125 in.; outside diameter, 0.497 in.); enriched to 3.4 wt.% $U^{235}$ and clad internally and externally with type 304 stainless-steel tubing (wall thickness, 28 mils). The annular fuel element was surrounded by a type 304 stainless-steel process tube (inside diameter, 0.725 in.; wall thickness, 25 mils) which formed a boundary between the external coolant passage and the moderator region. Data were obtained over a wide range of water-to-fuel ratios in the unit cell by varying the magnitude of the square lattice pitch (1.8 to 2.0 in.) and the material content of the central coolant passage (voided, flooded, or flooded with a 0.252-in.-OD void tube), the external coolant passage (voided or flooded), or the moderator region (0.625-in.-OD aluminum displacers or 0.252-in.-OD void tubes). Descriptions of the engineering design model as well as of calculations used to validate certain approximations in the engineering design model are given.

Measurements of the region-averaged thermal flux and the azimuthal variation of the thermal flux in a unit square superheater cell, made for comparison with the predictions of an analytical model and for use in the computation of flux-weighted superheater constants, are described in Ref. 23. The experiments were carried out in the full-size mockup of the Pathfinder reactor core, which consists of an annular boiler region with a central integral superheater region. The superheater fuel element contains two concentric annular stainless-steel-clad cermet fuel regions (20 wt.% highly enriched $UO_2$ alloyed with stainless steel), surrounded by a stainless-steel process tube. Two techniques were employed in the measurement of the region-averaged thermal flux. The first technique, which utilized manganese-copper wires lying in planes perpendicular to the axes of the element, gave results that could be considered only as a first-order approximation to the information desired. The second technique employed two uranium-aluminum foils that encompassed the entire cell with the exception of the annular region occupied by the process tube. The foil occupying the area interior to the process tube was sectioned to provide data for each distinct annular zone. Uranium-aluminum foilettes (0.047 in. in diameter), either irradiated individually in one quadrant of the moderator portion of the unit cell or punched from a large foil irradiated inside the process tube, were used to provide a detailed mapping of the thermal flux in the unit cell. A comparison of the experimental data with the predictions of an analytical model employing a SOFOCATE P-3 iteration scheme in a cylindricized cell indicated that the model was not adequate in describing the radial variation of the thermal flux. The experimental data were also used to compute flux-weighted thermal-group superheater constants for use in two-group diffusion-theory calculations of the superheater flooding coefficient. These calculated results were in better agreement with experimental measurements (of the flooding

coefficient) than were the results of flux-distribution calculations.

Reference 24 is a summary of critical experiments and their analysis carried out under the Army Boiling-Water Reactor Program in support of the design of the PL-2 reactor core. The experiments were designed to test calculational methods employed in the reactor design and to provide a direct measure of control-rod worth and shutdown margins under specific stuck-rod conditions. The major uncertainties in the analytical model were associated with the treatment of discrete poison elements and control rods. The PL-2 reference design core contains 9 stainless-steel-clad silver-cadmium-indium cruciform control rods and 24 subassemblies of 59 fuel elements and 3 boron–stainless-steel poison elements. The reactor-grade fuel elements used in all critical experiments were composed of 4.8 wt.% $U^{235}$-enriched ceramic $UO_2$ pellets (0.420 in. in diameter) clad in stainless-steel process tubing (inside diameter, 0.426 in.; wall thickness, 20 mils). The boron–stainless-steel poison elements were of four enrichments: 0, ¼, ½, and 1.1 wt.%; each rod was 0.420 in. in diameter and was jacketed with the same cladding structure as that used on the fuel elements. During the course of the experiments, approximately 38 distinct core loadings were examined in two phases. The first phase provided criticality data on small poisoned and unpoisoned cores, both with and without control rods. In several cores the effects of both poisoned- and unpoisoned-pin location, as well as boron enrichment, were measured by means of critical loadings and mappings of the power distribution. In the second phase, data on control-rod interactions, evaluation and adjustment of shutdown margin, stuck-rod conditions, uniform and radial zoning of poison elements, void coefficient, simulated hot-core conditions, and power mappings were obtained with the full-size core. The void coefficient and hot-core conditions were simulated by the use of aluminum tubing (outside diameter, 0.628 in.; wall thickness, 0.065 in.) positioned coaxially to individual fuel and poison elements. A detailed description of the analytical method and comparisons with experimental data are given.

Reference 25 presents a summary of the final results of critical tests performed during the startup of the Plutonium Recycle Test Reactor (PRTR). The PRTR is a vertical pressure-tube reactor, moderated and cooled by heavy water, with a power rating of 70 Mw(t). The unpressurized moderator is contained in a calandria with 85 fuel channels. Each fuel channel consists of the calandria tube, a helium thermal barrier, a Zircaloy-2 pressure tube, and a high-pressure coolant flowing through the fuel bundle. The heavy-water reflector is contained in a separate annular tank that is 24 in. thick, and it extends from the top of the calandria to 24 in. above the bottom of the calandria. The annular region beneath the reflector is connected to the interior of the calandria, and it serves as a moderator dump chamber. The moderator has a free surface at an annular weir extending around the base of the calandria inside the dump chamber. The primary control system of the reactor adjusts the height of the moderator above this free surface by controlling the helium gas pressure in the dump chamber. A secondary control system consisting of 18 shim control rods serves to modify axial and radial flux distributions as well as compensate for xenon poisoning.

Each fuel bundle is a cluster of nineteen 0.564-in.-OD fuel rods which are clad in 30-mil Zircaloy-2 and which contain either 1.8 wt.% plutonium (6% $Pu^{240}$, 0.45% $Pu^{241}$, < 0.01% $Pu^{242}$, and 93.55% $Pu^{239}$) in aluminum or natural $UO_2$. Three core loadings were investigated: (1) an annular region of plutonium-aluminum fuel bundles surrounding $UO_2$ fuel; (2) a three-zone annular core with a central $UO_2$ region, a plutonium-aluminum region, and an outer $UO_2$ annular zone; and (3) a uniform plutonium-aluminum core. Data were obtained on critical fuel loadings, moderator-level coefficients using period techniques and boron poisoning of the moderator, shim-rod calibrations, temperature coefficients, flux distributions, and substitution tests. The substitution tests provided data on reflector savings, spike enrichments, worth of gray and black shims, nuclear characteristics of in-reactor test-loop components, light-water substitution, and reactivity worth of a $UO_2$ fuel assembly. Measurements of the reactor transfer function by random noise techniques were not definitive because of fluctuations in the moderator level induced by the primary control system.

Previous critical experiments [see *Power Reactor Technology*, 5(4): 17], completed under the Spectral Shift Control Reactor (SSCR) basic

physics program, studied the properties of 4% enriched $UO_2$ fuel rods at a lattice metal-to-water ratio of 1.0 over a range of moderator compositions varying between 0 and 76.5% $D_2O$ in $H_2O$. A second phase of experimentation is designed to study the effect of varying the metal-to-water ratio and the enrichment. The former effect will involve critical experiments using the 4% enriched $UO_2$ at metal-to-water ratios of 1.195 and 0.7, whereas the second effect will be measured with 2.46% enriched $UO_2$ at a metal-to-water ratio of unity.

Reference 5 summarizes the results of clean critical experiments with the 4% enriched fuel at a lattice metal-to-water ratio of 1.195 and moderated by water containing 0% (core X) and 70.1% (core XI) $D_2O$. The 0.475-in.-OD stainless-steel-clad fuel rods were spaced on a square pitch of 0.571 in. The critical mass (clean and at reduced moderator height), worth of control elements, radial and axial flux traverses with bare and cadmium-covered gold foils, thermal disadvantage factor, and cadmium ratio of fissions in $U^{235}$ were measured in both cores. In core X, the reactivity worth of incremental changes in moderator level ($\partial\rho/\partial h$) was measured over a range of levels by varying the effective radius of the core. In core XI, the critical radius was so large that $\partial\rho/\partial h$ was measured at a fixed loading; additional data were obtained by varying the concentration of $D_2O$. The cadmium ratio of $U^{238}$ fissions was measured in core X by both chemical-separation and thermal-activation techniques to resolve discrepancies obtained previously at a metal-to-water ratio of 1.

Reference 27 presents a summary of the results of SSCR critical experiments employing the 4% enriched fuel in the same lattice as in Ref. 26 but with moderator water containing 50% $D_2O$. Measurements similar to those listed above are reported. Experiments employing the 2.46% enriched $UO_2$ in light-water moderator were initiated. The 0.475-in.-OD aluminum-clad fuel rods were spaced on a square pitch of 0.595 in. to give a metal-to-water ratio of 1.002.

A description of the final design of the small lattice experiments that are to be carried out in the Modified Lynchburg Source Reactor (MLSR) is given in Ref. 27. The purpose of these experiments is to apply the Physical Constants Testing Reactor technique to the measurement of $k_\infty$ and lattice parameters in the SSCR type epithermal systems. The assembly to be used for the initial experiments is described. The driver region will consist of the MLSR fuel and moderator, i.e., 93% enriched uranium-aluminum strips taped to 1.6-in.-square graphite bars. A 2-ft-square by 6-ft-high core tank will contain the following: (1) a test insert and inner buffer region containing 4% enriched fuel rods and (2) an outer buffer region with 93% enriched $UO_2$-$ThO_2$ fuel. The 18-in.-long test insert is positioned axially between two regions having the same composition as the inner buffer region. All regions in the core tank are to be moderated by the same $D_2O$-$H_2O$ mixture.

Reference 28 contains a summary of the results of neutron multiplication measurements on assemblies composed of 15- and 21-in.-diameter 93.2% enriched uranium disks. The assemblies were unreflected or reflected on one or both flat faces by various thicknesses of graphite, water, polyethylene, paraffin, and Lucite. Subcritical masses were assembled by supporting half of the assembly (including reflector) on a 19-mil-thick stainless-steel diaphragm, whereas the remaining part of the assembly, with its reflector, was supported on a 10-in.-high thin-walled aluminum pedestal atop the platen of a lift. Critical masses for the various configurations were deduced by extrapolation of the neutron multiplication curves. The reactivity worth of structural members was evaluated by measuring the change in extrapolated critical mass resulting from changes in dimensions of the structural component or the use of mirror images. Values of the reflector savings were evaluated from the decrease in critical core dimension brought about by the addition of a reflector with a given thickness to a normally bare surface. The values of the reflector savings, which were established at the relatively small ratios of assembly thickness to diameter employed in the experiments, were then used as guides to estimate the savings for infinite Oralloy slabs.

Because of an increasing interest in higher density uranium systems, a study[29] of the density effect and its relation to the maximum safe enrichment has been carried out at the Oak Ridge Gaseous Diffusion Plant (ORGDP). At ORGDP the maximum-safe-enrichment criterion for homogeneous, hydrogen-moderated

systems is set at 0.95% $U^{235}$ without regard to the usual criticality controls of mass or geometry. In addition, a maximum uranium density of 3.2 g of uranium per cubic centimeter is specified because of the generally greater reactivity of high-density nonhomogeneous uranium systems at low enrichment (e.g., the minimum critical enrichment of high-density uranium metal rods in light water is in the neighborhood of 0.71% $U^{235}$). Therefore, since the minimum critical enrichment of a nonhomogeneous system is less than that of a homogeneous system, it is necessary, from a nuclear safety standpoint, to distinguish between nuclearly homogeneous and nonhomogeneous systems. A specification of uranium enriched to 0.95% $U^{235}$ was established for nuclear homogeneity, and was arrived at by examining the available experimental data and using short, guided extrapolations. It was concluded that the condition of nuclear homogeneity will be maintained (1) if the uranium density is less than or equal to 3.2 g of uranium per cubic centimeter or (2) if, for densities ranging from 3.2 g of uranium per cubic centimeter up to a maximum of 18.9 g of uranium per cubic centimeter, one dimension of the uranium fuel is less than or equal to 0.02 in.

The results of a theoretical and experimental investigation to determine the extent to which very small subcritical assemblies can be used in the determination of reactor parameters are contained in Ref. 30. A general treatment of the exponential assembly with nonreflecting boundary conditions was carried through with age-diffusion theory. Complete solutions of the age-diffusion equation are found for a homogeneous, bare, cylindrical, subcritical assembly, fed from one end by a uniform, plane, thermal-neutron source and by a plane source having the distribution $J_0(2.405\ r/R)$. For any point in the assembly, the solutions yield the thermal flux due to source neutrons, the thermal flux due to neutrons born and moderated in the assembly, and the slowing-down density at any particular value of the neutron age. Methods of correction for source and leakage effects were developed for the measurement of lattice parameters. A detailed description of experimental procedures, the results of measurements made in lattices containing slightly enriched-uranium fuel in mixtures of $H_2O$ and $D_2O$, as well as detailed comparisons with theoretical predictions, are presented.

## References


1. W. K. Anderson and J. S. Theilacker (Eds.), *Neutron Absorber Materials for Reactor Control*, U. S. Government Printing Office, Washington, 1962.
2. G. H. Kear and M. H. Ruderman, An Analysis of Methods in Control Rod Theory and Comparisons with Experiment, USAEC Report GEAP-3937, General Electric Company, Vallecitos Atomic Laboratory, May 27, 1962.
3. A. F. Henry, A Theoretical Method for Determining the Worth of Control Rods, USAEC Report WAPD-218, Westinghouse Electric Corp., Bettis Plant, August 1959.
4. K. M. Case, F. de Hoffman, and G. Placzek, *Introduction to the Theory of Neutron Diffusion*, Volume I, U. S. Government Printing Office, Washington, June 1953.
5. G. C. Pomraning, Control Worth of $B_4C$ Rods, USAEC Report GEAP-3800, General Electric Company, Atomic Power Equipment Department, Aug. 30, 1961.
6. B. Davison and S. A. Kushneriuk, Linear Extrapolation Length for a Black Sphere and a Black Cylinder, Canadian Report MT-214, Mar. 30, 1946.
7. Argonne National Laboratory, Reactor Physics Constants, USAEC Report ANL-5800, July 1958.
8. R. W. Deutsch, Method for Analyzing Low-Enrichment Light-Water Cores, Supplementary Study Related to Bonus and Nuclear Superheat Programs, USAEC Report GNEC-133, General Nuclear Engineering Corp., Oct. 5, 1960.
9. Combustion Engineering, Inc., and General Nuclear Engineering Corp., Nuclear Superheat Development Program. Twelfth Quarterly Progress Report, April–June 1962, USAEC Report GNEC-241.
10. P. Meyer and W. C. Ballowe, An Experimental Parametric Study of the Effects of Control Rods on the Prompt Neutron Decay Constant in Multiplying Media, USAEC Report GEAP-4019, General Electric Company, Vallecitos Atomic Laboratory, April 1962.
11. I. Itkin, Analysis of the Neutron Capture Cross Section and Resonance Integral of Hafnium, USAEC Report WAPD-TM-324, Westinghouse Electric Corp., Bettis Atomic Power Laboratory, August 1962.
12. S. M. Feinberg, Heterogeneous Methods for Calculating Reactors, *Proceedings of the International Conference on the Peaceful Uses of Atomic Energy, Geneva, 1955*, Vol. 5, p. 484, United Nations, New York, 1956.
13. A. D. Galanin, Critical Size of Heterogeneous Reactor with Small Number of Rods, *Proceedings of the International Conference on the Peaceful Uses of Atomic Energy, Geneva, 1955*, Vol. 5, p. 462, United Nations, New York, 1956.

14. W. A. Horning, Small Source Model of a Thermal Pile, USAEC Report HW-24282, Hanford Atomic Products Operation, Apr. 30, 1952.
15. C. N. Klahr, L. B. Mendelsohn, and J. Heitner, Heterogeneous Reactor Calculation Methods, Final Report, April 1, 1959–June 30, 1961, USAEC Report NYO-2680, Technical Research Group, Inc., June 30, 1961.
16. H. Greenspan and I. G. Baksys, Differential Scattering Cross Sections for Slow Neutrons in Be and BeO, Reactor Physics Constants Center Newsletter No. 5, USAEC Report TID-16324, May 1962.
17. H. Greenspan and I. G. Baksys, Differential Scattering Cross Sections for Slow Neutrons in Graphite, Reactor Physics Constants Center Newsletter No. 6, USAEC Report TID-16772, June 1962.
18. H. Greenspan and I. G. Baksys, Differential Scattering Cross Sections for Slow Neutrons in Natural $UO_2$, Reactor Physics Constants Center Newsletter No. 7, USAEC Report TID-16801, July 1962.
19. D. H. Perkel, ROBESPIERRE: A Program for Calculating the Nelkin Scattering Kernel for Bound Hydrogen, USAEC Report GA-1803, General Atomic Division, General Dynamics Corp., Aug. 7, 1961.
20. M. S. Nelkin, Scattering of Slow Neutrons by Water, *Phys. Rev.*, 119: 741 (1960).
21. B. A. Kerr, Calculated Scattering Kernels for Light Water at 23°C, 42°C, 61°C, and 82°C, USAEC Report GEAP-3944, General Electric Company, Vallecitos Atomic Laboratory, May 27, 1962.
22. G. T. Petersen and F. G. Warzek, AEC Superheat Criticals—A Comparison of Experiment and Theory on Uniform Lattices, USAEC Report GEAP-3882, General Electric Company, Atomic Power Equipment Department, Januarv 1962. (See also errata issued June 1962.)
23. H. F. Finn and R. H. Vollmer, Pathfinder Atomic Power Plant Detailed Flux Measurements in Superheater Cells, USAEC Report ACNP-62020, Allis-Chalmers Mfg. Co., Aug. 27, 1962.
24. O. Gailar, R. S. Harding, and R. W. Knapp, Critical Experiments for PL-2 and Their Analysis, Report CEND-164, Combustion Engineering, Inc., August 1962.
25. J. R. Triplett, R. E. Dunn, V. W. Gustafson, R. E. Peterson, J. J. Regimbal, J. T. Russell, and L. C. Schmid, Plutonium Recycle Test Reactor Critical Test Results, USAEC Report HW-61900BA, General Electric Company, Hanford Atomic Products Operation, December 1961.
26. Babcock & Wilcox Co., Spectral Shift Control Reactor—Basic Physics Program. Quarterly Technical Report No. 6, January–March 1962, USAEC Report BAW-1250.
27. Babcock & Wilcox Co., Spectral Shift Control Reactor—Basic Physics Program. Quarterly Technical Report No. 7, April–June 1962, USAEC Report BAW-1259.
28. G. E. Hansen, D. P. Wood, and B. Peña, Reflector Savings of Moderating Materials on Large Diameter U (93.2%) Slabs, USAEC Report LAMS-2744, Los Alamos Scientific Laboratory, Oct. 8, 1962.
29. C. E. Newlon, The Effect of Uranium Density on the Safe U-235 Enrichment Criterion, USAEC Report K-1550, Oak Ridge Gaseous Diffusion Plant, Oct. 11, 1962.
30. J. C. Peak, I. Kaplan, and T. J. Thompson, Theory and Use of Small Subcritical Assemblies for the Measurement of Reactor Parameters, USAEC Report NYO-10204, Massachusetts Institute of Technology, Apr. 2, 1962.

Section

III

Power Reactor Technology

# Heat Transfer and Fluid Flow

## Conduction

A recent Pressurized-Water-Reactor technical progress report[1] contains an article on the thermal conductivity of $UO_2$. A "best estimate" equation was obtained by statistical-analysis techniques, although the particular data analyzed are not given. The best-fit equation, which is intended to apply over the temperature range 200 to 2600°F, is[1]

$$k = (4296fR)/(632 + T) \qquad (1)$$

where $k$ = thermal conductivity, Btu/(hr)(ft)(°F)
$f$ = fraction of theoretical density
$R$ = effect of irradiation
$T$ = temperature, °F

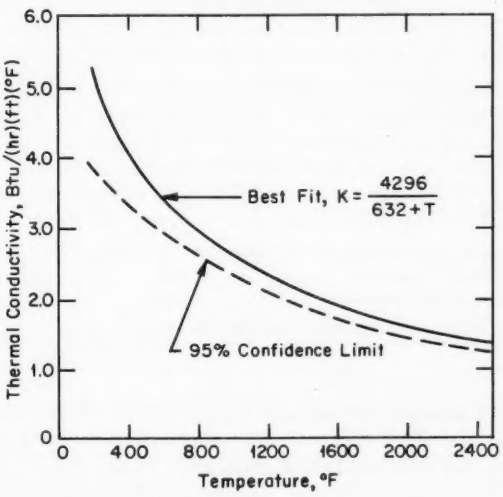


Fig. III-1 Thermal conductivity[1] of 100% dense unirradiated $UO_2$.

Equation 1 is plotted in Fig. III-1 with a value of unity for $fR$. Figure III-2 illustrates the functional relation between $R$ and burnup. More comprehensive reviews of $UO_2$ conductivity may be found in *Power Reactor Technology*, 4(2): 38-43 and in 5(1): 56-66.

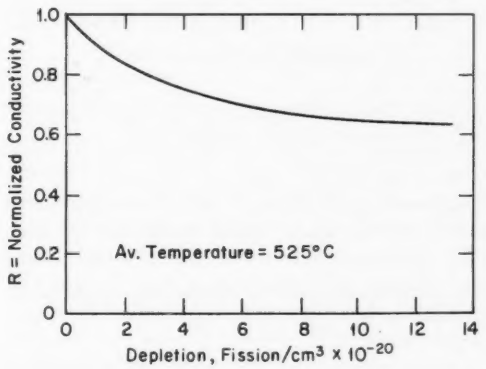


Fig. III-2 Normalized thermal conductivity[1] of irradiated $UO_2$.

References 2 to 6 deal with heat transfer in graphite. The effects of temperature, coolant flow rate, channel diameter, and graphite chemical reactivity are evaluated in order to determine the length of channel that can be cooled by flow of air.[2-5] The treatment in Ref. 6 applies the data to the specific problem of annealing out Wigner energy in a reactor. Although the work was done specifically for the Brookhaven graphite reactor, the results are of general interest in the design of graphite-moderated reactors. The thermal conductivity and electrical resistivity of a number of commercial and experimental graphites are given in Ref. 7. An expression relating thermal and electrical properties was developed which was found to hold for over

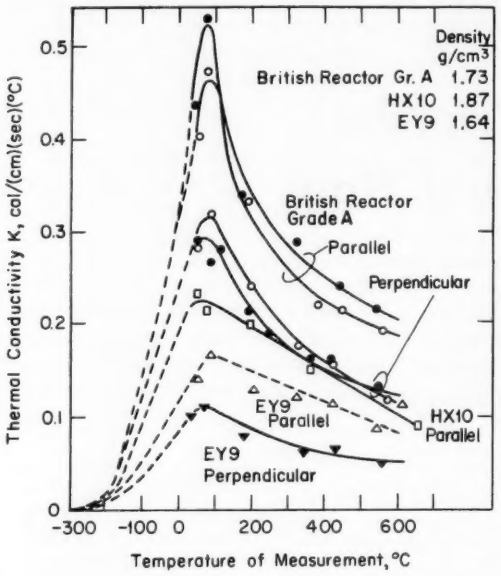


Fig. III-3 The variation of graphite thermal conductivity[7] with temperature of measurement.

40 different graphites. A method is proposed for estimating the thermal conductivity at elevated temperatures from room-temperature data. Figure III-3 illustrates the variation of thermal conductivity with temperature for various graphites.

Several conduction problems are treated in Refs. 8 to 10. These reports are interesting because of the mathematical complexities of the conduction problems they treat; in Ref. 10, for example, the boundary values are chosen to represent the case of nonuniform azimuthal power generation in a fuel rod.

# Single-Phase-Coolant Transfer

The development of explicit equations for pipe and rectangular-channel isothermal friction factors is the subject of Ref. 11. The data of Esselman et al.[12] were subjected to a least-squares analysis to obtain a correlation between the friction factor and Reynolds number with roughness as a parameter. The final correlation is given as

$$f = gN_{\mathrm{Re}}^{-h} \qquad (2)$$

where $g$ and $h$ are functions of $\epsilon_a/D_e$, the arithmetic average relative roughness:*

$$g = 0.1743 - 24.27\,(\epsilon_a/D_e) + 0.03695 \exp\left[-7219\,(\epsilon_a/D_e)\right] + 7.305 \times 10^8 \exp\left[-0.08886\,(D_e/\epsilon_a)\right]$$

$$h = 0.1960 - 20.95\,(\epsilon_a/D_e) - 2427\,(\epsilon_a/D_e)^2 + 0.01770 \exp\left[-10{,}350\,(\epsilon_a/D_e)\right] + 2.713 \times 10^8 \exp\left[-0.0589\,(D_e/\epsilon_a)\right]$$

Within the range of $2 \times 10^4 \leq N_{\mathrm{Re}} \leq 2 \times 10^5$, Eq. 2 reproduces the data of Esselman et al. with a maximum error of 2%.

The transfer of heat via forced convection in annular passages was treated in *Power Reactor Technology*, 4(2): 13-15. Reference 13, which is an addition to the literature on the subject, reports on an experimental program to investigate heat transfer and pressure drop in eccentric annuli. Table III-1 contains pertinent information on the test sections used. Eccentricities from 0 to 97% were studied, and the eccentricity, $e$, is defined as follows:

$$e = 2d/(D_2 - D_1)$$

where $d$ is the distance between the center lines of the inner and outer tubes and $D_2 - D_1$ is twice the annulus thickness if the tubes were centered. Figure III-4 illustrates the effect of eccentricity on the friction-factor ratio for a value of $D_2/D_1$ of 1.5. An attempted prediction of the effect of eccentricity was based on the concept of a local

Table III-1 TEST-SECTION DIMENSIONS FOR TESTS OF ECCENTRIC ANNULI[13]

| | Test section | | | |
|---|---|---|---|---|
| | 1 | 5 | 6 | 7 |
| Housing material | 61S Al | S.S. | S.S. | S.S. |
| Housing inside diameter, in. | 1.50 | 1.50 | 1.495 | 1.33 |
| Heater material | 61S Al | | "A" Ni | |
| Heater outside diameter, in. | 1.00 | | 1.003 | |
| Heater thickness, in. | 0.035 | | 0.020 | |
| Core-rod material | | S.S. | | S.S. |
| Core outside diameter, in. | | 1.03 | | 1.15 |

*Here $\epsilon_a$ is the roughness specified by Report MIL-STD-10A and $D_e$ is the equivalent diameter.

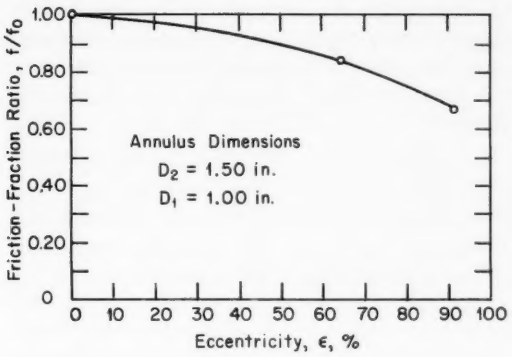


Fig. III-4 Friction-factor ratio vs. eccentricity.[13]

equivalent diameter. The eccentric annulus was divided into subareas, and a friction factor was computed for each subarea. The integrated-area average friction factor was then obtained; data are shown in Table III-2. Heat-transfer results were obtained for both concentric and eccentric annuli. The concentric-annulus heat-transfer coefficient was found to correlate by the Stein-Begell equation,[14] and the coefficient was found to be constant after 20 equivalent diameters. In contrast to this, the data for the eccentric annuli indicated that the coefficient did not approach a constant value, and the authors of Ref. 13 attribute this to the possibility of transverse mixing in the annulus. The heater-tube wall-temperature circumferential profile showed considerable variation; the difference between the maximum and minimum wall temperatures in one typical run was about 50% of the difference between the average surface temperature and the bulk average water temperature. The Stein-Begell equation did not adequately predict the heat-transfer coefficients, although empirical equations are presented in the reference which enable these temperature differences to be calculated.

Table III-2 COMPARISON OF PREDICTED AND EXPERIMENTAL RESULTS[13]

| | $D_2$, in. | $D_1$, in. | Eccentricity, % | $f/f_0$ |
|---|---|---|---|---|
| Predicted (integrated-area average friction factor) | 1.5 | 1.0 | 90 | 0.67 |
| Experimental test section: | | | | |
| 1 | 1.50 | 1.00 | 90 | 0.68 |
| 5 | 1.50 | 1.03 | 96 | 0.71 |
| 6 | 1.495 | 1.003 | 92 | 0.76 |

References 15 and 16 both present analytical approaches to determining heat and mass transfer in smooth tubes. Although the reports are quite specialized, both dealing with the solution of the equations for heat and mass transfer, there are some results of general interest. In Ref. 16, for example, the distinction between the laminar sublayer, the buffer zone, and the turbulent core is removed, and a single equation is postulated which relates the velocity within the fluid to the distance from the tube wall. The approach taken in Ref. 15 includes body forces to allow for the contribution of natural convection.

# Boiling-Water Heat Transfer

## Hydrodynamics

Savannah River Laboratory (SRL) has conducted an experimental program to measure the pressure drop for the flow of boiling water at high pressure.[17] The test conditions and apparatus are summarized in Table III-3. Refer-

Table III-3 EXPERIMENTAL CONDITIONS FOR SRL EXPERIMENTS

| | |
|---|---|
| Pressure, psia | 400 to 1000 |
| Test-section geometry | Tubular |
| Test-section length, ft | 18 |
| Test-section diameter, in. | 0.5 |
| Inlet subcooling, °F | 52 to 173 |
| Mass velocity, lb/(hr)(sq ft) $\times 10^{-6}$ | 0.8 to 7.9 |

ence 17 contains a discussion of the behavior of forced-convection flow of boiling water in a heated channel and the various "supply" and "demand" curves that characterize the system. This subject has been reviewed in *Power Reactor Technology*, 5(2): 14-15. The following is quoted from Ref. 17: "...knowledge of the relationship between flow and pressure drop in the heated channels is essential in estimating the stability of a boiling water system and in designing the pumping system to overcome potential instability." Approximately 74 pressure-drop runs were made, and the data are compared to the results of the homogeneous method of calculating pressure drop. The homogeneous method is discussed in some detail. In general,

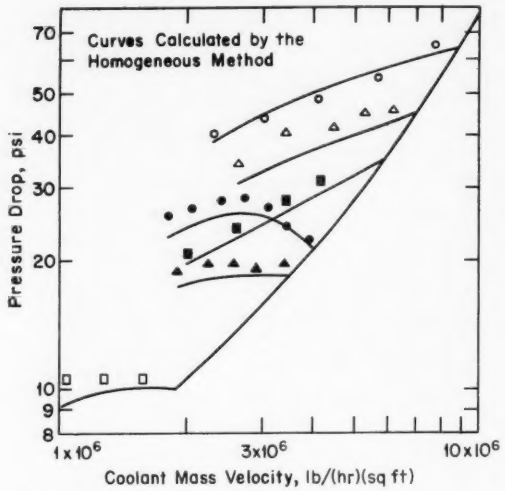


| Pressure, psia | Power Input Mw/sq ft | Inlet Subcooling, °C |
|---|---|---|
| ○ 420 | 127 | 29 |
| ● 665 | 141 | 48 |
| △ 780 | 150 | 37 |
| ▲ 815 | 135 | 61 |
| □ 850 | 104 | 96 |
| ■ 1010 | 144 | 44 |

Fig. III-5 Comparison of measured and calculated pressure drops for the flow of boiling water.[17]

for exit qualities from 15 to 25%, the experimental and calculated data agreed within ± 10%. The comparison is illustrated in Fig. III-5. Wall temperatures were also measured during about 54 runs to make possible the evaluation of heat-transfer coefficients; the correlation of Schrock[13] was found to agree with the experimental data.

The material in Ref. 17 pertains to the case of a forced-circulation system. Reference 19 contains a discussion of a natural-circulation system and the stability of such a system. A mathematical model is formulated which is based upon a force balance along an increment of channel length, and the resulting equation is investigated for stability by the methods of Liapunov. It is shown that the channel is asymptotically stable if the derivative of the pressure drop with respect to flow rate is positive when evaluated at the equilibrium flow rate. The term "asymptotically stable" implies that small perturbations in flow will tend to die out as time proceeds. The criteria presented defined regions of stability in terms of channel power, geometry, coolant properties, and slip ratio, for a single uniformly heated channel.

## Burnout

A French bibliographical study on the subject of boiling burnout has been issued.[20] Approximately 35 references are reviewed and discussed. Reference 21 presents results of a Euratom program conducted at Centro Informazioni Studi Esperienze, Milan. This program was reviewed in *Power Reactor Technology*, 5(2): 18-19. Reference 21 contains the data obtained with the annular test section utilizing bilateral heating. Experiments were conducted to measure pressure drop during two-phase flow, burnout heat fluxes, and heat-transfer coefficients. All tests employed two-phase flow at the inlet to the test section since the work was done in support of the fog-cooled-reactor concept. For bilateral-heating burnouts, the power was continuously increased on the inside or outside of the annulus while the power supplied to the other wall of the annulus was held constant. The test-section dimensions and the ranges of other variables are given in Table II-9 in *Power Reactor Technology*, 5(2): 18. Reference 21 lists the results of approximately 500 runs, and some of the data are graphically displayed. No analyses are reported in the reference, but the data are of interest per se.

A Russian correlation of burnout data has recently been published in translated form.[22] The correlation is stated to be valid in both the subcooled and quality regions for round, rectangular, and annular channels. The range of parameters over which the correlation is said to hold is given in Table III-4.* The correlation states

Table III-4 RANGE OF PARAMETERS FOR RUSSIAN BURNOUT CORRELATION[22]

| | |
|---|---|
| Pressure, psia | 15 to 3240 |
| Flow velocity, ft/sec | 1 to 79 |
| Quality | 0 to 0.7 |
| Hydraulic diameter, in. | 0.04 to 1.18 |
| Length, in. | 1.37 to 71 |

*Table III-4 is reprinted here by permission from the *Journal of Nuclear Energy*.[22]

that the burnout heat flux is a function of the following variables: $\phi_{bo} = f$ (flow velocity, surface tension, density, viscosity, quality, equivalent diameter, total length, boiling length). The author states that the flow velocity is determined "...from the total flow divided by the area of the channel and the density, at a mean temperature and vapour content...." Although this implies that a homogeneous flow model would be used, no direct statement to that effect is made; if separated flow were assumed, then a statement as to the void-fraction quality correlation employed would be very useful since a number of such correlations are available.

The results of an extensive program at General Electric's Atomic Power Equipment De-

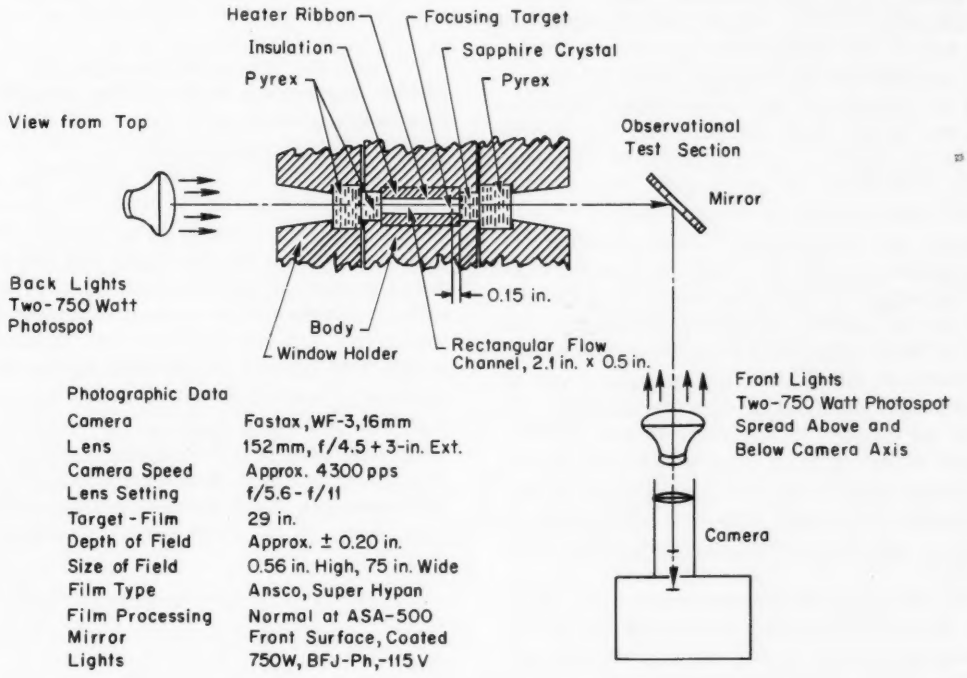


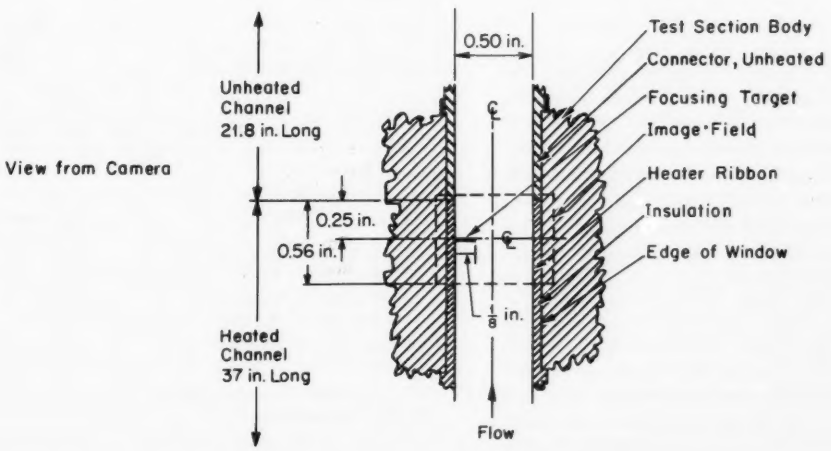


Fig. III-6 Schematic of the observational test section.[23]

partment (GE-APED) are reported in Ref. 18. The correlation of Ivashkevich[22] and many other publications on boiling burnout are discussed. The reference presents both experimental data and theoretical analysis of burnout. The particular test section used for the experimental program consisted of the "observational test section," so named because it contained a sapphire "window" to enable observation of a portion of the interior. The basic geometry was rectangular in cross section, with a total length of 58.8 in., and the test section was mounted vertically. The rectangular channel was about 2 in. wide and was either 0.5 or 0.25 in. thick. The channel was heated uniformly on either one or both of the two wide sides; the thickness of the heated walls was either 6 or 10 mils. Figure III-6 shows the geometrical arrangement of the test section and observation window. Burnout was determined by a detector that monitors the voltage unbalance of two tapped sections at the exit end of the heated section. This detector was also utilized to provide information for manual initiation of the camera operation in order to photograph conditions within the channel at the point (in time) of critical heat flux or burnout. Three types of runs were made: (1) camera operation only to achieve photographs of flow patterns; (2) burnout runs with no camera operation; and (3) burnout runs with camera operation.

Approximately 80 burnout runs were made, and about 30 motion pictures resulted. The following quotation from Ref. 23 describes the operation of the burnout detector:

> The character of the traces of the Detector output signal at onset of the critical heat flux condition shows a definite general similarity throughout the entire range of steam qualities, mass velocities, and heater element geometries.... Typically, as the heat flux was slowly raised to the critical condition, the first indication of abrupt change of the heater element temperature occurred at heat fluxes about 94 to 99 per cent of the heat flux at which the Detector would trip the power or physical damage to the heater ribbons would occur. At this point the recorded Detector output signal would commence pulsing slightly. As the heat flux was raised further, a definite fluctuation or oscillation would usually develop with a characteristic frequency of about 2 to 5 cycles per second and a minimum deflection about equal to or slightly above the previous steady-state level. Further increases in heat flux would increase the amplitude of fluctuation to the power trip point (6 mm deflection of the recorder pen to the right) or would cause an abrupt transient rise of the output signal through the power trip point, depending on the levels of steam quality and heat flux. Occasionally the Detector response was too slow to trip the power in time to prevent damage to the heater element.... At the lower steam qualities and higher critical heat flux levels the span of heat fluxes between initial indication of onset of critical conditions and the power trip point tended to be least and the Detector output signal tended to rise more abruptly than at the higher steam qualities and lesser critical heat flux levels....

An analysis was conducted to derive a theoretical expression involving the critical heat flux and the system variables. The analysis assumes a model wherein liquid flows in a layer or film adjacent to the wall while vapor flows in the core. Stability of the liquid film is measured by whether a small disturbance at the interfacial surface of the liquid and gas grows with the passage of time, and the limit of stability is interpreted as a significant limit on the liquid film thickness. The model further assumes that burnout occurs when the liquid film adjacent to the heated wall becomes discontinuous; thus patches of vapor contact the wall. The final analytical correlation contains three constants that were chosen to achieve best agreement between the analytical and experimental data. Although the correlation will not be pre-

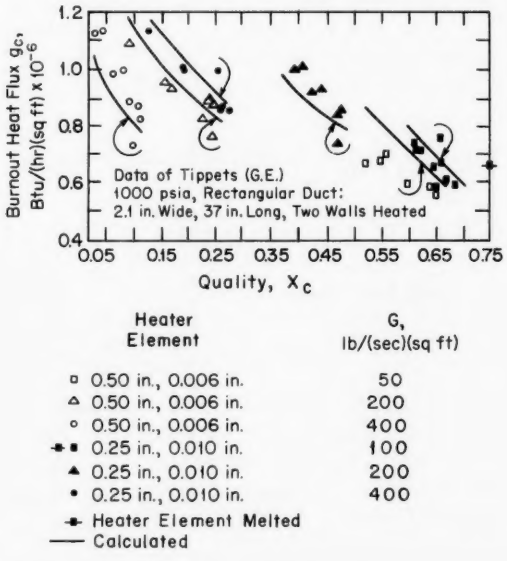


Fig. III-7 Comparison of data taken with observational test section and the correlation.[23]

sented here in detail, the comparison between the experimental data and the correlation is illustrated in Fig. III-7. The conclusions derived from the study are as follows:[23]

1. The critical heat flux to water in conditions of bulk boiling (X > 0) with steady forced flow has the following trends, over the range of conditions investigated experimentally and analytically:
   (a) $q_c$ decreases with increasing mass velocity over the range from 50 lbs/sec-ft$^2$ to 900 lbs/sec-ft$^2$.
   (b) $q_c$ decreases with increasing pressure over the range from 600 psia to 2500 psia.
   (c) $q_c$ decreases with increasing hydraulic diameter over the range of duct dimensions "b" from .084 in. to .24 in. and increases slightly with hydraulic diameter for the range of duct dimensions "b" less than .084 in. down to .024 in. ("b" is the radius for circular tubes and one-fourth the hydraulic diameter for annular and rectangular ducts.)
   (d) $q_c$ decreases monotonically with increasing steam quality over the range from 0.00 to 0.75.
   (e) $q_c$ increases with increasing ratio of heated surface to total surface.
   (f) $q_c$ is approximately independent of heated length over the range from 12 in. to 108 in. and range of length to diameter ratios from about 100 to 400. The Russian data indicate $q_c$ increases with decreasing $L/D_e$ ratios for $L/D_e < 100$.
   (g) $q_c$ appears to be calculable using local fluid properties and local flow conditions such as mass velocity, steam quality and pressure.
   (h) The critical heat flux condition appears to be a distinct repeatable phenomenon rather than subject to significant statistical variation.
2. There is substantial evidence in the high speed motion pictures that the general arrangement of the flow, over the range of variables investigated, at heat fluxes near and including the critical heat flux level, is characteristically a wavy turbulent liquid film in which there is vapor formation, flowing along the channel walls with the balance of the liquid being carried as either dispersed droplets or as an emulsion with the vapor in an adjacent more rapidly and steadily moving core. This conclusion is not indisputable, due to lack of corresponding precise measurements of the arrangement of the flow pattern.
3. Theoretical analysis based on a representation of the flow pattern which is generally consistent with conclusion 2 resulted with a useful working equation which relates the critical heat flux to the significant local fluid properties and flow parameters.... Critical heat fluxes calculated by this expression are in good general agreement with measured values over the range of variables considered. The expression includes three empirical constants which were determined by application to a limited portion of the data treated.

Reference 24 presents a new method of plotting burnout data. The technique consists of plotting the burnout heat flux, $\phi_{bo}$, against a quantity called "steam energy flow." The steam-energy flow bears the units of heat flux and is computed as the product of mass flow, quality, and vaporization enthalpy, $Gxh_{fg}$. Since uniformly heated test sections almost always burn out at the exit of the test section, the quality can be taken as the exit quality, whereas $G$ is the superficial mass velocity. The steam-energy-flow (SEF) plot has the characteristic of separating burnout data into at least two regimes, as shown in Fig. III-8.* These are represented by curves labeled "DNB-1" and

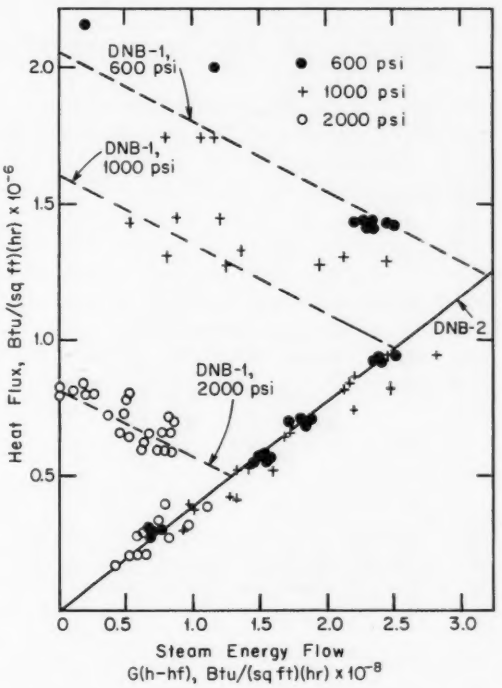


Fig. III-8 DNB heat-flux data and correlation curves at three pressures.[24]

*Figure III-8 is reprinted here by permission from *Nuclear Science and Engineering*.[24]

"DNB-2." The author suggests that the DNB-2 data result from test loops "burning out" from hydrodynamic instability, whereas the DNB-1 data are caused by transition from nucleate boiling into film boiling. By defining quality on an enthalpy basis, it is possible to plot data (from the left), the data depart from the DNB-1 curve and trace out a curve labeled "DNB-3." The 08-075 data show similar behavior; however, the experiments were run starting in the quality region, and $G$ was increased until subcooled-burnout data were taken. Also plotted

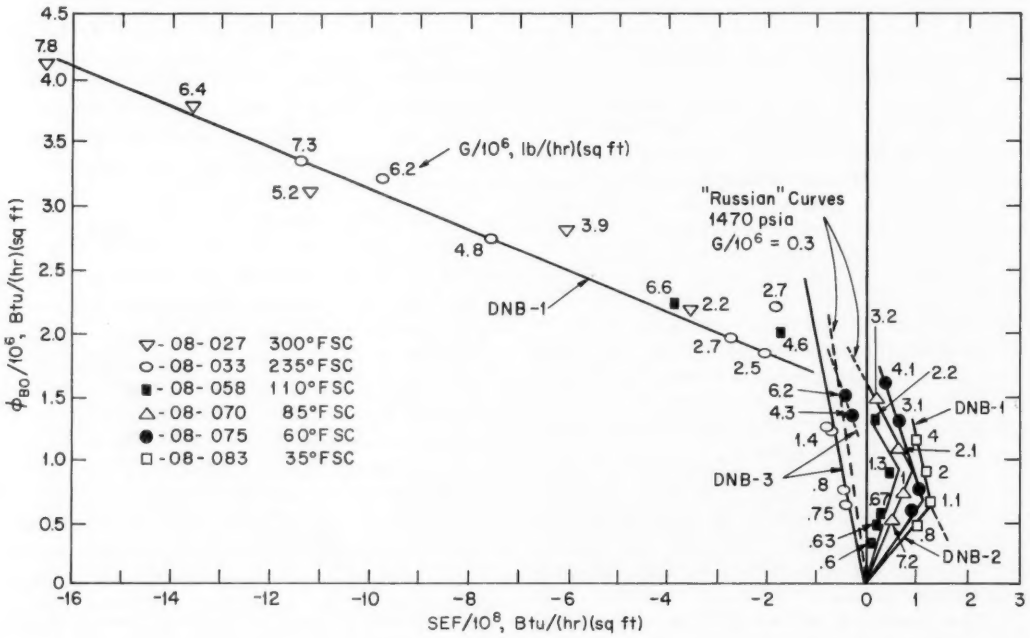


Fig. III-9 Burnout data[25] at a pressure of 2000 psia.

from both the subcooled and quality regimes on the same plot; an example of this is given in Ref. 24.

Further SEF analyses of burnout data were presented at the winter meeting of the American Nuclear Society.[25] Some of the conclusions can be obtained by considering the data presented in Fig. III-9.* Each set of points is identified with a number, e.g., 08-027; the first two-digit number identifies the table in WAPD-188 (Ref. 26), from which the data were taken, whereas the three-digit number identifies the run number commencing the series.

Figure III-9 contains burnout data at 2000 psia and constant inlet subcooling. The 08-033 set of data show that, as zero SEF is approached

*Figure III-9 is reprinted here by permission from *Transactions of the American Nuclear Society*.[25]

are "Russian" curves taken from Fig. 5 of Ref. 27. The DNB-3 type Russian line represents "pulsating" burnout, whereas the DNB-1 type line represents data from "nonpulsating" burnout. The reference suggests that, since the DNB-3 line lies close to SEF = 0, these instabilities may be associated with subcooled boiling, where it is possible to get high void volumes.

## Miscellaneous Reports

In the Research and Reactor Group of the United Kingdom Atomic Energy Authority (UKAEA), both the Chemical Engineering Division and the Reactor Development Division have been studying heat-transfer and fluid-flow characteristics of steam-water mixtures. The magnitude of the effort can be seen in a number of recent reports[28–39] issued by the UKAEA. The

reports are concerned with quite specialized topics in two-phase flow and heat transfer and will not be reviewed in detail. A perusal of the titles, however, indicates the detail to which the topic is being investigated and suggests that interesting results should be forthcoming.

References 40 to 44 deal with the expansion of two phases, steam and water, through nozzles or in discharge from a pipe. Like the above-mentioned UKAEA reports, they are not written to aid in reactor design and are quite specialized. The reports in fact are motivated to some extent by the attempt to attain an understanding of two-phase flow through a nozzle in order to maximize the transfer of potential energy to kinetic energy for the production of useful work. In general, however, the mechanics of two-phase flow are of interest to the reactor designer in safety calculations where it is postulated that a rupture has occurred in the primary piping and a knowledge of the rate of loss of coolant is important. In addition, critical flow phenomena place limits on the amount of coolant that can be handled by a flow system.

Film boiling is treated in Refs. 45 and 46. The purpose of the experiments reported in Ref. 45 is to obtain data necessary for the design of once-through boilers in which the feedwater is completely vaporized in a single pass through the boiler. An equation of the following type is recommended for computing the film-boiling heat-transfer coefficient:[45]

$$\mathrm{Nu} = K(\mathrm{Re})^{0.8}(\mathrm{Pr})^{0.4}$$

The symbols have their conventional meanings. The coefficient $K$ was determined to be a pressure-dependent "constant"; at 3000 psia, it has the value 0.076, and at 2600 psia, 0.050. The properties were evaluated at the surface temperature. Most of the experiments utilized smooth tubing; however, some runs were made with an internally ribbed tube. Concerning this point, the authors conclude that "...certain configurations of internally ribbed surfaces in steam generating tubes will maintain nucleate boiling at lower velocities and much higher steam qualities than a smooth tube. Therefore the possibility of tube failures resulting from high tube-wall temperatures associated with the departure from nucleate boiling can be avoided by using ribbed tubes." The film-boiling heat-transfer correlation proposed in Ref. 46 is for pool film boiling instead of forced-convection film boiling. The correlation is not entirely empirical, however, because it employs a term to account for the effect of Taylor instabilities in rupturing the vapor film surrounding the heat-transfer surface. The correlation is said to be applicable over a range of diameters from 0.00022 to 1.895 in.

# Mathematical Analyses

The transient thermal behavior of $UO_2$ fuel elements in the Sodium Reactor Experiment (SRE) is reported in Ref. 47. The results of a study on an analog computer and an experimental program are reported, and, although the details are peculiar to the SRE, the analog equations are of general applicability. Computer programs to solve complex conduction problems are described in Ref. 48, whereas Refs. 49 to 52 present programs to aid in the study of single-phase and two-phase hydrodynamics and associated phenomena.

## References


1. Westinghouse Electric Corp., Bettis Atomic Power Laboratory, Pressurized Water Reactor (PWR) Project, Technical Progress Report, April 24, 1962, to June 23, 1962, USAEC Report WAPD-MRP-98.
2. Donald G. Schweitzer, George C. Hrabak, and Robert M. Singer, Oxidation and Heat Transfer Studies in Graphite Channels. I. The Effect of Air Flow Rate on the C-$O_2$ and CO-$O_2$ Reactions, *Nucl. Sci. Eng.*, 12(1): 39 (January 1962).
3. Donald G. Schweitzer and David H. Gurinsky, Oxidation and Heat Transfer Studies in Graphite Channels. II. Thermal Changes with Time and Distance in Air-Cooled Graphite Channels, *Nucl. Sci. Eng.*, 12(1): 46 (January 1962).
4. Donald G. Schweitzer and Robert M. Singer, Oxidation and Heat Transfer Studies in Graphite Channels. III. The Chemical Reactivity of BNL Graphite and Its Effect on the Length of Channel Cooled by Air, *Nucl. Sci. Eng.*, 12(1): 51 (January 1962).
5. Donald G. Schweitzer, Oxidation and Heat Transfer Studies in Graphite Channels. IV. Combined Effect of Temperature, Flow Rate, Diameter, and Chemical Reactivity on the Length of Channel Cooled by Air, *Nucl. Sci. Eng.*, 12(1): 59 (January 1962).
6. Donald G. Schweitzer, Thermal Properties of Air-Cooled Graphite Channels, *Nucl. Sci. Eng.*, 13(3): 275 (January 1962).

7. I. B. Mason and R. H. Knibbs, The Thermal Conductivity of Artificial Graphites and Its Relationship to Electrical Resistivity, British Report AERE-R-3973, March 1962.
8. R. Bee and L. R. T. Gardner, A Slide Rule Method of Calculating the End Fitting Temperatures of Fuel Elements, British Report TRG-Report-306, June 6, 1962.
9. R. J. Hill, The Theoretical and Experimental Temperature Distribution in a Fuel Pin of a Thermionic Convertor, British Report AERE-R-4075, June 1962.
10. J. Randles, Heat Diffusion in Cylindrical Fuel Elements of Water Cooled Reactors, British Report AEEW-R-96, September 1961.
11. R. F. Clements, Explicit Equations for Pipe and Rectangular Channel Isothermal Friction Factors, in Reactor Technology Report No. 21—Engineering, USAEC Report KAPL-2000-18, Knolls Atomic Power Laboratory, June 1962.
12. W. H. Esselman, I. H. Mandil, S. J. Green, P. C. Ostergaard, and R. A. Fredrickson, Thermal and Hydraulic Experiments for Pressurized Water Reactors, in *Proceedings of the Second United Nations International Conference on the Peaceful Uses of Atomic Energy, Geneva, 1958*, Vol. 7, pp. 758-773, United Nations, New York, 1958.
13. T. Diskind, Heat Transfer and Pressure Drop in Eccentric Annuli, USAEC Report NYO-9649, Columbia University, Engineering Research Laboratories, Sept. 30, 1961.
14. R. P. Stein and W. Begell, Heat Transfer to Water in Turbulent Flow in Internally Heated Annuli, *A.I.Ch.E. J.*, 4(2): 127 (June 1958).
15. M. S. Ojalvo and R. J. Grosh, Combined Forced and Free Turbulent Convection in a Vertical Tube (thesis). Technical Report No. 12, USAEC Report ANL-6528, Argonne National Laboratory, January 1962.
16. V. R. Gowariker, Analysis of Mass and Heat Transfer in Smooth Tubes at High Reynolds Numbers, British Report AERE-M-1055, June 1962.
17. N. Dinos, Pressure Drop for Flow of Boiling Water at High Pressure, USAEC Report DP-698, Savannah River Laboratory, May 1962.
18. V. E. Schrock and C. M. Grossman, Forced Convection Boiling in Tubes, *Trans. Am. Nucl. Soc.*, 3(2): 472-473 (December 1960).
19. A. Carnasale, Hydraulic Stability in Heated Parallel Channels (thesis), Drexel Institute of Technology, June 1961.
20. A. de la Harpe, Literature Survey of Burnout Heat Fluxes for Two-Phase Water-Steam in Forced Convection, French Report CEA-Bib-28, 1961.
21. N. Adorni, S. Bertoletti, J. Lesage, C. Lombardi, G. Peterlongo, G. Soldaini, F. J. Weckermann, R. Zavattarelli, Results of Wet Steam Cooling Experiments: Pressure Drop, Heat Transfer and Burnout Measurements in Annular Tubes with Internal and Bilateral Heating, USAEC Report TID-12469, January 1961.
22. A. A. Ivashkevich, Critical Heat Fluxes for Forced Convection of Liquid in Channels, *J. Nucl. Energy: Pts. A&B*, 16: 171 (March 1962).
23. F. E. Tippets, Critical Heat Flux and Flow Pattern Characteristics of High Pressure Boiling Water in Forced Convection, USAEC Report GEAP-3766, General Electric Company, Atomic Power Equipment Department, April 1962.
24. William J. Levedahl, Two Regimes of Burnout (DNB) Correlated with Steam Energy Flow for Uniformly-Heated Channels, Letters to the Editors, *Nucl. Sci. Eng.*, 14(2): 201 (October 1962).
25. John S. Wiley, Analysis of High-Pressure Burnout Data, *Trans. Am. Nucl. Soc.*, 5(2): 474-476 (November 1962).
26. R. A. DeBortoli, S. J. Green, B. W. LeTourneau, M. Troy, and A. Weiss, Forced-Convection Heat Transfer Burnout Studies for Water in Rectangular Channels and Round Tubes at Pressures Above 500 psia, USAEC Report WAPD-188, Westinghouse Electric Corp., Bettis Atomic Power Laboratory, October 1958.
27. I. T. Alao'yev et al., Boiling Crisis in Tubes, in *International Developments in Heat Transfer*, Part II, Section A, p. 237, American Society of Mechanical Engineers, 1961.
28. G. F. Hewitt and P. C. Lovegrove, The Application of the Light Absorption Technique to Continuous Film Thickness Recording in Annular Two-Phase Flow, British Report AERE-R-3953, July 1962.
29. J. G. Collier and D. J. Pulling, Heat Transfer to Two-Phase Gas-Liquid Systems, Part II. Further Data on Steam/Water Mixtures in the Liquid Dispersed Region in an Annulus, British Report AERE-R-3809, March 1962.
30. G. B. Wallis, Flooding Velocities for Air and Water in Vertical Tubes, British Report AEEW-R-123, December 1961.
31. G. F. Hewitt, R. D. King, and P. C. Lovegrove, Techniques for Liquid Film and Pressure Drop Studies in Annular Two-Phase Flow, British Report AERE-R-3921, March 1962.
32. D. J. Pulling, The Deposition of Solids in a Vertical Tube Evaporator, British Report AERE-R-3807, September 1961.
33. L. E. Gill and G. F. Hewitt, Further Data on the Upwards Annular Flow of Air-Water Mixtures, British Report AERE-R-3935, April 1962.
34. J. G. Collier, Pressure Drop Data for the Forced Convective Flow of Steam/Water Mixtures in Vertical Heated and Unheated Annuli, British Report AERE-R-3808, March 1962.
35. H. J. Ivey and D. J. Morris, On the Relevance of the Vapour-Liquid Exchange Mechanism for Sub-Cooled Boiling Heat Transfer at High Pressure, British Report AEEW-R-137, January 1962.

36. G. B. Wallis, The Transition from Flooding to Upwards Cocurrent Annular Flow in a Vertical Pipe, British Report AEEW-R-142, February 1962.
37. G. F. Hewitt, Some Calculations on Holdup, Heat Transfer and Nucleation for Steam-Water Flow in a 0.5 cm Bore Tube, British Report AERE-R-3984, April 1962.
38. G. B. Wallis, One-Dimensional Waves in Two-Component Flow (with Particular Reference to the Stability of Fluidised Beds), British Report AEEW-R-162, April 1962.
39. N. Hall-Taylor and G. F. Hewitt, The Motion and Frequency of Large Disturbance Waves in Annular Two-Phase Flow of Air-Water Mixtures, British Report AERE-R-3952, June 1962.
40. R. A. Brown, Flashing Expansion of Water Through a Converging-Diverging Nozzle (thesis), USAEC Report UCRL-6665-T, University of California Lawrence Radiation Laboratory, Oct. 24, 1961.
41. R. A. Fiedler, Shock Location During Two-Phase Flow in an Overexpanded Nozzle (thesis), USAEC Report UCRL-6676, University of California Lawrence Radiation Laboratory, Nov. 1, 1961.
42. D. J. Maneely, A Study of the Expansion Process of Low-Quality Steam Through a de Laval Nozzle (thesis), USAEC Report UCRL-6230, University of California Lawrence Radiation Laboratory, Jan. 25, 1962.
43. K. F. Neusen, Optimizing of Flow Parameters for the Expansion of Very Low-Quality Steam (thesis), USAEC Report UCRL-6152, University of California Lawrence Radiation Laboratory, Jan. 25, 1962.
44. F. R. Zaloudek, The Low Pressure Critical Discharge of Steam-Water Mixtures from Pipes, USAEC Report HW-68934(Rev.), Hanford Atomic Products Operation, March 1961.
45. H. S. Swenson, J. R. Carver, G. Szoeke, The Effects of Nucleate Boiling Versus Film Boiling on Heat Transfer in Power Boiler Tubes, *J. Eng. Power*, 30A(4): 365 (October 1962).
46. B. P. Breen and J. W. Westwater, Effect of Diameter of Horizontal Tubes on Film Boiling Heat Transfer, *Chem. Eng. Progr.*, 58(7): 67 (July 1962).
47. J. T. Ream and R. P. Varnes, Transient Thermal Behavior of Experimental $UO_2$ Fuel Elements in the Sodium Reactor Experiment (SRE), *Nucl. Sci. Eng.*, 13(4): 325 (August 1962).
48. David Bagwell, SIFT—An IBM-7090 Code for Computing Heat Distributions, USAEC Report K-1528, Oak Ridge Gaseous Diffusion Plant, July 6, 1962.
49. D. G. Dight, A. B. Jones, STABLE-3—Hydraulic Flow Stability Analysis, in Reactor Technology Report No. 21—Engineering, USAEC Report KAPL-2000-18, Knolls Atomic Power Laboratory, June 1962.
50. J. E. Meyer and J. S. Williams, Jr., A Momentum Integral Model for the Treatment of Transient Fluid Flow, Bettis Technical Review. Reactor Technology, USAEC Report WAPD-BT-25, Westinghouse Electric Corp., Bettis Atomic Power Laboratory, May 1962.
51. A. B. Jones and D. G. Dight, Hydrodynamic Stability of a Boiling Channel, Part 2, USAEC Report KAPL-2208, Knolls Atomic Power Laboratory, Apr. 20, 1962.
52. J. Dugone, Calculation of Departure from Nucleate Boiling Conditions for the SPERT III Reactor in the High Pressure Region, USAEC Report IDO-16774, Phillips Petroleum Co., Apr. 18, 1962.

Section

# IV

Power Reactor Technology

# Fuel Elements

## Performance of Packed-Powder Fuels

An expanding program of fuel irradiation is being carried on in conjunction with the packed-powder $UO_2$ fuel effort previously reviewed in *Power Reactor Technology*, 6(1): 26-38. These activities stem from the widespread interest in the economic potential associated with the production of $UO_2$ fuel by use of various packed-powder techniques. Although the initial experiments were largely comparison studies between packed-powder and pressed-and-sintered fuels, their success has permitted recent investigations to assume a more general character. Broadly stated, the goals of the present irradiation program are to obtain a better understanding of the behavior of packed-powder fuel elements during reactor operation and to assess the effect of various materials and fabrication methods upon the performance of the packed-powder product. The following review presents some typical results of the irradiations conducted to date.

The first packed-powder-fuel irradiation specimens were of the solid, cylindrical, rod type and consisted of a Zircaloy or stainless-steel jacket tube which contained ground, ceramic-grade $UO_2$ and which was tamp-packed to between 40 and 60% of theoretical density. This technique was chosen as the simplest application of the packed-powder approach because (1) it utilized only those materials commonly available and (2) it represented a minimum of fabrication effort. A typical 1-in.-OD sample of this type[1] was exposed to $2 \times 10^{20}$ nvt (3000 Mwd/ton burnup) at a heat flux in excess of $10^6$ Btu/(hr)(sq ft). Postirradiation examination of this and three other companion specimens disclosed a marked contraction and relocation of the $UO_2$. This relocation and its relation to environmental neutron flux are shown in Fig. IV-1. The observed shrinkage of the $UO_2$ is attributed to the extensive in-reactor sintering and grain growth sustained by the $UO_2$, as shown in Fig. IV-2.

Reference 2 describes the results of the irradiation of three test elements, each containing thirty-six ¼-in.-OD type 304 stainless-steel-jacketed $UO_2$ fuel rods. Three methods of densification (vibratory compaction, swaging, and pressing and sintering) were used to fabricate the various test rods. The as-packed densities ranged from a low of 56% of theoretical for vibratory-compacted fuel to 90% of theoretical for the pressed-and-sintered material. Swaged fuel averaged 80% of theoretical density. Exposures of up to about 20,000 Mwd/ton at heat fluxes of up to 410,000 Btu/(hr)(sq ft) were obtained. Table IV-1 contains a résumé of data compiled for representative specimens. Figures IV-3 to IV-6 are cross-sectional photomicrographs that are typical of the vibratory-compacted, swaged, and pressed-and-sintered rods used in the test.

It is significant to note that only Fig. IV-3 exhibits the characteristic structure associated with $UO_2$ that has operated at temperatures conducive to grain growth. The lack of grain growth in Fig. IV-4 (a companion specimen to that of Fig. IV-3) may be explained by the low heat flux [194,000 Btu/(hr)(sq ft)] at which the specimen operated, the high initial density (89% of theoretical density), and the small diameter of the rod. Moreover, it is unlikely that operation at this low power produced any substantial degree of sintering in the specimen shown in Fig. IV-4. This contention is further supported by the clearly discernible particulate structure of the $UO_2$ which normally is obliterated by the sintering process.

Figure IV-5 suggests the extremely porous structure usually found in solidified melts. This structure may have resulted from the low initial density (56%) rather than actual melting. Paradoxically, the postirradiation structure of the pressed-and-sintered specimen shown in Fig. IV-6 is radically different from that usually associated with this form of $UO_2$. The reference calls attention to this fact as follows: "The polished and etched structure is startling and has no relation to the original microstructure. It appears that the pellet has been fused into an amorphous glass. There is no discernible grain structure except for a few spots near the cladding. The structure is honeycombed with irregular smooth-edged voids. Elongated voids form a radial pattern with its center at the axis of the fuel. A 700-$\mu$-diameter central void is noted." Unfortunately the reference gives no explanation for the observed result. An explanation cannot be deduced without a more detailed knowledge of the materials and fabrication history of this specimen.

The experiments of Refs. 1 and 2 also contributed some useful gas-release information that is reproduced here as part of Table IV-1 and as Table IV-2. The data of Table IV-2 are of particular interest in that both specimens contained $UO_2$ of the same batch and subjected to the same processing conditions, except that the $UO_2$ of specimen II-a had been exposed to the atmosphere for a period of approximately 13 weeks.

Similar results were observed by other investigators[3] during the irradiation of four 0.57-in.-OD swaged rods of stainless-steel-jacketed fused $UO_2$. The rods were irradiated to exposures of from 1580 to 3390 Mwd/ton and at powers of 3.7 to 7.9 kw/ft [85,000 to 181,000 Btu/(hr)(sq ft) heat flux]. Fission-gas releases of 1.7 to 13.7% of the total fission gas generated were observed. However, as shown in Table IV-3, concomitant releases of nitrogen and carbon dioxide accounted for 80% of the total gas released, even in rods releasing the greatest amount of fission gas. The unexpectedly large

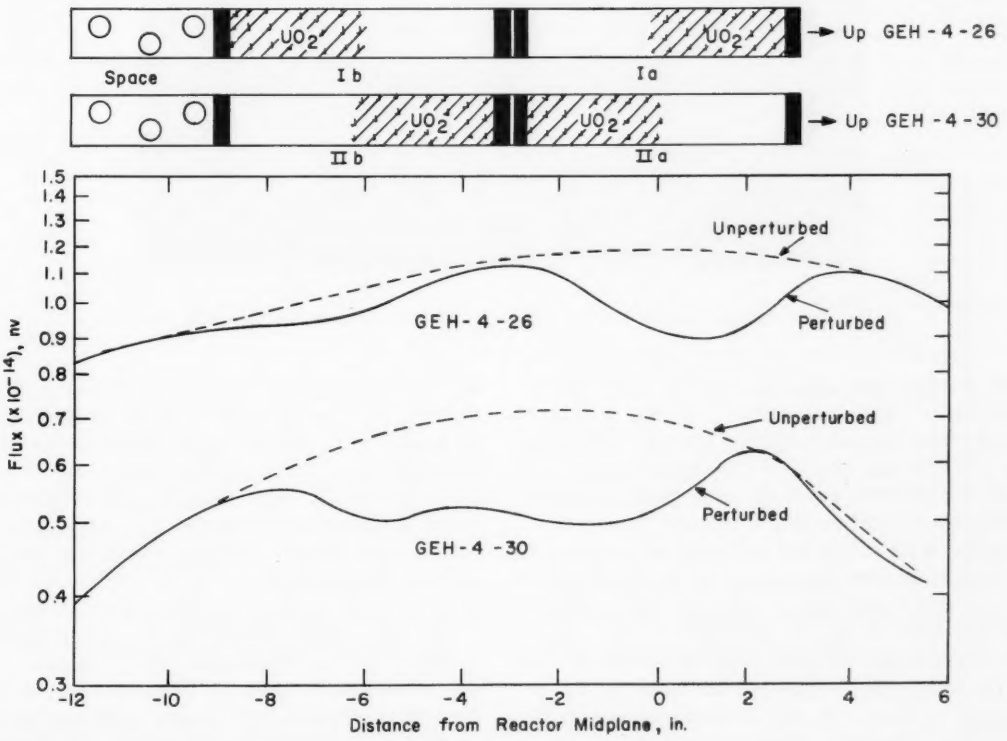


Fig. IV-1 Vertical flux pattern of $UO_2$ powder fuel elements.[1]

gas release may have been due, partially, to the excess oxygen in the fused $UO_2$ which exhibited oxygen-to-uranium ratios of 2.087 and 2.132.

In view of the modest power levels at which these specimens operated, the quantity of fission-product and atmospheric gas liberated is significant. The implication is for a more severe gas-release problem than that indicated for pressed-and-sintered $UO_2$ by previous irradiation studies. From those studies one would expect the total fission-gas release to be only a fraction of 1% of that generated in rods operated at 85,000 Btu/(hr)(sq ft) and to be about 1 or 2% of that generated in the rods operated at 181,000 Btu/(hr)(sq ft). Moreover, little if any atmospheric gas release would be expected.

The difference in gas-release behavior is, of course, related to the differences in void structure. Porosity exists in pressed-and-sintered fuel of more than 92% theoretical density almost exclusively as isolated voids. Measurements indicate that only 0.2 to 0.4% of the porosity is interconnected.[4a] Conversely, packed-powder fuel consists of particles of fused $UO_2$ that are considered to be 100% dense and, therefore, to contain no voids. If a fuel element using this material exhibits a bulk density of less than theoretical density, the element must contain voids between the $UO_2$ particles and, furthermore, these voids must be connected to some degree. Investigations using pressed-and-sintered fuel have established that, when operating below the grain-growth temperature (1500°C), $UO_2$ crystals give up fission gas by diffusion. Characteristically, the rates applicable to this diffusion process[5] are approximately $10^{-12}$ $cm^2/sec$. At the irradiation times of interest ($10^7$ to $10^8$ sec), the diffusion-path length is of the order of $10^{-2}$ cm; thus little of the gas can diffuse from internal regions of the fuel body to the

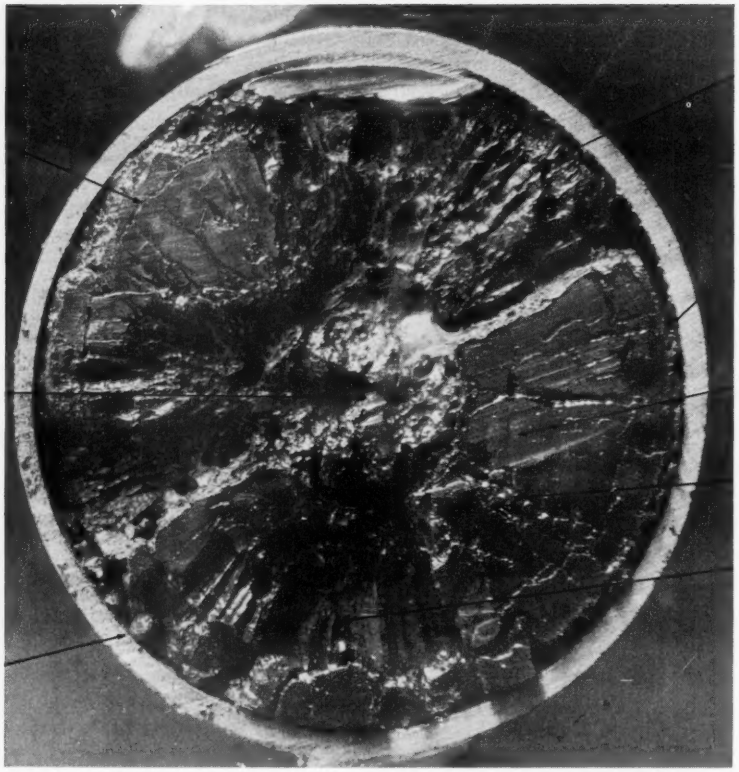


Fig. IV-2 Cross section[1] of irradiated test element originally filled with $UO_2$.

surface unless most of the diffusion path is bypassed by interconnected voids or cracks. The effects of open porosity upon fission-gas release have been demonstrated previously by comparing the release rates of pressed-and-sintered material exhibiting low open porosity (bulk densities greater than 92% of theoretical density) and that having extensive open porosity (bulk densities less than 90% of theoretical density). The unsintered packed-powder fuels represent a still more pronounced case of open porosity.

The presence of gases, normally found as constituents of the atmosphere, in the gas spaces of irradiated fuel elements is attributed to surface adsorption which results from prolonged exposure of the $UO_2$ to air.[1,3] This opinion is sustained by investigations[4a-c] employing the standard laboratory techniques of autoclaving and vacuum degassing of both irradiated and nonirradiated $UO_2$. Typical results of experiments of this type are contained in Table IV-4. It is significant to note that, even after a 1700°C sintering operation, the fused-and-ground product released is in some cases more than 20 times as much adsorbed gas as pressed-and-sintered material.[4a] As illustrated by Fig. IV-7, this effect may be a function of the greater total surface area exhibited by the packed-powder $UO_2$. All the above references suggest vacuum degassing as an effective means of removing surface-adsorbed gases from either type of oxide.

Two deleterious effects of the release of substantial quantities of atmospheric gas may be visualized. The first is the obvious problem of high internal fuel-jacket pressures that result from the volume of gas to be contained.

Table IV-1 DATA RÉSUMÉ[2]

| | | Fuel | | | Burnup | | Peak heat flux,§ | $Kr^{85}$ | Central void | |
|---|---|---|---|---|---|---|---|---|---|---|
| Element | Rod | Powder type | Density* | Fabrication† | Peak,‡ % | Av.,‡ % | 1000 Btu/(hr)(sq ft) | release,¶ % | Length, in. | Character |
| Group 1: | | | | | | | | | | |
| G1 | H1 | Fired | 56 | V | 0.97 | 0.77 | 360 | 63 | 28 | Wandered |
| | I6 | | 56 | V | 1.10 | 0.88 | 410 | 89 | 28 | Wandered |
| | N5 | | 53 | V | 1.07 | 0.86 | 380 | 83 | 28 | Wandered |
| Group 2: | | | | | | | | | | |
| G1 | E5 | | 55 | V | 2.24 | 1.72 | 230 | | 21 | Centered |
| | I1 | | 56 | V | 2.34 | 1.80 | 250 | | 23 | Wandered |
| | K6 | | 54 | V | 2.60 | 2.00 | 270 | | 18 | Centered |
| Group 3: | | | | | | | | | | |
| G2 | A2 | | 61 | V | 0.91 | 0.73 | 370 | 47 | 19 | Centered |
| | B1 | | 59 | V | 0.87 | 0.72 | 350 | 55 | 16 | Centered |
| | N4 | | 53 | V | 0.87 | 0.70 | 310 | 80 | 28 | Wandered |
| Group 4: | | | | | | | | | | |
| G2 | A3 | | 64 | V | 1.78 | 1.30 | 220 | | 3 | Centered |
| Group 5: | | | | | | | | | | |
| G4 | 21 | | 89 | S | 0.60 | 0.46 | 190 | 14 | 0 | |
| | 39 | | 79 | S | 0.81 | 0.63 | 250 | 64 | 2 | Centered |
| | 42 | Ceramic grade | 90 | P | 0.84 | 0.65 | 220 | 68 | 7 | Centered |
| | Y3 | Fired | 81 | S | 0.87 | 0.67 | 270 | 11 | 0 | |
| Group 6: | | | | | | | | | | |
| G4 | 34 | | 82 | S | | (0.65)** | (220) | 33 | | |
| | V4 | | 87 | S | | (0.46)†† | (190) | 26 | | |
| | Y6 | | 86 | S | | (0.46)†† | (190) | 21 | | |

*Percent of theoretical $UO_2$ density (10.96).
†V, vibratory packed; S, swaged; P, pellet.
‡By cerium analysis, atomic percent of total uranium.
§Heat flux at peak point of rod, Vallecitos Boiling-Water Reactor at 30 Mw.
¶Based on gamma-count sample and cerium burnup analysis.
**Based on similar position to rod 42 of group 4.
††Based on similar position to rod 21 of group 4.

The second is the concern that these gases or the products of their interaction with impurities in the uranium may have a detrimental effect upon the fuel-element-jacket material. Jacket deterioration, caused by internally contained gases, is considered to be the major factor in the failure of several swaged, Zircaloy-2-jacketed, tubular $UO_2$ fuel elements during irradiation.[6a,6b] Although the $UO_2$ was vacuum degassed prior to irradiation, postirradiation investigations of the processes used to fabricate the unsuccessful elements indicated that the $UO_2$, upon initiation of irradiation, could have contained from 20 to 110 ppm water (contributing 2 to 12 ppm hydrogen) and from 3 to 10 ppm free hydrogen. The $UO_2$ also contained uranium nitride and uranium carbide, which react with water to produce, respectively, free nitrogen and free hydrogen plus methane. As shown in Table IV-5, both methane and nitrogen were found in gas samples removed from nondefected fuel tubes. These sources are believed to be more than sufficient to account for the increase from the 1 to 3 ppm hydrogen, existing as impurity in the preirradiated jacket material, to the 6 to 7 ppm hydrogen observed in postirradiation inspections of extensively hydrided test specimens that had not failed during the test.[3] Substantially greater quantities of hydrogen would probably exist in $UO_2$ that had not been vacuum degassed.

An additional question regarding the characteristics of packed-powder fuels is the effect

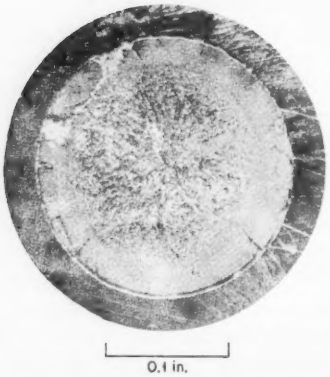


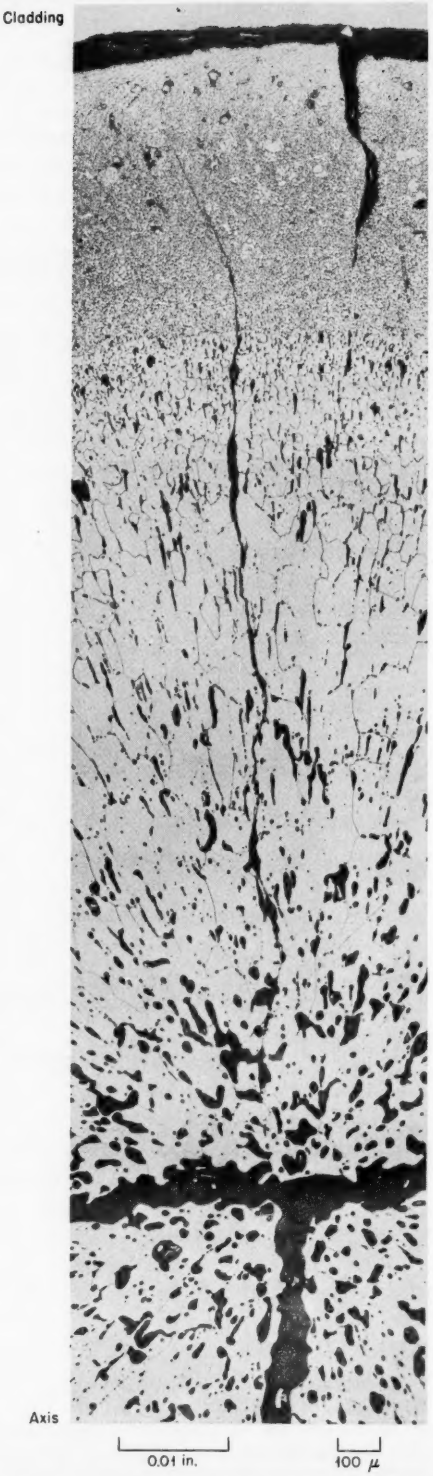


Fig. IV-3 Polished and etched, irradiated, swaged $UO_2$ + 1% $TiO_2$ powder[2] (−325 mesh and 79% dense). This specimen was exposed at a heat flux of 248,000 Btu/(hr)(sq ft).

of flowing coolant upon the compacted fuel in the event of a jacket tube rupture. Investigations to determine the extent of any erosion have been conducted both in the laboratory and during irradiation using either high-temperature water or steam as the working fluid.[4a,8c,6d] The results given in Ref. 6*d* are typical of those reported for jacket defects occurring in packed-powder fuel used at high power density. In this case the jacket failure occurred after 24 days of irradiation at a point where the maximum heat flux was about 600,000 Btu/(hr)(sq ft). The coolant used was water, at 2000 psi and 477°F, flowing past the jacket surface at a velocity of 4.7 ft/sec. The defected fuel element was operated for about 15 hr after the failure. Postirradiation inspection disclosed a split in the jacket tube which was about 1 in. long. It was estimated that approximately 10% of the volume of $UO_2$ in the vicinity of the rupture was lost to the coolant.

The experiments of Ref. 4*a* involved the exposure of two defected, stainless-steel-jacketed $UO_2$ fuel elements, one containing pressed-and-sintered compacts and the other packed-powder fuel, to flowing steam heated to 1050°F. As shown in Figs. IV-8 and IV-9, the amount of erosion sustained by the two elements appears to be roughly comparable. The degree of erosion observed in the pressed-and-sintered material appears to be greater than that produced by high-temperature water. This may be due in part to the conversion of some of the sintered


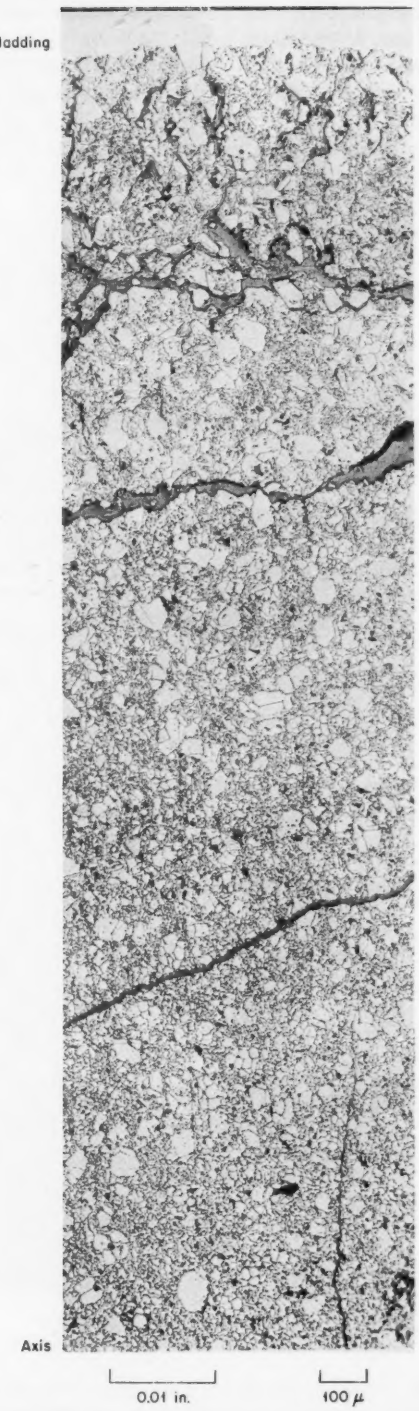


Fig. IV-4 Polished and etched, irradiated, swaged $UO_2$ + 1% $TiO_2$ powder[2] (−200 + 325 mesh and 89% dense). This specimen was exposed at a heat flux of 194,000 Btu/(hr)(sq ft).

$UO_2$ to unsintered $U_3O_8$ and $U_4O_9$ which results from steam oxidation.

These experiments indicate that, although some erosion is to be expected if a sizable rupture of the fuel jacket occurs, the effect is not likely to be catastrophic on a short-time basis, particularly in fuel that has undergone a reasonable degree of sintering.

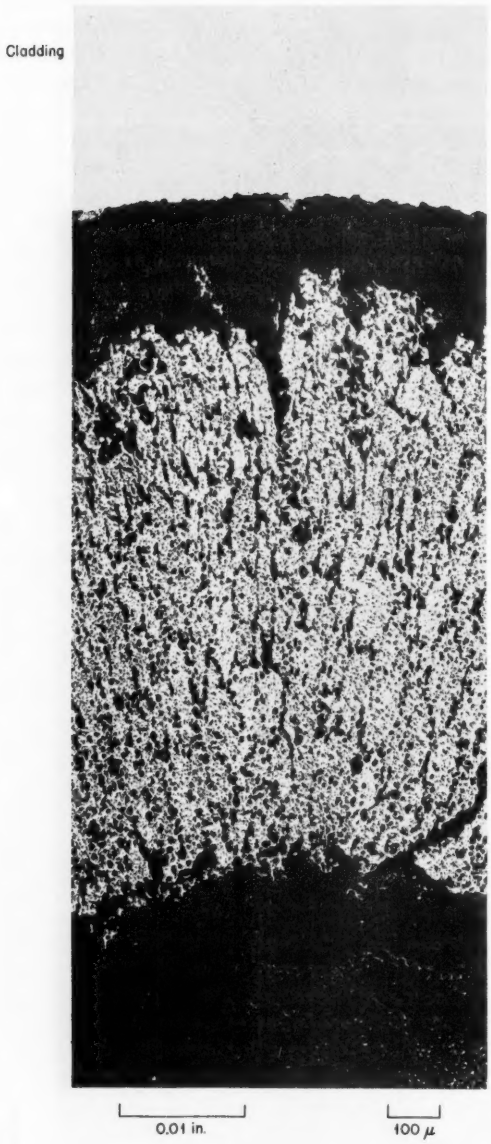


Fig. IV-5 Polished and etched, irradiated, vibratory-packed $UO_2$ powder[2] (−200 + 325 mesh and 53% dense). This specimen was exposed at a heat flux of 310,000 Btu/(hr)(sq ft).

The information gained from the investigations discussed and from others of a similar nature may be summarized as follows:

1. Packed-powder fuel of low preoperational density undergoes densification with attendant changes in the volume and location of the fuel when sintering and/or grain growth occurs during irradiation.
2. The behavior of packed-powder fuel of high preoperational density (approximately 90% of theoretical density) does not differ importantly, during irradiation, from that of pressed-and-sintered $UO_2$ if sintering and/or grain growth does occur.
3. When operating at elevated temperatures (above 1000°C), fused and ground $UO_2$ releases comparatively large quantities of surface-adsorbed gases.
4. High-temperature vacuum degassing prior to irradiation is effective in removing surface-adsorbed gases and moisture from $UO_2$ powder.
5. The erosion of packed $UO_2$ powder, which results from jacket-tube failures, is not expected to be a major disadvantage, particularly if the fuel has experienced extensive sintering or grain growth.

As a result of such conclusions, present and projected efforts in packed-powder technology have been directed toward attaining higher compacted densities and toward the establishment of effective gas-removal operations as part of the overall fabrication process.

Perhaps the most significant result of the packed-powder irradiations conducted to date is the evidence that high-bulk-density $UO_2$ fuel elements perform in much the same manner regardless of whether packed-powder techniques or pressed-and-sintered techniques are used in their fabrication. The mechanisms affecting grain growth in the $UO_2$ fuel as well as the effective thermal conductivity of the operating fuel elements appear to be relatively independent of the fabrication method. In-reactor sintering of packed-powder fuel occurs, to some degree, in that portion of the $UO_2$ operating at temperatures conducive to sintering. Moreover, there is evidence that sintering is produced at lower temperatures in-pile than out-of-pile, although the reasons are not yet understood. With respect to outgassing, packed-powder fuel exhibits a greater propensity to release gen-

erated fission-product gases and surface-adsorbed atmospheric gases than its pressed-and-sintered counterpart. However, for fuel operating at temperatures conducive to grain growth, the difference in fission-gas release appears to be negligible.

As a consequence of these findings, it appears possible to apply the data from packed-powder $UO_2$ irradiation programs to the behavior of $UO_2$ fuel in general rather than to only that produced by a particular fabrication technique. This change in emphasis has permitted better integration of packed-powder results with those of pressed-and-sintered programs. An illustration of the benefits attendant to this generalization of approach is the work being done to determine the effective thermal conductivity of operating $UO_2$ and to explain the observed $UO_2$ crystal-structure changes occurring during irradiation.

The operation of $UO_2$ fuel at high power levels and hence high central temperatures produces the characteristic structures shown in Figs. IV-10 and IV-11. The regions shown in Fig. IV-10 may be described as follows:[7] The centrally located void is formed by solidification shrinkage and/or the migration of porosity, from that portion of the $UO_2$ undergoing grain growth, up the thermal gradient to the thermal center of the fuel material. The hollow thermal center is surrounded by a region of heavily voided large columnar grains extending outward to a radius of about 0.3 cm. This region is followed by a relatively void-free ring of large columnar grains, extending to a radius of about 0.4 cm, and a ring of material containing small columnar grains and some

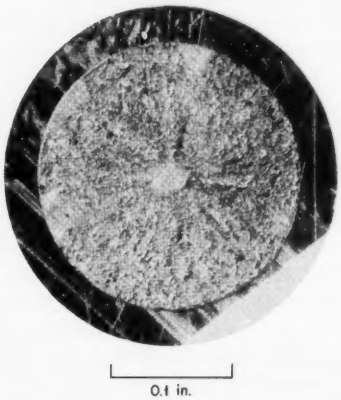


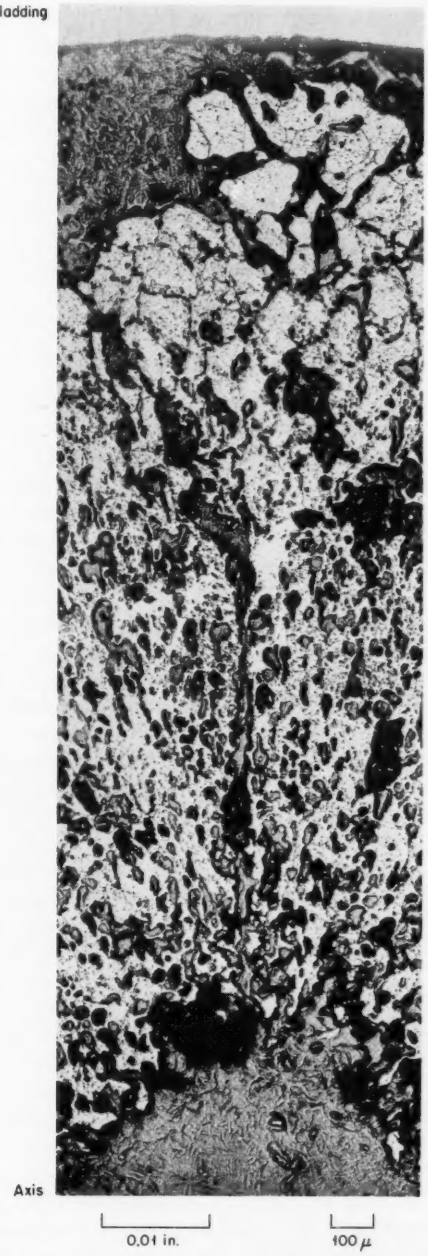


Fig. IV-6 Polished and irradiated, ceramic-grade $UO_2$ pellet[2] that was sintered at 1700°C for 3 hr (85% dense). This specimen was exposed at a heat flux of 225,000 Btu/(hr)(sq ft).

voids. The latter region extends to a radius 0.48 cm, which is considered to be the limit of grain growth in this specimen. The remaining annular ring of material retains the original sintered structure.

Figure IV-11 exhibits the same general arrangement and structure as Fig. IV-10, although the various regions may terminate at different radial distances; since Fig. IV-11 shows a packed-powder element, a ring of unsintered $UO_2$ can be found adjacent to the inner surface of the cladding. Until recently the consensus of the investigators was that the structures shown in Figs. IV-10 and IV-11 were all produced at temperatures below the melting point of $UO_2$.

Table IV-2 RESULTS[1] OF INTERNAL GAS ANALYSIS, MOLE PERCENT

| Test element | $CO_2$ | Ar | $O_2$ | $N_2$ | $H_2O$ | CO | $CH_4$ | He | $H_2$ | $Xe^{131}$ | $Kr^{84}$ |
|---|---|---|---|---|---|---|---|---|---|---|---|
| I-b | 0.66 | 0.02 | <0.01 | 15.5 | 0.86 | <0.01 | 0.04 | 0.30 | 63.4 | 17.8 | 2.23 |
| II-a | 54.6 | 0.25 | 0.08 | 1.15 | 0.10 | <0.01 | 0.07 | 33.2 | 2.43 | 7.33 | 0.91 |

It is generally considered[7] that the interface between the heavily voided and void-face regions of the large columnar grains is at a temperature of about 2400 to 2700°C and that the temperature at the interface between the large and small columnar grains is about 2100°C. The lower limit for grain growth is thought to be about 1500°C. Further substantiation for the no-melting viewpoint was the difference between the appearance of solidified, previously molten material, which is composed of large, porous, equiaxial grains typified by the central region shown in Fig. IV-2 and that of the heavily voided central regions shown in Figs. IV-10 and IV-11. However, a theory has now been advanced which considers that the central regions shown in Figs. IV-10 and IV-11 were operated in the molten state for a brief time early in their irradiation period.[8]

The new performance model is based upon the following considerations: First, it has been observed in laboratory demonstrations that the threshold temperature for porosity migration is in the range of 1800 to 2000°C and that the rate of migration up the thermal gradient increases with temperature. Second, the thermal conductivity of $UO_2$ operating below the grain-growth region is in the range of 1 to 1.5 Btu/(hr)(ft)(°F) and perhaps less in the case of unsintered packed-powder fuel. Third, as a consequence of both grain growth and temperature, the average effective thermal conductivity of high-rated $UO_2$ fuel is greater after an initial short period of irradiation than at the beginning of life.

Under these assumptions the highest temperatures exist at the beginning of irradiation, and thus the central portion of the $UO_2$ is in the molten state. This can be demonstrated, within experimental error, for a large number of specimens if a value of between 1 and 1.5 is assumed to be appropriate for the as-sintered or as-packed thermal conductivity. Enclosing the molten core is a thick ring of solid $UO_2$, and the temperatures experienced range from about 1500°C at the outermost limit of this ring to about 3000°C (the melting point of $UO_2$) at the molten core. The phenomenon of grain growth occurs throughout this region. The remainder of the fuel operates below the grain-growth temperature and, in the case of sintered fuel, retains its original structure. Packed-powder fuel, however, will undergo some sintering.

In this picture the final structure results from changes originating near the periphery of the fuel element and progressing inward. As a result of grain growth (and sintering in the case of packed-powder fuel), the average effective thermal conductivity of the element is markedly improved and solidification of the molten core begins. Concurrently, voids in the region experiencing grain growth begin to migrate rapidly up the thermal gradient and into the molten region and thus produce fuel densification and a continued improvement in the effective thermal conductivity of the element. This process proceeds, with steadily decreasing temperatures and a shrinking grain-growth region, until complete solidification of the molten core has occurred. The fuel is then frozen into the characteristic structure observed in postirradiation examinations except for minor changes resulting from cracks and the slow migration of voids toward the thermal center of the fuel.

The new model's greatest appeal lies in the convincing explanations it provides for the existence of a void-free region between two adjacent voided regions and for the varied types of grain-growth structures observed. These explanations are based upon the previously stated premise that the $UO_2$ experiences the highest internal temperatures at the beginning of life. Moreover, because of these temperatures and because the molten zone extends some distance outward from the center of fuel, the thermal gradient through the nonmolten fraction of the fuel operating above the grain-growth temperature is also the greatest at beginning of life.

From laboratory demonstrations it appears that the rate at which sublimation and condensation occur increases with temperature. Consequently, in fuel operating above the grain-growth temperature and in the presence of a steep thermal gradient, one would expect void migration to proceed slowly in the outermost reaches of the fuel undergoing grain growth but at a steadily increasing rate as the molten core is approached. Under these conditions voids are swept from the highest temperature region (the zone of essentially void-free large columnar grains) and into the molten core faster than they are contributed by the cooler outlying regions of small columnar grains. Upon solidification of the molten center, the porous, equiaxed grain structure is obtained and, if irradiation were terminated at this time, the typical structure of solidified $UO_2$ shown in Fig. IV-2 would be observed. However, if irradiation continues, the voids entrapped in the solidified melt begin to migrate toward the thermal center and produce the refined central structure shown in Figs. IV-10 and IV-11. It should be noted that these high temperatures and steep thermal gradients probably persist for only a relatively short period of time; otherwise the entrapment of voids in the solidified molten zone could not have occurred to the extent observed.

One can also use the theory of changing thermal conductivity, and hence internal temperatures, to explain the presence of small columnar grains and large columnar grains in the grain-growth region. If, as the theory proposes, the boundary of temperatures at the melting point and above recedes toward the center of fuel, it is likely that the boundary of grain-growth temperatures also recedes toward the center of the fuel. Predicated upon this assumption and the apparent effect of temperature upon the rate at which grain growth

Table IV-3 FUEL-ROD INTERNAL GAS ANALYSIS DATA[3]

| Rod No. | Quantity of gas,* $cm^3$ of gas at STP per gram of oxide | | | | | | Fractional release of fission gases,† % |
|---|---|---|---|---|---|---|---|
| | Total | $N_2$ | $O_2$ | $CO_2$ | Xe | Kr | |
| 428H | $1.5 \times 10^{-2}$ | $1.0 \times 10^{-2}$ | $6.5 \times 10^{-4}$ | $0.3 \times 10^{-2}$ | $0.6 \times 10^{-3}$ | $1.2 \times 10^{-4}$ | 1.7 |
| 431C | $5.8 \times 10^{-2}$ | $1.8 \times 10^{-2}$ | $0.32 \times 10^{-4}$ | $2.9 \times 10^{-2}$ | $10.2 \times 10^{-3}$ | $16 \times 10^{-4}$ | 13.7 |
| 428C | $5.2 \times 10^{-2}$ | $1.8 \times 10^{-2}$ | $2.4 \times 10^{-4}$ | $2.8 \times 10^{-2}$ | $4.4 \times 10^{-3}$ | $6.3 \times 10^{-4}$ | 6.6 |
| 431H | $5.4 \times 10^{-2}$ | $2.5 \times 10^{-2}$ | $33 \times 10^{-4}$ | $2.2 \times 10^{-2}$ | $3.2 \times 10^{-3}$ | $4.6 \times 10^{-4}$ | 5.2 |
| 428C‡ | $0.40 \times 10^{-2}$ | $0.30 \times 10^{-2}$ | $5.9 \times 10^{-4}$ | $0.030 \times 10^{-2}$ | $0.038 \times 10^{-3}$ | $0.12 \times 10^{-4}$ | |

*Also traces ($2.4 \times 10^{-4}$ maximum) of helium, argon, and hydrogen.
†"Released" Kr + Xe as a fraction of that produced by fission.
‡Repunched.

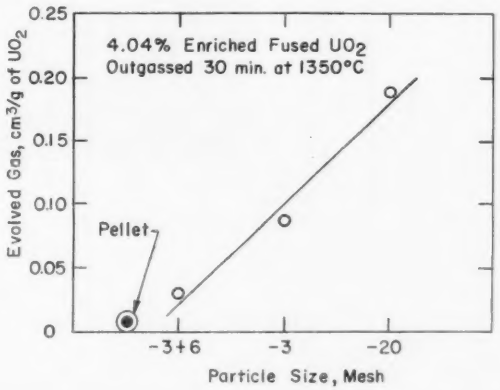


Fig. IV-7 Effect of particle size[6c] on amount of gas evolved from fused $UO_2$.

Table IV-4 COMPOSITION OF GASES EVOLVED FROM FURNACE-SINTERED $UO_2$ PELLETS WITH BINDER AND ARC-FUSED $UO_2$ POWDER[4a]

| Temp. | Type | Sample No. | Total gas* | $H_2$ | $O_2$ | $H_2O$ | $CO_2$ | CO | $N_2$ | Hydrocarbons | Accuracy |
|---|---|---|---|---|---|---|---|---|---|---|---|
| 400°C | | 5 | 1.64 | 0.48 | 0.02 | 0.06 | 0.51 | 0.32 | 0.15 | 0.05 | ±10% |
| 400 + 1500°C (15 min) (30 min) | | 3 | 6.89 | 2.70 | Trace | Trace | 0.49 | 2.47 | 1.05 | 0.29 | ±5% |
| 1700°C | Arc-fused powder after sintering | 25 | 149.3 | 51.7 | 0.12 | Trace | 16.8 | 74.2 | 4.3 | 3.0 | ±1% |
| 1700°C | Arc-fused powder after sintering | 26 | 158.2 | 19.9 | 0.6 | Trace | 6.1 | 101.4 | 10.8 | 1.6 | ±1% |

*Microliters of gas per gram of $UO_2$ at atmospheric pressure and 22°C.

Table IV-5 RESULTS OF PUNCTURE AND MOISTURE TESTS ON COMPACTED OXIDE* TUBES[6b]

| Tube No. | Fabrication history | | | | | Core weight, g | Core volume, $cm^3$ | Total gas release, $cm^3$ | Gas composition, vol.% | | | | | | | | Moisture, ppm |
|---|---|---|---|---|---|---|---|---|---|---|---|---|---|---|---|---|---|
| | Vacuum outgassed | Vibratory compaction | Swaged | Dried | Autoclaved† | | | | $H_2$ | He | $N_2$ | $O_2$ | A | Co | $CO_2$ | $CH_4$ | |
| Z-169B | No | Yes | No | No | No | 5940 | 96 | 154 | 41 | 50.4 | 0.63 | 0.09 | 7.93 | | 0.03 | | 10 to 30 |
| Z-166B | No | Yes | No | No | Yes | 5620 | 102 | 645 | 75.4 | 10.1 | 4.56 | 0.05 | 0.84 | | 0.27 | 8.83 | nd |
| Z-168B | No | Yes | No | No | Yes | 5660 | 98 | 236 | 14.5 | 35.5 | 12.0 | 0.08 | 3.04 | 0.65 | 0.16 | 34.1 | 30 |
| Z-165A‡ | No | Yes | No | No | Yes | 5880 | 85 | 184 | | 38.8 | 0.06 | 0.06 | 7.32 | | 0.01 | 53.8 | nd |
| Z-204A | No | Yes | Yes | Yes | No | 5810 | 53 | 33 | 0.42 | 95.8 | 0.85 | 0.29 | 2.64 | | 0.02 | | 9 to 12 |
| Z-205D | No | Yes | Yes | Yes | Yes | 5860 | 55 | 123 | 0.55 | 48.0 | 28.6 | 0.12 | 2.04 | | 0.03 | 20.6 | 7 to 13 |

*Arc-fused $UO_2$ with following composition: oxygen/uranium, 2.01; carbon, 50 ppm; nitrogen, 70 to 140 ppm.
†Autoclaved in steam for three days at 750°F.
‡Autoclaved eight months after loading and sealing.

occurs, changes in that portion of the fuel residing at the outer limit of the grain-growth region could be expected to proceed slowly and to persist for only a relatively short time. The small columnar grain region may then be described as an incipient or incomplete zone of grain growth in which the initial rate of void migration was less than the rate at which the grain-growth temperature boundary receded toward the center of fuel.

Reasoning similar to that used above was applied to obtain an estimate[7] of the operating thermal conductivity of $UO_2$ [see *Power Reactor Technology*, 6(1)] which is more representative of actual operating experience. Early curves of the thermal conductivity of $UO_2$ indicated that conductivity decreased with increasing temperature until it approached a relatively constant value of between 1 and 1.5 Btu/(hr)(ft)(°F) at about 1200°C. Most of the data used to develop these curves were obtained by the postirradiation examination of small fuel specimens whose operating temperatures were largely unknown. The latest estimate is also based upon postirradiation examinations but, unlike its predecessor, benefits from a better knowledge of the operating temperatures which results from the improved understanding of temperature-induced grain growth. The new estimate retains the thermal-conductivity values of the early curves below about 1200°C but predicts that at about 1600°C the effective conductivity of $UO_2$ begins to increase with temperature, rising to a value of about 4.9 Btu/(hr)(ft)(°F) at the melting point. This increase in effective conductivity is attributed to improved radiative heat transfer, probably associated with grain growth. It is also probable that conductive heat transfer is improved as a result of grain growth, if for no other reason than the observed densification.

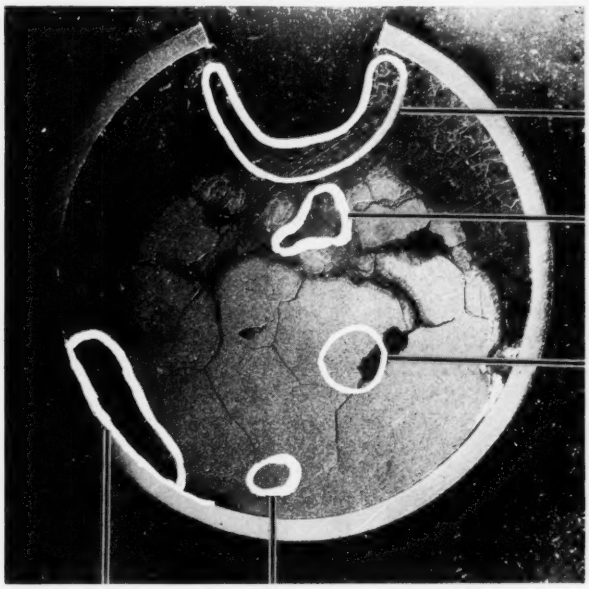


| Sampled Area | Results Of X-Ray Diffraction Studies |
|---|---|
| 1 | $U_3O_8$ |
| 2 | $U_3O_8$ |
| 3 | $UO_2$ |
| 4 | $UO_2$ |
| 5 | $U_3O_8$ |

No Other Phases Detected

Fig. IV-8 Cross section of a pellet-filled specimen[4a] exposed in flowing steam for 1000 hr.

Support for the new estimate is based upon considerations similar to those described below.

Since grain growth is considered to begin at about 1500°C, at some time during irradiation this temperature existed at a point about 0.48 cm out on the radius of the specimen shown in Fig. IV-10. If a surface temperature of about 850°F is assumed for the given heat flux of 230 watts/cm$^2$ [approximately 730,000 Btu/(hr)(sq ft)], the following simple equation can be used to solve for the approximate average effective thermal conductivity of the $UO_2$ which would permit grain growth at the observed radial location:

$$T_r = T_s + \frac{q''}{12kD}(b^2 - r^2)$$

If the neutron-flux depression in the fuel is neglected,

$T_r$ = temperature at fuel radius of interest (°F)
$T_s$ = temperature at fuel surface (°F)
$k$ = thermal conductivity [Btu/(hr)(ft)(°F)]
$q''$ = volumetric heat generation [Btu/(hr)(cu ft)]
$b$ = fuel radius (in.)
$r$ = fuel radius at point of interest (in.)
$D$ = fuel diameter (in.)

When the values for heat flux, temperature, and radial position cited previously are used, the fuel in the fuel rod shown in Fig. IV-10 must exhibit a thermal conductivity of about 1.6 Btu/(hr)(ft)(°F) to produce the observed extent

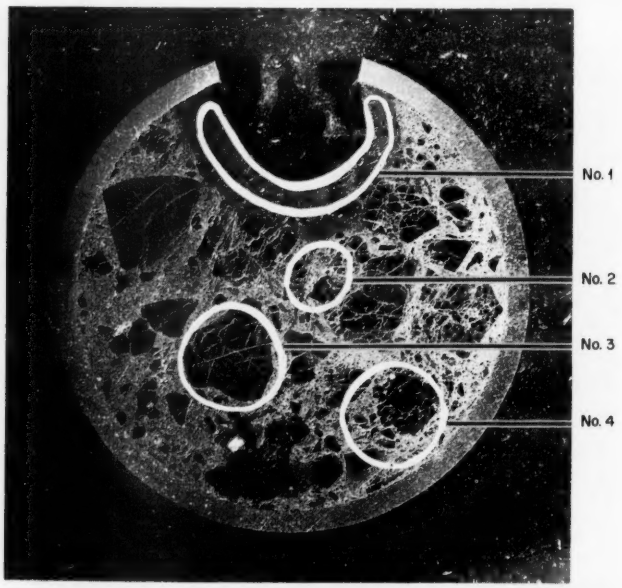


| Sampled Area | Results Of X-Ray Diffraction Studies |
|---|---|
| 1 | $U_3O_8$ - No Other Phases Detected |
| 2 | $UO_2$ - Major Phase<br>$U_3O_8$ - Minor Phase, Very Weak |
| 3 | $UO_2$ - Major Phase<br>- No Minor Phases Detected |
| 4 | $UO_2$ - Major Phase<br>- No Minor Phases Detected |

Fig. IV-9 Cross section of a powder-filled specimen[4a] exposed in flowing steam for 1000 hr.

of grain growth. However, re-solving the equation to determine the minimum average thermal conductivity necessary to attain a center temperature just below the melting point yields a value of about 1.8 Btu/(hr)(ft)(°F). It is unlikely that two related regions in the same cross-sectional plane of the element, both containing the same as-fabricated fuel, can have thermal conductivities differing to this extent. One must therefore conclude, in light of the observed grain growth, that either the center of the fuel was molten during its entire irradiation period or that the thermal conductivity of at least the central region of the element was improved during the course of irradiation. In view of the dissimilarity between the structure of molten $UO_2$ that has not been subjected to postsolidification irradiation and that shown in Fig. IV-10, the center of Fig. IV-10 does not appear to be molten at the end of irradiation, although it could have been at some time earlier in life. One is therefore left with the conclusion that the average thermal conductivity of the element was higher at the end of irradiation than at the beginning.

A further indication of improved high-temperature thermal conductivity may be obtained from the specimen shown in Fig. IV-2. The

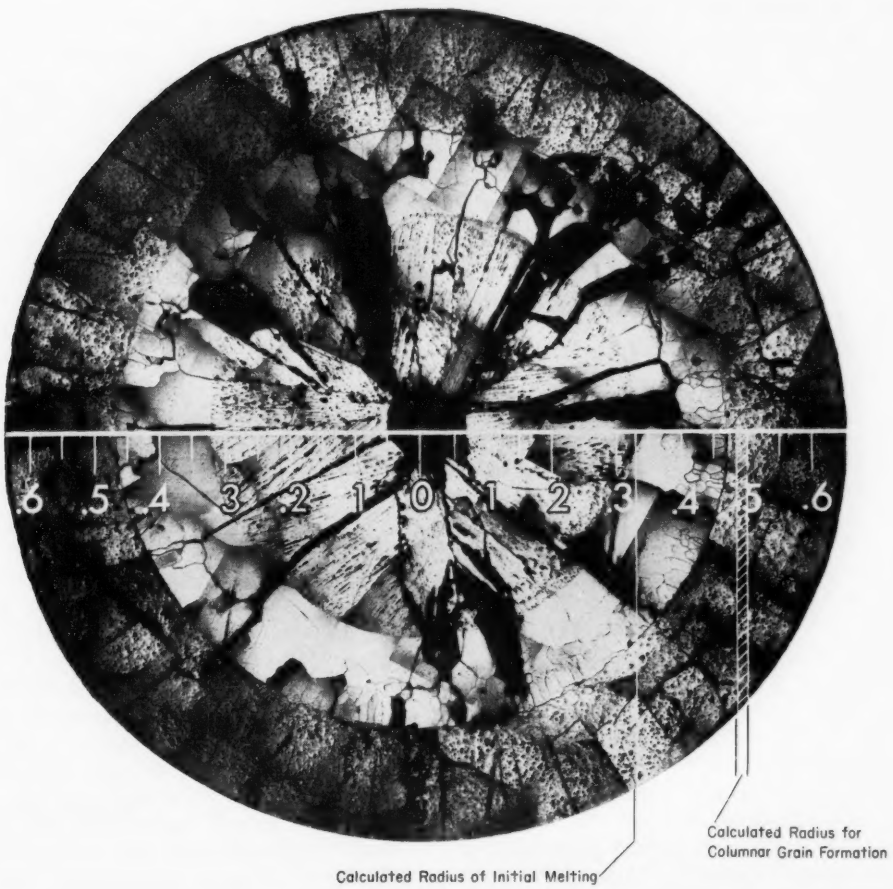


Fig. IV-10 Microstructure of a 1.28-cm-diameter sintered-pellet $UO_2$ fuel rod[7] after 12.3 days of irradiation. Surface heat flux = 235 watts/cm$^2$ (scale across pellet gives radius in centimeters).

sample was operated at a surface heat flux of $1 \times 10^6$ Btu/(hr)(sq ft); the surface temperature is assumed to have been about 600°F. The radius of the molten zone is estimated from the figure as 0.15 in., on the basis of the 0.970-in. diameter of $UO_2$ specified in the reference. If these values and the previously described equation are used, an average effective thermal conductivity of more than 4 Btu/(hr)(ft)(°F) for the nonmolten fraction of $UO_2$ is necessary to limit the molten radius to that observed. It should be noted that the errors possible in the assumed fuel surface temperature and the estimated radius of the molten zone will not affect this result importantly.

## Low-Temperature Sintering of $UO_2$

Results obtained by early investigators indicate that a $UO_2$-pellet fabrication process based on low-temperature (1300°C or lower) sintering in an inert atmosphere would be technically feasible and could have a significant economic advantage over the conventional high-temperature (1600 to 1700°C) sintering process in a hydrogen atmosphere. Reference 9 is the final report on the development of such a low-temperature sintering process. This work was sponsored under the AEC Fuel Cycle Develop-

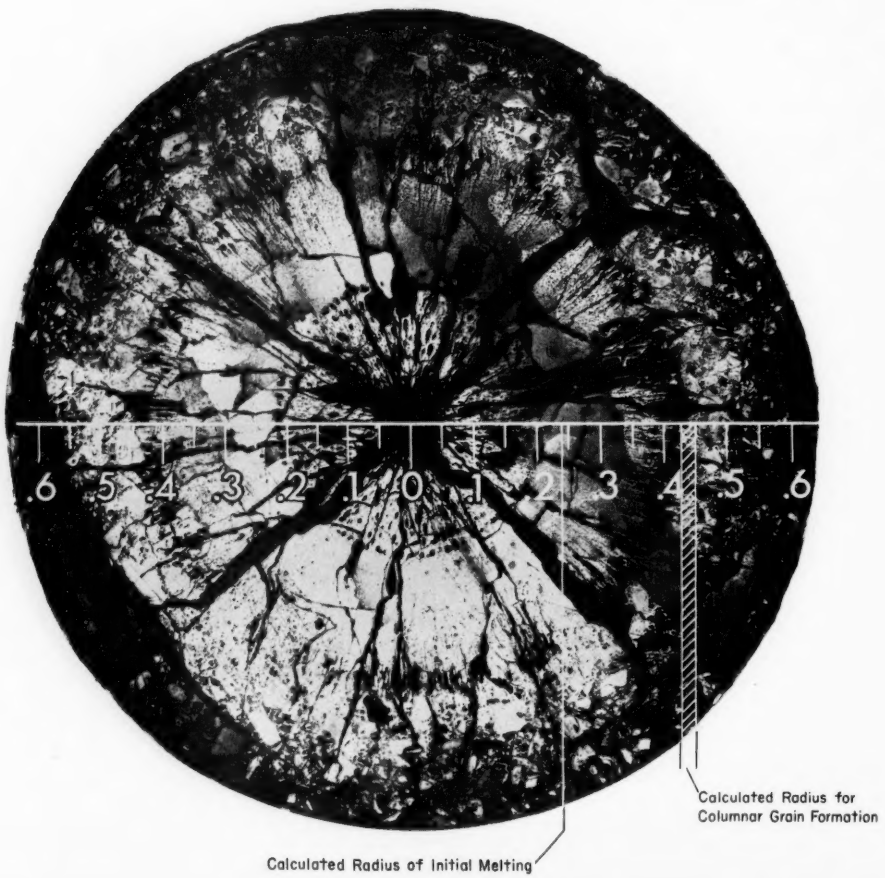


Fig. IV-11 Microstructure of a 1.28-cm-diameter swaged $UO_2$ fuel rod[7] after 12.3 days of irradiation. Surface heat flux = 195 watts/cm$^2$ (scale across pellet gives radius in centimeters).

ment Program and was performed by the Fuels Division of United Nuclear Corporation during the period Apr. 15, 1959, to Dec. 31, 1961. The reference is concerned only with the process-development phase of the program; radiation behavior of $UO_2$ pellets prepared by the process developed will be the subject of a subsequent report to be issued upon completion of irradiation testing, which was already under way at the time the current report was issued.

A near-optimum low-temperature two-stage sintering process for the fabrication of $UO_2$ pellets was developed. A comparison of the estimated cost of preparing oxide pellets by the process developed with that of the conventional high-temperature hydrogen process is presented in the reference, and a potential cost saving of about \$0.86/lb of $UO_2$ product is indicated. This saving occurs mainly in the lower acquisition and maintenance costs of the furnaces and accessories for the lower temperature process. Such a saving would represent a significant fraction of the normal cost of preparing sintered $UO_2$ pellets, which is about \$5 to \$6/lb. The total fabrication cost of $UO_2$ pellet type fuel is currently in the range from about \$40 to \$60/lb.

The low-temperature process developed consists basically of (1) pretreatment of commercial ceramic-grade (ADU) uranium oxide, (2) granulation and pressing, and (3) a two-stage sintering operation. The pretreatment operation consists of one or more cycles of oxidation reduction to activate the oxide and a final air-roasting operation to introduce the excess oxygen that was found to be essential for low-temperature sintering. Repetition of the oxidation-reduction activation cycle up to some optimum number (which was indicated to be about three cycles) was found to be effective in increasing the density of the sintered $UO_2$ product obtained. The investigation showed that oxidation-reduction cycling removes fluoride impurities which inhibit sintering and which may have other detrimental effects such as chemical reaction with the metal cladding of the fuel element. Results of this study suggest that the enhancement of sinterability by oxidation-reduction pretreatment may involve, in addition to the removal of inhibiting impurities in general, an increase of the surface area of the $UO_2$ particles.

After granulation and pressing into green compacts by the usual techniques, the pellets are sintered in a two-stage operation. The first stage consists of sintering in a nitrogen atmosphere at 1100 to 1300°C. The second stage consists of a relatively short exposure of about 1 hr to a hydrogen atmosphere, also at 1100 to 1300°C. This second stage removes the excess oxygen required for the low-temperature sintering and produces the stoichiometric $UO_2$ pellets required for satisfactory performance as a reactor fuel.

In addition to the potential economic advantages, the results persented in the reference are also of interest because they indicate that, by the utilization of several cycles of the pretreatment oxidation-reduction, it is possible consistently to produce $UO_2$ pellets with densities greater than 95% and up to 98% of theoretical density.

Reference 10, which was originally issued as a classified report on Dec. 5, 1960, has recently been released for distribution on an unrestricted basis. The report is mentioned here because it provides a good summary of most of the methods for $UO_2$ powder processing, forming and sintering of $UO_2$, machining of $UO_2$ shapes, and preparation of dense $UO_2$ fuel particles developed up to 1960. Many, if not most, of these methods are still being used.

## Uranium Carbide as a Nuclear Reactor Fuel

Although uranium carbide has been considered as a possible fuel material much earlier, intensive research on the material was started only about three or four years ago. Interest in this material was stimulated at that time by indications that it would offer attractive performance advantages for certain types of reactors. Uranium carbide is of particular interest because of its high thermal conductivity, high uranium density, high melting point, and temperature stability. Liquid-metal and organic-cooled reactors would be particularly attractive applications for the carbide: the former because carbide fuel could match the heat-transfer capability of metal coolants without the extremely fine subdivision of the fuel which is necessary with $UO_2$ in order to avoid excessive central temperatures; the latter because the more massive fuel elements possible with the carbide would give a welcome improvement in

neutron economy. The problems associated with the use of uranium carbide as a reactor fuel material in those coolants with which it is compatible are primarily (1) the lack of development of methods of preparation and fabrication and (2) a general lack of information on the effects of irradiation on the material.

The Third AEC Uranium Carbide Meeting[11] was held at Oak Ridge National Laboratory on Dec. 1 and 2, 1960. Representatives from France, Germany, and the United Kingdom Atomic Energy Authority (UKAEA) participated in this meeting.

On Apr. 4, 1961, the AEC conducted an unclassified symposium on the use of uranium carbides as reactor fuel materials.[12] The principal purpose of this symposium was to acquaint industry and other interested parties with the research being conducted by the AEC to develop uranium monocarbide and uranium dicarbide as fuel materials for nuclear reactors.

As a result of the Fourth Plansee Seminar on Powder Metallurgy in Nuclear Engineering, held at Reutte, Tyrol, Austria, in June 1961, a bibliography of 209 references, most with appended abstracts, on uranium carbides was issued.[13]

Recent efforts on developing uranium carbides for use as a fuel material for nuclear reactors can generally be divided into two categories: (1) their preparation and fabrication and (2) their irradiation behavior. Two methods of fabrication have been proposed: (1) casting and (2) powder metallurgy. Both of these methods are being investigated by the United Nuclear Corporation Fuels Division Research Laboratory at New Haven, Conn. (formerly the Metallurgical Laboratories of Olin Mathieson Chemical Corporation). The results of this work are presented in a first[14] and second[15] annual report, each entitled "The Development of Uranium Carbide as a Nuclear Fuel." The third annual report in this series should, presumably, be forthcoming in the near future.

After establishing methods for producing uranium carbide materials by consistent methods and with controlled composition, this group has started to determine the effect of compositional and fabricational variables on the properties of uranium carbides. This includes its compatibility with other materials, especially potential cladding metals, and the effects of irradiation.

Another program to investigate the properties of uranium carbides, particularly the effects of irradiation, is being pursued by Atomics International.[16] From the results obtained to date, this group has concluded that, "fission gas release or diametral increase of fuel do not represent limitations on the use of U-C fuel elements, under presently conceived Na-cooled reactor conditions."

The UKAEA is also investigating the application of uranium carbides as reactor fuels. They have shown[17] that about 85% of the irradiation damage to uranium carbide is annealed out at temperatures of about 640°C and that essentially all the damage is annealed out at about 700°C. Reference 18 summarizes the results obtained to date at the United Kingdom's Atomic Energy Research Establishment on the oxidation behavior of uranium monocarbide. This includes the behavior of sintered and cast material in various gases, including $CO_2$, CO, and steam, at temperatures within the range 150 to 1000°C.

Fuels based on uranium carbide appear to be particularly attractive for use in fast reactors because of the relatively high thermal conductivity of the material. Since any fast-reactor fuel system of importance must provide for the use of plutonium, it would be desirable to use a mixture of PuC-UC in such reactors. The UKAEA is sponsoring work to investigate several alternate ways of obtaining such a material. Probably the simplest method is to form a solid solution of these compounds by "chemical" methods such as arc-melting a mixture of the carbides. Reference 19 presents observations on the sintering behavior of such a 15% solid solution of plutonium carbide in uranium carbide. An alternate method of producing such a material is to blend the desired fraction of PuC with uranium and graphite powder and then to sinter the mixture. Reference 20 presents the results of an investigation of this method of preparation.

## Flat-Plate Ceramic Fuel Elements

Reference 21 describes the development of a process for fabricating thin, flat plates of urania potentially suitable for use in fuel elements. The process developed calls for rolling a mixture of $UO_2$ powder and organic binder

into a thin strip from which pieces of the desired shape are punched or cut and then sintering to a density up to 90 to 97% of theoretical. Present equipment permits the production of pieces up to $3 \times 6$ in. and from 0.02 to 0.06 in. thick. These dimension ranges could apparently be extended if necessary, by the application of other equipment, with the possible exception of reductions of thickness; the current lower limit appears to be about the minimum thickness practical for handling purposes. Similar pieces of 90% $ThO_2$–10% $UO_2$ were also prepared successfully. The next problem to be attacked in this development is that of cladding the plates and incorporating them into a fuel-element structure. Cooperative work with Battelle Memorial Institute on pressure bonding of such ceramic strips into metal sheaths is being initiated.

## References


1. J. L. Bates and W. E. Roake, Irradiation of Fuel Elements Containing $UO_2$ Powder, USAEC Report HW-60578, General Electric Company, Hanford Atomic Products Operation, June 15, 1959.
2. F. A. Brandt, T. J. Slosek, and B. Weidenbaum, Irradiation and Examination of $UO_2$ High Burnup Program Fuel Elements, USAEC Report GEAP-3108(Pt. 3), General Electric Company, Vallecitos Atomic Laboratory, Jan. 15, 1962.
3. G. R. Cole, Preliminary Irradiation of Fused $UO_2$, USAEC Report DP-662, Savannah River Laboratory, January 1962.
4. Meeting on Characterization of Uranium Dioxide, Held at Oak Ridge National Laboratory, December 12 and 13, 1961, USAEC Report TID-7637, Oct. 1, 1962:
   *a.* C. N. Spalaris and W. R. Raymont, Gaseous and Trace Impurities in $UO_2$. Their Effect on Fuel Element Performance in Superheated Steam Applications.
   *b.* G. R. Cole, Volatile and Nonvolatile Impurities in Fused $UO_2$.
   *c.* R. H. Gale, G. S. Golden, and G. Zuromsky, Thermally Activated Gas Release from Fused $UO_2$.
5. R. C. Daniel, M. L. Bleiberg, H. B. Meieran, and W. Yeniscavich, Effects of High Burnup on Zircaloy-Clad Bulk $UO_2$, Plate Fuel Element Samples, USAEC Report WAPD-263, Westinghouse Electric Corp., Bettis Atomic Power Laboratory, September 1962.
6. Combustion Engineering, Inc., Symposium on Powder Packed Uranium Dioxide Fuel Elements, November 30–December 1, 1961, USAEC Report CEND-153:
   *a.* G. R. Caskey, Jr., G. R. Cole, and W. G. Holmes, Failures of $UO_2$ Fuel Tubes by Internal Hydriding of Zircaloy-2 Sheaths.
   *b.* W. G. Holmes, Control of Hydrogen in the Fabrication of Tubular $UO_2$ Fuel Elements.
   *c.* J. W. Lingafelter, The Performance Evaluation of Compacted Powder $UO_2$ Fuel Rods.
   *d.* E. A. Evans, Irradiation Testing of Powder-Containing Fuel Elements.
7. W. E. Roake, Irradiation Alteration of Uranium Dioxide, USAEC Report HW-73072, General Electric Company, Hanford Atomic Products Operation, March 1962.
8. W. A. Snyder and J. E. Brown (Eds.), Research and Development Programs Executed for the Division of Reactor Development, Quarterly Progress Report, April–June 1962, USAEC Report HW-74761, General Electric Company, Hanford Atomic Products Operation, Nov. 15, 1962.
9. N. Fuhrman, L. D. Hower, Jr., and R. B. Holden, Low Temperature Sintering of Uranium Dioxide. Final Report on Process Development, April 15, 1959–December 31, 1961, USAEC Report UNC-3006, United Nuclear Corporation, Mar. 1, 1962.
10. D. W. Brite and R. J. Anicetti, Uranium Dioxide Fabrication, USAEC Report HW-64684, General Electric Company, Hanford Atomic Products Operation, Dec. 5, 1960.
11. Proceedings of the Uranium Carbide Meeting Held at Oak Ridge National Laboratory, Oak Ridge, Tennessee, December 1–2, 1960, USAEC Report TID-7603.
12. Proceedings of the Symposium on Uranium Carbides as Reactor Fuel Materials Held at Atomic Energy Commission Headquarters Building, Germantown, Maryland, April 4, 1961, USAEC Report TID-7614.
13. H. H. Hausner and H. C. Friedemann, Bibliography on Uranium Carbides, Report NP-11407, 1961.
14. H. S. Kalish, F. B. Litton, F. E. Bowman, J. Crane, and W. C. Hahn, The Development of Uranium Carbide as a Nuclear Fuel, Annual Report No. 1 [for] May 1, 1959, to April 30, 1960, USAEC Report NYO-2688, Olin Mathieson Chemical Corporation, June 13, 1960.
15. H. S. Kalish, F. B. Litton, J. Crane, and M. L. Kohn, The Development of Uranium Carbide as a Nuclear Fuel, Second Annual Report (Phase 2), May 1, 1960–August 31, 1961, USAEC Report NYO-2694, United Nuclear Corporation, Nov. 30, 1961.
16. D. I. Sinizer, B. A. Webb, and S. Berger, Irradiation Behavior of Uranium Carbide Fuels, USAEC Report NAA-SR-7248, Atomics International, Aug. 15, 1962.
17. M. D. Rogers and J. Adam, Radiation Damage and Its Thermal Recovery in Uranium Monocarbide and Uranium Mononitride, British Report AERE-R-4046, June 1962.
18. J. E. Antill and K. A. Peakall, Oxidation of

Uranium Monocarbide, British Report AERE-M-1100, August 1962.

19. J. D. L. Harrison, W. G. Roberts, and L. E. Russell, Observations on the Sintering Behaviour of Uranium Carbide and 15 Per Cent Plutonium–85 Per Cent Uranium Carbide, British Report AERE-R-4151.
20. M. C. Regan and J. W. Isaacs, The Effect of Additions (UC, $UC_2$, PuC) on the Reaction Sintering Behaviour of Compacted U + C Powders, British Report AERE-R-4153, September 1962.
21. J. J. Fargo, Summary Report on Development of Flat Plate Ceramic Fuel Elements, USAEC Report TID-15373, Aug. 28, 1961.

Section

V

Power Reactor Technology

# Materials

## Zirconium and Zircaloy

In view of the rapid rate of expansion of zirconium-alloy technology, the standard books on the subject have aged rapidly, and current reviews of the literature and data compilations are especially valuable. The United Kingdom Atomic Energy Authority has released a Zirconium Data Manual,[1] the tenth in a series of manuals covering uranium, thorium, niobium, vanadium, beryllium, plutonium, aluminum, magnesium, and uranium ceramics. Data were compiled from 81 references under the general headings of: Physical Properties, Mechanical Properties, Chemical Properties (including compatibility and corrosion), and The Effects of Irradiation. The information is briefly and conveniently presented in tabular form or as curves.

An Oak Ridge study[2] to determine the feasibility of replacing the N.S. *Savannah* stainless-steel fuel-element containers with Zircaloy-2 or Zircaloy-4 has resulted in the compilation of data of general interest to those using zirconium alloys. The fuel-element containers (about 9 in. square) make up the permanent core structure of the *Savannah* reactor. The study covers the same topics as the British manual, but critical evaluations and discussion are included. Seventy-six references are cited. Both compilations include quite recent information, but important questions such as the degree to which corrosion rates are increased by irradiation (given by Ref. 2 as less than a factor of 5) and the limiting amount of hydrogen that can be safely absorbed in Zircaloy remain unresolved. In regard to the second question, Whitmarsh[2] suggests 500 ppm as an upper limit for Zircaloy-2 and calculates, on the basis of stated assumptions, a 150-ppm hydrogen content for a 125-mil Zircaloy-4 plate after 30 years of exposure to N.S. *Savannah* conditions. A 400-ppm hydrogen content for a 125-mil Zircaloy-2 sheet was calculated for the same time and conditions.

In addition to hydrogen absorption and the deterioration of materials as a result of corrosion, a third major consideration in the broad corrosion problem is that of the control of the formation of what is commonly called crud. The control of *p*H by means of lithium hydroxide offers a method of limiting the formation of this inconvenient corrosion product. Since LiOH might have serious side effects, particularly when used in the concentrations necessary for the higher alkalinities, an investigation was made at Westinghouse[3] of the effects of LiOH on corrosion rates. Zircaloy-2, "nickel-free" (0.005% nickel) Zircaloy-2, and Zircaloy-4 were investigated in autoclaves, replenished autoclaves, and in two loops. The autoclave temperatures were 680°F, and the loops operated at 615°F. A wide range of LiOH concentrations was covered. No significant differences in behavior of the three alloys were found, and it was concluded that with these alloys no accelerated corrosion or increased hydrogen absorption took place at a *p*H below 11.3. Crud control with LiOH is then indicated to be feasible. However, the warning should be noted that, if crevices exist in the Zircaloy parts of the core, concentration of the LiOH may occur in them which might result in heavy corrosive attack if the *p*H exceeded 13.

Investigations of LiOH at Knolls Atomic Power Laboratory[4] have revealed that such crevice corrosion did occur under nucleate-boiling conditions in 587°F water. Considerably greater hydrogen absorption was found in LiOH solutions in these experiments than was reported in the Westinghouse study.

Although hydrogen is important in any wrought zirconium in the core, it could well be even

more important in the weld metal joining zirconium parts, particularly as it affects fatigue. Fatigue tests at Knolls[5] at 400 and 600°F on specimens machined from weld metal showed that hydrogen contents up to 500 ppm had little effect on fatigue behavior at these temperatures.

Programs for the development of zirconium alloys with improved corrosion resistance to steam and water at temperatures higher than those presently employed are under way at several laboratories. The 15th paper in a series covering such a program at Harwell describes work on niobium-zirconium ternary alloys containing such elements as tin, copper, tungsten, and molybdenum.[6] Niobium was selected as the basic addition element for this set of alloys because it is the only element of sufficiently low cross section which has a relatively high solubility in zirconium. The higher content niobium alloys (20 to 60 wt.%) were found to be subject to cracking and pitting, but, at contents of 5 wt.% and below, resistant alloys were developed. The corrosion properties were sensitive to heat-treatment and cold working. Of the heat-treatments, a 24-hr anneal at 585°C was found optimum for resistance to 400°C steam in a 200-day test. For resistance to steam at 300 to 500°C, copper and iron at the 1 wt.% level were found to be the most beneficial alloying additions to a base that consisted of 1% niobium–balance zirconium. Several alloys showed considerably lower rates of hydrogen uptake than Zircaloy-2.

One of the alloys studied at Harwell (2½% niobium–balance zirconium) is of the same nominal composition as one intensively investigated at Chalk River[7] for use in pressure tubes. The major requirement for the alloy was strength; this permitted the reduction of the tube-wall thickness below that possible with Zircaloy-2 and thereby reduced total neutron absorption. Corrosion resistance is less important in this application since the use temperatures are relatively low. Specimens, heat-treated at 880°C, were quenched and then tempered at 500°C. The effects of irradiation exposures of $1.3 \times 10^{20}$ neutrons/cm$^2$ (>500 ev) at 50°C and of $1.0 \times 10^{20}$ neutrons/cm$^2$ (>500 ev) at 250°C were investigated. No metallurgical instability of the alloy was found after these exposures. The strength at 300°C was 50% higher than that of Zircaloy-2. The higher temperature irradiation resulted in a decrease from 14.2 to 13.3% in total elongation for a 300°C temperature test, and the total elongation of the irradiated specimen was 10.5% at room temperature. The effects on impact behavior were comparatively small, and the alloy was quite superior in this regard to Zircaloy-2.

# Materials for Reactor Control

The recently published book *Neutron Absorber Materials for Reactor Control*[8] is the eleventh technical book published under the sponsorship of the Naval Reactors Branch of AEC. It gives comprehensive, up-to-date treatment of the control materials applicable to water-moderated reactors, and it contains, in addition, a large amount of information of more general applicability. The first two chapters of the book give a general survey of the applications of control materials to power reactors and treat the neutron physics of these applications in thermal reactors. This portion of the book is reviewed separately in Sec. II of this issue of *Power Reactor Technology*. Chapters 3 to 6 treat the various control materials under the headings: Hafnium, Boron Materials, Silver and Silver-Base Alloys, and The Lanthanons. The last three chapters treat specific applications of the materials, including fabrication, under the headings: Control Rods; Unshielded Burnable Poison Materials; and Discrete, Self-Shielded, Burnable Poison Elements.

Several recent reports have given new information on specific control materials and their applications. These are reviewed briefly below.

From the points of view of economics and control effectiveness, boron is one of the most attractive control materials, and borated stainless steels are widely used in power reactors despite the difficulties encountered with embrittlement and helium formation. The embrittlement usually found when boron or its compounds are dispersed in stainless steel can be attributed in large part to the fact that such cermets must be sintered at relatively high temperatures. This usually causes an alloy-boron reaction, and in any case it initiates diffusion of the boron through the matrix metal. One approach that should avoid such interactions has been investigated by General Electric.[9] The method investigated consists of the

codeposition of nickel and boron carbide by an electrolytic technique at aqueous-solution temperatures. The codeposition technique is a proprietary process of Platecraft of America, Inc.; therefore little detail on the actual plating method is available. Plates of 30 vol.% $B_4C$ in nickel which were $\frac{1}{16}$ in. thick were produced by this Company. Thicknesses as great as $\frac{1}{4}$ in. and volume percentages of 40% appear to be possible. Testing at General Electric consisted of determining the corrosion resistance of such plates and of investigating their thermal and radiation stability.

The thermal stability of nickel-$B_4C$ was determined by holding cold-pressed compacts of 26.7 vol.% $B_4C$ at 1000, 800, 600, and 375°C in vacuum. X-ray diffraction was used to determine the presence or absence of nickel borides in the exposed coupons. At 600°C, 29% of the boron had reacted with the nickel in 50 hr, and interactions were much faster at the higher temperatures. At 375°C (706°F), however, no reaction was found in 800 hr; therefore the material can be considered for use in water reactors.

Corrosion behavior was determined in a dynamic loop in 546°F, 1000-psi steam moving at a velocity of 20 ft/sec. One of the test coupons consisted of a type 304 stainless-steel base that was plated on both sides with 27 vol.% $B_4C$ in nickel. The other coupon was similar, but the exposed surface was coated with 2 mils of nickel. Metallographic examination showed good corrosion resistance for these coupons, and further tests are in progress.

Twelve specimens (six coated with nickel and six bare) were exposed at surface temperatures of 170 to 210°C to burnups of 92 to 97% of the $B^{10}$ atoms. Integrated thermal-neutron fluxes were calculated from cobalt and aluminum monitors to be from 1.81 to $2.01 \times 10^{24}$. Helium release averaged 12% from these samples, and little difference was shown between the bare and clad (2 mils of nickel) surfaces. Small blisters (75 mils in diameter) were found in 3 of the 12 specimens. Mechanical tests were not performed on the exposed specimens, but there was some evidence that excessive embrittlement had not occurred.

Reference 10 treats the use of boron in control rods for the High-Temperature Gas-Cooled Reactor (HTGR). This reactor employs graphite control rods that are intended to contain 20 to 40 wt.% boron. Investigation has shown[10] that graphite-$B_4C$ compacts containing up to 45 wt.% boron could be made. Crushing strength of these compacts was optimum in the 10 to 30 wt.% range. Exposures of the compacts to 100% of the HTGR design exposure [$9.8 \times 10^{20}$ nvt (fast)] at temperatures from 330 to 780°C resulted in some strengthening of the 20 wt.% boron specimens and no significant changes in the other compositions. Diametral changes in the exposed cylindrical specimens were small, but the lengths increased up to 4%, depending on exposure. Gas-release behavior was not reported.

Hafnium, an extremely attractive control-rod material, has had its use restricted almost entirely to military reactors. The metal may become more generally available as present production contracts end, and information on the behavior of hafnium control rods may be of correspondingly greater interest. Westinghouse[11] has reported on the destructive testing of a control rod that had operated in the Shippingport reactor for one seed life [$3.85 \times 10^{21}$ nvt (fast)]. Specimens from the more heavily irradiated portions of the rod were removed for tensile testing; also, electrical-resistivity measurements were made, and the effects of annealing were determined. The $3.85 \times 10^{21}$ nvt exposure resulted in a 168% increase in yield strength (to 73,900 psi) and a 41% increase in ultimate strength (from 58,000 to 82,000 psi). The total elongation decreased by a factor of $\frac{1}{3}$ to $\frac{1}{2}$, but the reduction in area showed smaller changes. Annealing tests showed that most of the radiation-induced changes could be annealed out in 1 hr at 700°C. Effects of irradiation on strain-rate sensitivity and notch effects were small. Notch strengthening was essentially the same for irradiated and non-irradiated hafnium. Plots of the mechanical-property data vs. increasing dosages showed that the radiation-induced changes were saturating in the $2.15 \times 10^{21}$ nvt range, and it was concluded that hafnium could be used through several seed lives of the Shippingport reactor.

A recent German paper[12] reports on an investigation of dicadmium tantalate, $Cd_2Ta_2O_7$. The compound decomposes in air above 1000°C, but below this temperature it is reportedly stable chemically and undergoes no allotropic transformations with temperature. The compound was compatible with copper to 1000°C and supposedly also with silver.

## Stainless Steels

The most important factor limiting the use of the austenitic stainless steels in several important reactor applications is the susceptibility of these alloys to stress-corrosion cracking. A rather extensive basic program on stress corrosion at Armour Research Foundation has been summarized in a recent report.[13] Experimental work was carried out on stressed type 304 stainless-steel wires in boiling solutions with the test cells so arranged that potential measurements could be made of the stressed wires during testing. A mapping technique was also developed which made it possible to chart the potential and various degrees of cathodic or anodic activity of the whole area of a stressed cylinder. This mapping technique showed that the appearance of a strong anodic zone marked the development of a visible crack. Work in several types of solutions, organic solvents, and molten salts led to the conclusion that no specific ion or compound is essential to produce stress-corrosion failure but that such failures can be produced by several substances. The only requirement for a stress-corrosion-producing medium was that it could establish a "partial passivity with areas of local activity" on the surface of a stressed specimen. Such areas of local activity could be found by using the mapping technique described. Support was developed for earlier theories that the cracking process is gradual and consists of two stages. The first stage or incubation stage is short and requires a stressed condition. This leads to the second stage, which is the crack-propagation period, and failure. The incubation stage, although the least understood, is apparently the more rewarding area of investigation.

Another approach to the stress-corrosion problem has been reported by Lang,[14] who investigated impurities in austenitic stainless steels and their role in stress corrosion. Alloys that basically consisted of 20% chromium, 18% nickel, and the balance iron were prepared from high-purity constituents and were carefully melted in vacuum to produce high-purity materials. As compared with the nominal compositions of conventional stainless steels, carbon contents were reduced from 0.1 to 0.001%, manganese from 2.0 to 0.01%, and silicon from 1.0 to 0.001%. Minor constituents such as nitrogen, arsenic, antimony, bismuth, $O_2$, and sulfur were reduced to extremely low levels. Additions of elements such as carbon, silicon, titanium, lead, aluminum, and nitrogen were made to the high-purity base. Tests were made on stressed U-bend specimens in boiling $MgCl_2$. Although the high-purity alloy specimens survived for 17 to 20 days, it was found that small additions of $N_2$, phosphorus, aluminum, arsenic, antimony, and bismuth produced failure in much shorter periods, depending usually on the amount added. Additions of carbon back to the normal 0.1% level and silicon to the 2.0% level produced considerable resistance to stress corrosion. Some of these specimens containing the carbon and silicon additions survived for more than four months as contrasted with failures of most of the alloys in less than 30 days. The report appears to identify some quite deleterious elements, such as phosphorus, which are always found in stainless steel, and emphasizes the beneficial effects of carbon and silicon. The author suggests that, although alloys of normal purity require 45 to 50% nickel to produce immunity to stress-corrosion cracking, purification of the alloy may reduce the required nickel content to 20%. A high-purity normal-carbon alloy that contained 14% nickel was not, however, particularly resistant to cracking; therefore there may be definite lower limits to the nickel content that will suffice for protection.

A specialized, but important, case of stress corrosion is that of the precipitation hardening of stainless steels. The high strength and hardenability of 17-4 PH have made it particularly attractive for control-rod drives. In view of the failures encountered with 17-4 PH drives in the Dresden reactor, tests were carried out at Savannah River[15] with the 1100°F, lower hardness heat-treatment as tested in *p*D 10.5 heavy water. Failures were not encountered at 3914 hr in any of the alloy specimens that had been heat-treated for 4 hr at 1100°F, either in the liquid or vapor phase, on notched or unnotched specimens, or even on specimens that had been cold worked 48% prior to heat-treating. Comparison specimens heat-treated at 900°F failed under the test conditions.

Although the usual important interaction between an alloy and its environment manifests itself as corrosion, there may frequently be a considerable effect of the environment on the creep behavior—a phenomenon often encoun-

tered in gas environments and of particular concern in connection with the Experimental Gas-Cooled Reactor (EGCR). The helium EGCR coolant is expected to be contaminated with various impurities and decomposition products from the graphite moderator and other sources. In Oak Ridge National Laboratory studies of creep behavior,[16] experiments were carried out in each contaminant gas separately. Air, CO, $CO_2$, and $N_2$ were found to strengthen type 304 stainless steel in creep tests. Oxygen weakened the alloy at 1500°F, but it had a strengthening effect at 1700°F, whereas hydrogen had the opposite effect at these two temperatures. The strengthening and the related loss of ductility in $CO_2$ and CO were attributed to carburization. Carbon contents as high as 2.43% were found in type 304 stainless steel exposed for 1939 hr at 1700°F at a 1200-psi stress. Copper plating of the specimens (carbon has a solubility of only 0.001% in copper at 1100°F) decreased carburization, as long as the plate remained intact, but did not prevent it entirely.

## Joining Methods

Pressure-tube reactor designs require that the "working" part of the pressure tube be made of a low-cross-section material such as a Zircaloy. The Zircaloy must be joined to the stainless steel of the rest of the coolant circuit. The great disparity in thermal expansion between Zircaloy and stainless steel complicates the design of mechanical joints connecting them, whereas the formation of the brittle nickel-zirconium eutectic makes conventional welding impossible. However, it has been demonstrated that, if Zircaloy and stainless steel are tandem extruded under the proper conditions, a strong and reliable bond is formed. The process consists of the extrusion of a canned composite billet consisting of a cone of stainless steel followed by a cone of Zircaloy, as shown in the sketch in Fig. V-1. Extrusion ratios as high as 10:1 result in tapered interface lengths up to 12 in. in the product. The interface or bond zone is very thin but mechanically quite strong. A set of such coextruded tubes as prepared by Nuclear Metals, Inc., the originator of the process, was tested by Du Pont at Savannah River.[17] The tubes ranged from 1.59 to 3.8 in. in outside diameter and had wall thicknesses in the 0.2-in. range. The major test consisted of cycling these tubes, while pressurized to 1000 psig, between 260°C and room temperature. Failures were not encountered in such tests, even when they were prolonged to 500 cycles. Testing of the tubes in tension resulted in failures in the Zircaloy section at stresses to be expected for the normal material. Some of the specimens had received 20% cold work and two of them had been prepared with an interlayer material of either niobium or titanium. The use of interlayers was found to furnish no advantage, but cold working after extrusion provided useful strength increases. Tests under irradiation are planned, but this

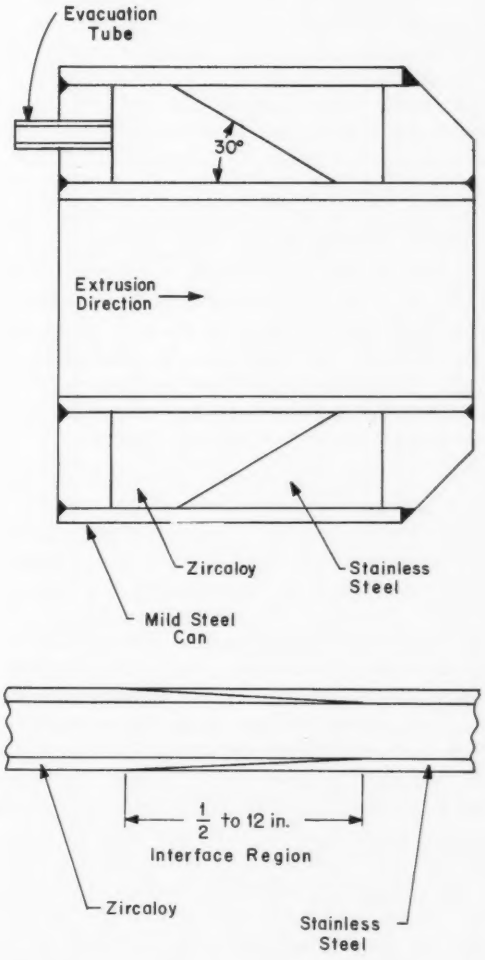


Fig. V-1 Composite billet before tandem extrusion (above) and finished coextruded joint with protective can removed (below).[16]

out-of-pile work indicated successful use of the tandem-extruded joints.

Work on the bonding of Zircaloy to stainless steel by other techniques has been reported by Battelle.[18] The first method, friction welding, a technique recently developed in Russia, consists of revolving one part against another when positioned coaxially under axial load. Motion between the surfaces in contact produces heat, breaks down the surface films, and provides intimate contact between the surfaces, thereby providing a weld at the contact. The heat-affected zone is small, but the parts to be welded are limited in shape since they must be revolved, and heavy unit pressures are required for bonding. Fortunately, reactor pressure tubes and fuel elements have shapes suitable for welding by this method. The preliminary or exploratory work carried out at Battelle was concerned with joining type 410 stainless steel to Zircaloy-2. Both rod-to-rod and tube-to-tube joints were investigated. The considerable difference in hot strength of the two alloys was probably responsible for many of the difficulties encountered, and the test work was limited by the lack of heavy equipment. A representative weld cycle consisted of a 2- to 4-sec revolution at 1500 rpm with the application of 10,000 psi pressure. Although completely successful welds were not made, it was concluded that the technique was probably feasible.

The joining of sintered aluminum powder (SAP) by friction welding was also investigated as a possible method for attaching end caps to fuel-element tubes. Since the SAP alloys depend for their strength on the presence of a network of $Al_2O_3$ and since this network is disrupted or destroyed by fusion welding, a successful joining technique for the material is badly needed. Experiments with the friction welding of 6061 aluminum rods to rods of the same material were successful, but SAP-to-SAP bonds were not obtained. "Cold-friction" bonding, in which high pressures are used with speeds low enough to generate little or no heat, was more successful with SAP, but the best welds had only a 50 to 70% bond at the interface. Heating of the rods with an oxyacetylene flame before the welding cycle produced good joints with rod specimens but was less successful with tube-to-tube joints. A method of closing SAP tubes was developed which consisted of deforming the end of the tube down to a small diameter by forcing it into a rotating die. This small opening could then be closed by hot forging.

Work on the bonding of flat plates of Zircaloy-2 to type 410 stainless steel by cold reduction in one pass through a rolling mill showed that, if surface preparation was adequate, relatively strong bonds could be obtained at reductions between 34 and 75%. The bonding was a combination of mechanical interlocking and metallurgical bonding of the surfaces. Such bonding was not achieved with a tube-rolling technique similar to that used in joining tubes to headers in boiler practice. With a conventional tube roller the walls of a Zircaloy-2 tube could be expanded into grooves machined into a stainless-steel header, but, since only one metal was deformed, metallurgical bonding did not take place.

Substitution of the force of an explosion to deform the metal gave better joints than did tube rolling. A small explosive charge transmitting its energy through either water or air could be used successfully to deform a tube into a header to produce a mechanically strong bond. The tube could be forced to conform to quite complex groove shapes machined in the header, but simple sleeve joints were found preferable as well as cheaper. Air, when trapped in the grooves, became heated, owing to compression by the explosion, to the point that brittle iron-zirconium intermetallics were formed. Although explosive joining would appear a promising method for materials that cannot normally be bonded, the nature of the process may make it difficult to apply to some cases.

Another possible technique for the joining of SAP is magnetic-force welding, now under study at Hanford.[19] This method differs from conventional resistance butt welding in that the electrode pressure comes from a magnet acting on the electrode rather than from mechanical or hydraulic pressure. The magnet is part of the welding circuit; therefore the resistance welding current and the electrode pressure are synchronized. In the Hanford program, tubes and rods containing either 7 or 10% oxide were employed. Close control of welding variables was found to be essential, but under proper conditions the welds showed complete bonding when examined metallographically, and, of some 25 tube specimens tested in tension at room temperature, only 3 failed in the weld interface. Considerable deformation takes place during welding; therefore a broadened weld interface

results. The photomicrographs,[19] however, indicate that the SAP structure is little affected outside the interface.

## Briefly Noted Reports

Wanklyn and Jones of Harwell have reviewed[20] the literature to late 1961 on the corrosion behavior in water of the common reactor materials such as the stainless steels (including stress-corrosion cracking), the mild steels, the zirconium alloys, the aluminum alloys, uranium, and the fuel alloys. Short discussions are included on Inconel, titanium, magnesium, beryllium, niobium, hafnium, the silver alloys, cadmium, thorium, and plutonium. The sources have been critically evaluated, and the review succeeds in being both reasonably brief (31 pages of text) and comprehensive (393 references are cited).

Finding sufficiently sensitive and rapid inspection methods that will provide full examination of fuel-element Zircaloy tubing at a reasonable price is one of the major problems limiting the use of this material in power reactors. Progress to date on a long-term program to develop nondestructive testing methods at Hanford has been described in an interim report.[21] Work has been concentrated on ultrasonic techniques. An electromachining method for producing standard defects has been developed, instrumentation has been improved, and Lamb-wave phenomena are under study as a possible tool for the location of defects. The objective is to develop a method that will inspect 200 in. of $\frac{1}{2}$-in. tubing per minute.

A specialized method for determining the total wall thickness of annular $UO_2$-containing fuel elements has been reported by Savannah River.[22] The technique depends on magnetic-reluctance measurements, and the method is applicable to either annular or flat elements. The measurements obtained represent the distance between a sensing probe and ferrous material that is placed inside the annular elements or underneath the flat elements.

The Radiation Effects Information Center at Battelle has prepared a review of the state of the art (1961–1962) on radiation effects for the Air Force.[23] Although the review is mainly concerned with space-environment radiation, brief chapters cover structural metals, ceramics, lubricants, and other subjects of interest to reactor designers. Institutions and laboratories carrying out specific research programs are listed for each heading. In this connection, Los Alamos[24] has prepared a list of abstracts of recent papers on radiation effects on semiconductor devices.

## References


1. B. J. Seddon (Comp.), Zirconium Data Manual—Properties of Interest in Reactor Design, British Report TRG-Report-108, Nov. 3, 1961.
2. C. L. Whitmarsh, Review of Zircaloy-2 and Zircaloy-4 Properties Relevant to N. S. *Savannah* Reactor Design, USAEC Report ORNL-3281, Oak Ridge National Laboratory, July 23, 1962.
3. E. Hillner and J. N. Chirigos, The Effect of Lithium Hydroxide and Related Solutions on the Corrosion Rate of Zircaloy in 680°F Water, USAEC Report WAPD-TM-307, Westinghouse Electric Corp., Bettis Atomic Power Laboratory, August 1962.
4. W. K. Anderson and M. J. McGoff, Corrosion of Zircaloy in Crevices Under Nucleate Boiling Conditions, USAEC Report KAPL-2203, Knolls Atomic Power Laboratory, Apr. 13, 1962.
5. S. Beitscher, Effect of Hydrogen on the Strain Fatigue Properties of Zircaloy-2 Weld Metal, USAEC Report KAPL-2221, Knolls Atomic Power Laboratory, Apr. 26, 1962.
6. B. Cox, P. G. Chadd, and J. F. Short, the Oxidation and Corrosion of Zirconium and Its Alloys. XV. Further Studies of Zirconium-Niobium Alloys, British Report AERE-R-4134, August 1962.
7. C. R. Crupp, The Effect of Neutron Irradiation on the Mechanical Properties of Zirconium–$2\frac{1}{2}$% Niobium Alloy, *J. Nucl. Mater.*, 6(3): 241 (August 1962).
8. W. K. Anderson and J. S. Theilacker (Eds.), *Neutron Absorber Materials for Reactor Control*, U. S. Government Printing Office, Washington, 1962.
9. H. E. Williamson, D. L. Zimmerman, and K. C. Antony, Investigation of $B_4C$-Ni Electro Dispersions for Control Rod Applications, USAEC Report GEAP-3831, General Electric Company, Atomic Power Equipment Department, Nov. 3, 1961.
10. W. V. Goeddel, Development and Evaluation of $B_4C$-Graphite Control-Rod Materials for the HTGR, USAEC Report GA-2827, General Atomic Division, General Dynamics Corp., Apr. 4, 1962.
11. G. J. Salvaggio, The Properties of Hafnium from a PWR Core I Control Rod After One Seed Life Exposure, USAEC Report WAPD-TM-336, Westinghouse Electric Corp., Bettis Atomic Power Laboratory, June 1962.

12. F. Haessner, G. Petzow, and E. Preisler, Eignung von Cadmiumtantalat als Kontrollmaterial für Hochtemperaturreaktoren, *J. Nucl. Mater.*, 7(1): 46 (September–October 1962).
13. Armour Research Foundation, The Mechanism of Stress Corrosion in Stainless Steels. Final Report, May 15, 1959, to May 15, 1960, USAEC Report ARF-2181-12, September 1962.
14. F. S. Lang, Effects of Stress-Corrosion Cracking of Austenitic Stainless Steels in Chloride Solutions, *Corrosion*, 18(10): 378 (October 1962).
15. R. P. Jackson, Stress-Corrosion Cracking of 17-4 PH Stainless Steel, USAEC Report DP-779, Savannah River Laboratory, September 1962.
16. H. E. McCoy, Jr., and D. A. Douglas, Jr., Effect of Environment on the Creep Properties of Type 304 Stainless Steel at Elevated Temperatures, USAEC Report ORNL-2972, Oak Ridge National Laboratory, Sept. 18, 1962.
17. J. W. Joseph, Jr., Evaluation of Tandem-Extruded Joints Between Zircaloy and Stainless Steel, USAEC Report DP-723, Savannah River Laboratory, June 1962.
18. S. J. Paprocki and S. W. Porembka (Eds.), Joining Zircaloy–Stainless Steel and SAP Alloys by Friction, Rolling, and Explosive Techniques, USAEC Report BMI-1594, Battelle Memorial Institute, Sept. 4, 1962.
19. L. E. Mills, Magnetic Force Welding Sintered Aluminum Powder Materials, USAEC Report HW-72379, Hanford Atomic Products Operation, March 1962.
20. J. N. Wanklyn and P. J. Jones, The Aqueous Corrosion of Reactor Metals, *J. Nucl. Mater.*, 6(3): 291 (August 1962).
21. C. E. Fitch, H. E. May, and V. E. Kahle, Ultrasonic Testing of Zircaloy Sheath Tubing for Fuel Elements, Interim Report, USAEC Report HW-72802, Hanford Atomic Products Operation, June 1962.
22. T. R. Herold, Wall Thickness Tester for Tubular Oxide Fuel, USAEC Report DP-738, Savannah River Laboratory, July 1962.
23. Battelle Memorial Institute, Radiation Effects Information Center, Radiation Effects State of the Art 1961–1962, Report REIC-24, June 30, 1962.
24. C. S. Schwiening (Comp.), Radiation Effects on Semiconductor Devices, USAEC Report LAMS-2706, Los Alamos Scientific Laboratory, Aug. 9, 1962.

Section

VI

Power Reactor Technology

# Systems Technology

## Shippingport Operation Without Purification

Data are now available covering the results of operating a pressurized-water reactor for periods as long as two to three months without primary coolant purification.[1] These data were obtained as part of the Shippingport Pressurized-Water Reactor (PWR) program to advance the technology of water-cooled reactors. The Shippingport plant was operated on the following schedule: 770 EFPH (effective full-power hours) with only one of two purification systems in use and at 1478 EFPH with no purification; a second period with one system in operation lasted approximately 1300 EFPH. This operation was carried out during core 1 seed 2 life.* It produced no noticeable buildup in deposited long-lived activity; the buildup of short-lived reactor coolant activity was due primarily to $I^{133}$ (20.8 hr) and $I^{131}$ (8.05 days) and did not result in any operational difficulties.

The primary coolant system[2] for the PWR operates at 2000 psia and 508 to 538°F. Wetted materials consist primarily of types 304 and 304L stainless steel and Zircaloy-2. The specified range of *p*H for the coolant water is 9.5 to 10.5. For the scavenging of radiolytically produced oxygen, hydrogen is added to the system as necessary to maintain a concentration of 50 to 60 ml (standard temperature and pressure) per kilogram of coolant.

The two identical purification systems, each of which is suitably connected to serve the entire primary coolant system, consist essentially of resin-bed ion exchangers with appropriate regenerative and nonregenerative heat exchangers which are used to reduce the temperature of the purification stream to 120°F at the inlets to the ion exchangers. Each system is designed for a normal flow of 20,000 lb/hr and a maximum flow of 25,000 lb/hr. At the normal flow rate, with both purification systems operating, the purification half-life for the primary coolant system is 2 hr; with one system operating, the half-life is 4 hr.

The design of the purification systems is based upon the assumption of a maximum corrosion rate for the approximately 35,000 sq ft of surface exposed to the coolant of 10 mg/(dm$^2$)(month), accompanied by a maximum fuel-element failure rate of 1000 per core life. The main requirements of the systems are set by considerations of primary system maintenance and of crud deposition and fouling of heat-transfer surfaces. The design is also based on a maximum primary coolant activity level of $1 \times 10^7$ dis/(sec)(cm$^3$) and a maximum of 1 ppm of suspended impurities in the coolant. The lithium hydroxide resins in the demineralizers serve the additional function of helping to maintain the *p*H of the coolant at the nominal value of 10.0. However, a system for the addition of lithium hydroxide directly to the coolant is also provided.[2] During the test with no purification system, four additions of lithium hydroxide were required to maintain the desired *p*H level; normally two or three additions would have been necessary for a comparable period of operation with purification. The coolant conductivity increased only slightly during the test period.[1]

The effects of operation without the purification system were evaluated by noting: (1) radiation levels about the primary coolant piping, (2) radiation-level buildup on the reactor vessel

*Earlier, during seed 1 life, the plant was operated for 2000 EFPH with only one purification system in use.

head, (3) primary coolant crud levels, (4) crud specific activity, (5) corrosion-product activity, (6) fission-product activity, (7) 15-min gross nonvolatile activity, (8) iodine activity in the secondary coolant (due to primary-to-secondary leakage), (9) pressure drop across the reactor core, (10) activity buildup on walls of the hairpin test loop in the purification system, and (11) coolant chemistry. Data points pertaining to these 11 conditions were taken during the tests, and most of them are plotted as functions of EFPH in Ref. 1. Of these, only the fission-product activities appear to correlate closely with the changes in purification-system operation. Plots of the data related to items 1, 3, and 6 above are reproduced in Fig. VI-1. It is stated[1] that the specific activities of the soluble fission products such as $Cs^{136}$, $Cs^{137}$, $Br^{83}$, $I^{131}$, and $I^{133}$, having half-lives appreciably longer than 4 hr, increased during the no-purification operation as would be expected. Part of the increase in the iodine activities is attributed to the effects of frequent power startups during the early portion of the no-purification operation. This is borne out by subsequent steady-state reactor operation during which iodine-activity levels declined steadily until the end of the purification run.

The following conclusions as to the effect of the interruption of purification-system operation are quoted from Ref. 1:

(1) The trend of long-lived radiation-level buildup on primary system piping and on the reactor head did not differ significantly from that observed during operation with purification.

(2) Operation without purification resulted in no significant changes in coolant crud concentrations; crud bursts of comparable magnitudes (10 to 36 ppb daily average for one week) occurred at all purification flow rates. Steady-state concentrations were essentially the same, that is 0.5 ppb for full purification operation versus 2 ppb with half or no purification.

(3) Crud specific activity remained constant during operation with half purification and no purification, then increased following the return to full-purification flow. Whether the increase was coincidental or related to operation with full purification was not determinable.

(4) Corrosion product activity in the primary coolant remained within the scatter observed during operations with purification.

(5) Fifteen-minute gross nonvolatile gamma activity levels, iodine activity in the secondary system due to primary-to-secondary leakage, and spe-

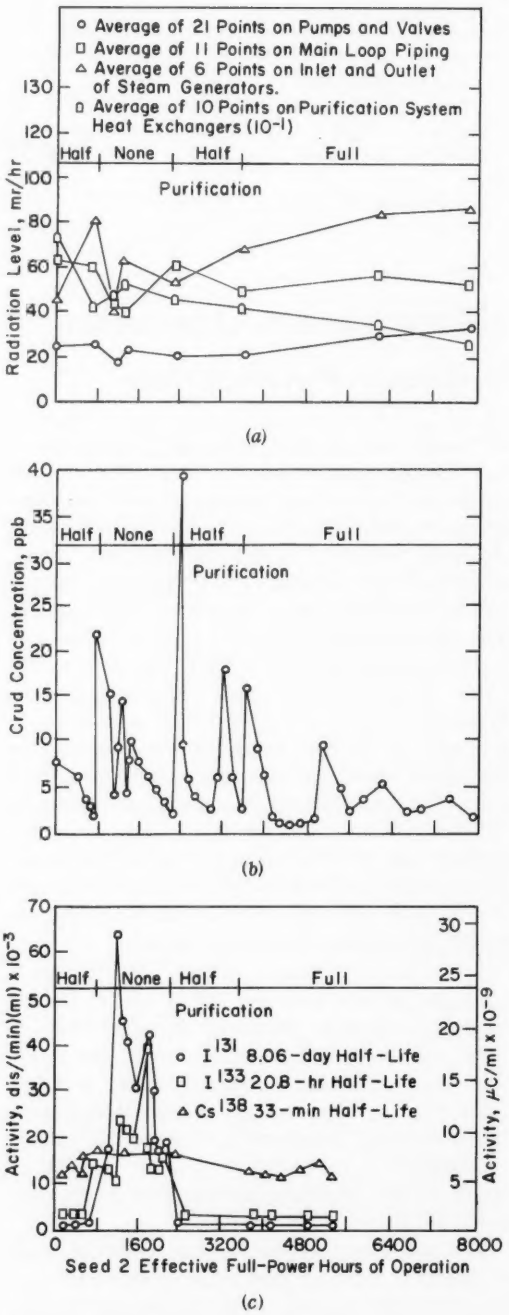


Fig. VI-1 Plots of data taken during variations in operation of the PWR purification system.[1] (*a*) PWR radiation levels based on 30-hr survey, contact readings. (*b*) PWR crud concentration in primary coolant. (*c*) PWR $I^{131}$, $I^{133}$, and $Cs^{138}$ activity levels for ion-exchange influent.

cific activities of the fission products with a half life appreciably longer than 4 hours increased during operation without purification, as expected. However, this did not present an operation or maintenance problem.

(6) Within the accuracy of instrumentation there was no change in pressure drop across the core, regardless of the extent of purification system operation.

(7) Survey results from the hairpin loop[*] were, in general, indicative of overall plant behavior during the test, since there was no increase in radiation levels of the plant or the hairpin loop during operation without purification. The radiochemical data from the hairpin loop are inconclusive.

(8) Summing up the overall results, the plant, as a whole, showed no change within the scatter of the data in the trend of long-lived activity buildup during operation without purification.

## Organic-Coolant Impurities Removal

The problem of removing impurities from organic reactor coolants is an important one, and the reader may wish to consult the review in *Power Reactor Technology*, 6(1): 65-67, for a more general discussion of the problem. The importance of impurities removal can be considered from three points of view:

1. The impurities establish the radioactivity level of the primary coolant system.
2. Since many of the impurities concentrate in the waste stream, they contribute to the difficulty of contaminated-waste disposal.
3. The impurities may contribute to the fouling of heat-transfer surfaces.

Reference 3 describes the design and construction of the Organic-Moderated Reactor Experiment (OMRE) particulate removal loop. Reference 4 describes the results of an experimental investigation designed to study removal of film-forming impurities from high-temperature organic coolants. Reference 4 will be emphasized in this review.

The study presented in this report emphasized impurities removal by both filtration and adsorption techniques. The equipment used in the filtration testing (shown in Fig. VI-2) was constructed of carbon steel and was designed to operate at 700°F and 150 psia. The coolant used in the tests was a mixture of fresh organic, Santowax OM or OMP, and "high boilers" (HB); the latter was high-molecular-weight

*The hairpin loop or purification test loop is a small loop that is incorporated just upstream of the purification loop to provide a location for the monitoring of coolant contamination.

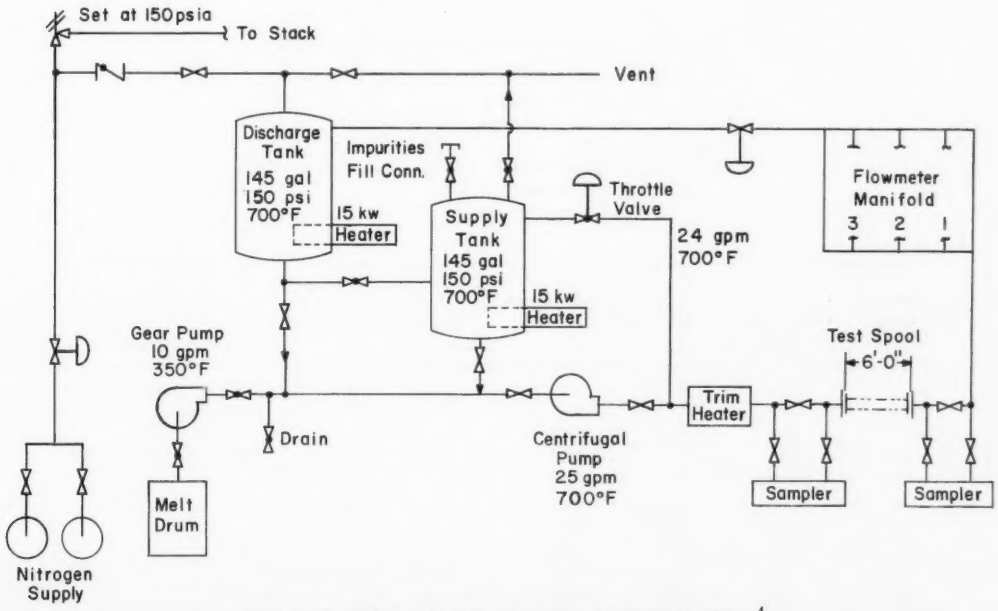


Fig. VI-2 Schematic flow diagram of impurities loop.[4]

"decomposition" product removed from the organic coolant of the OMRE at the time when that coolant contained very high levels of impurities which were concentrated in these decomposition products. Many commercial filtering devices were tested. With this very impure coolant, simple cartridge type units plugged rapidly. The most promising type tested employed a precoated sintered stainless-steel filter and a filter aid mixed with the organic coolant. The efficiency of the filter in removing inorganic particulate material was measured by the Pyrolytic Capsule Fouling Test (PCFT) and by the amount of radioactivity removed from the organic coolant. The PCFT measures the weight of the film deposited on an electric resistance heater in 24 hr when the heater is immersed in 240 ml of a test liquid. The liquid temperature is maintained at 600°F, whereas the heater temperature is maintained at 1050°F. The weight of the film thus obtained is usually expressed in milligrams. The ash content of the coolant upon ignition also was used as a measure of filtration efficiency.

Various grades of diatomaceous earths were used in the experiments for filter aids and precoats; asbestos was also studied as a precoat. Data taken in a typical run are given in Table VI-1. Although an appreciable amount of coolant cleanup was achieved, the results showed that the purity of the product nevertheless remained somewhat poorer than desired for reactor operation.

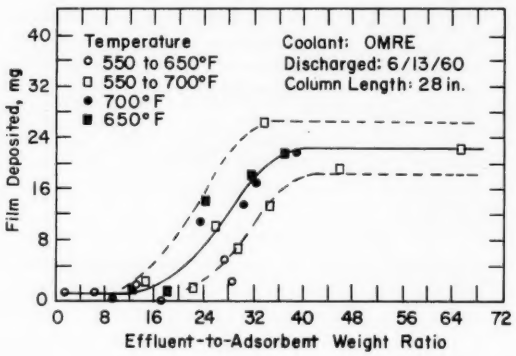


Fig. VI-3 Attapulgus clay adsorption reference tests.[4]

A higher degree of purification was achieved by an adsorption technique, also described in this report. The equipment consisted primarily of a column filled with an adsorbent through which the synthetic coolant was passed. Attapulgus clay, one of the better adsorbents for impurity removal, was used for most of the tests. Illustrative data are given in Fig. VI-3. Owing to the high levels of impurities in the feed material, breakthrough of impurities took

Table VI-1 TYPICAL PRECOAT FILTRATION TEST[4]

Filter Support: 40-$\mu$ sintered stainless steel
Precoat: Asbestos, 3.2 oz/sq ft
Filter Aid: Filter-Cel, 0.115 wt.%
Temperature: 575°F
Test Liquid: Synthetic coolant, 30 wt.% HB in Santowax OM
Ash = 165 ppm
PCFT wt. = 86 mg

| Quantity filtered, gal | Flow rate, lb/(hr)(sq ft) | $\Delta p$, psig, | Removal, gross gamma activity, % | Filtrate | | Remarks |
|---|---|---|---|---|---|---|
| | | | | Ash, ppm | PCFT weight, mg | |
| | | 14 | | | | Precoat applied |
| | 368 | 31 | | | | Begin run |
| 13 | 336 | 47 | 92.0 | 7 | | |
| 16 | 327 | 49 | 93.0 | | 14.2 | Begin constant pressure |
| 25 | 239 | 49 | 93.2 | 1 | | |
| 32 | 175 | 49 | 93.2 | | 7.9 | |
| 35 | 170 | 49 | 92.6 | 2 | | |
| 41 | 133 | 49 | 92.4 | 1 | | |
| 45 | 96 | 49 | 93.5 | | 14.5 | |
| 48 | 83 | 49 | 92.7 | | | |

place at relatively low weight ratios of effluent to adsorbent. Some runs were made using both precoat filtration and fixed-bed adsorption, and the results were encouraging in that no breakthrough was obtained at effluent-to-adsorbent weight ratios up to 62. This contrasts with the behavior shown in Fig. VI-3, where breakthrough came at ratios from 10 to 20.

Recent operation at the OMRE with a feed of very pure coolant (PCFT film weight of 1 mg) has indicated that attapulgus clay adsorption columns could be operated to effluent-to-adsorbent weight ratios in excess of 4000 prior to impurity breakthrough.

## References


1. Westinghouse Electric Corp., Bettis Atomic Power Laboratory, Bettis Technical Review, Reactor Technology, p. 49, USAEC Report WAPD-BT-26, September 1962.
2. *The Shippingport Pressurized Water Reactor*, Addison-Wesley Publishing Co., Inc., Reading, Mass., 1958.
3. H. Cataldo, Design and Construction of the OMRE Particulate Removal Loop, USAEC Report NAA-SR-6646, Atomics International, Dec. 30, 1961.
4. G. O. Haroldsen and J. W. Florence, Organic Coolant Impurities Removal, USAEC Report NAA-SR-6905, Atomics International, Aug. 15, 1962.

Section

VII

Power Reactor Technology

# Operating Experience

## Dresden Nuclear Power Station

The operation and performance of the Dresden Nuclear Power Station were the subjects of a series of papers[1–6] given at the March 1962 meeting of the American Power Conference. References 1 and 2, which cover the plant description and the modification and inspection of various reactor components, were reviewed in *Power Reactor Technology*, 4(4): 56-58; 5(2): 56-59. This review will be devoted primarily to the remaining references.

The operation of the Dresden plant can be divided into three main periods: The first period covered the time between the beginning of "commercial" power operation (August 1960) and shutdown (November 1960). The second period covered the time between resumption of power operation (June 1961) and shutdown for inspection purposes (October 1961). The inspection was accomplished over a period of about nine weeks. The third period, which began when the plant returned to power operation, was continuing at the time of the writing of Ref. 3. A summary of the operating statistics is given in Table VII-1.* The load schedules for the Dresden plant are shown in Figs. VII-1 to VII-3. Load schedule 1 was designed to achieve a 79.9% weekly capacity factor; this schedule is typical of the schedule used during 1960. Schedule 4, which raised this weekly factor to 89.8%, was used during July, August, and September 1961. Schedule 5, which was in use at the time of the report,[3] represents essentially base loading at full rated load.

*Table VII-1 and Figs. VII-1 to VII-4 are reprinted here by permission from *Proceedings of the American Power Conference*.[3]

As is apparent in Table VII-1, the plant net heat rate improved steadily over the three operating periods. The most significant factors contributing to this improvement are stated[3] to be (1) the reduction of auxiliary power requirements caused by station outage, which reduces the yearly net generation; (2) the condenser water temperature, which was lower in January and February; and (3) the improved load schedules. The January and February 1962 values of the plant heat rate are about normal;[3] about 4.7% of the gross was used for auxiliary power requirements.

In addition to statistics pertinent to power generation, Ref. 3 also discusses the water chemistry and radioactive waste handling. Although most of the nuclides observed in the reactor water are the same as those found in other water-cooled reactor systems constructed of stainless steels, a small amount of copper was also detected; this copper was interpreted to originate in the feedwater heaters. These heaters, which employ copper-nickel and monel tubes, were thought to be responsible also for much of the nickel in the water. Nickel, via the $(n,p)$ reaction, is converted to $Co^{58}$, which is the principal source of radioactivity in the water after a one-day shutdown. During the first two months of 1962, the *p*H of the feedwater to the secondary flow loop was maintained at about 8.5 by the addition of ammonia. This decreased the nickel concentration from 20 ppb to about 8 ppb; the ammonia was prevented from entering the reactor by the condensate demineralizer just ahead of the primary system feedwater pump.

The specific activities of most of the nuclides in the water have apparently leveled off at equilibrium values; the specific activity of the crud has stabilized at about $1.5 \times 10^7$ counts/min per milligram of iron. A previous discussion of the Dresden-plant water chemistry may be found in Ref. 7.

Table VII-1 SUMMARY OF DRESDEN OPERATING STATISTICS[3]

| | 1960 | 1961 | Jan.-Feb. 1962 |
|---|---|---|---|
| Reactor operating (critical) hours | 2647.9 | 3452.9 | 1199.6 |
| Turbine-generator operating hours | 2135.3 | 3340.4 | 1160.4 |
| Number of reactor criticals | 397 | 211 | 9 |
| Number of unit starts | 43 | 5 | 2 |
| Gross electric-power generation, kw-hr | 275,634,000 | 555,140,000 | 212,480,500 |
| Net electric-power generation, kw-hr | 252,038,000 | 521,872,600 | 202,511,300 |
| Auxiliary power, % of gross | 8.56 | 5.99 | 4.69 |
| Plant capacity factor | 16.3 | 33.0 | 78.2 |
| Plant capacity factor (based on operating hours) | 67.0 | 86.6 | 95.4 |
| Plant heat rate, Btu/kw-hr (net) | 12,413 | 11,950 | 11,431 |

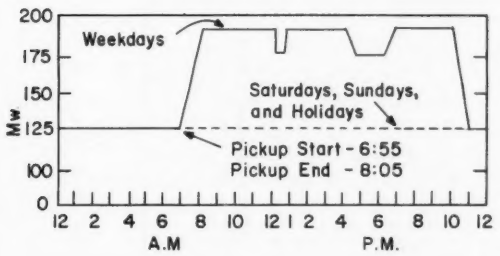


Fig. VII-1 Dresden-plant load schedule No. 1, gross generated.[3]

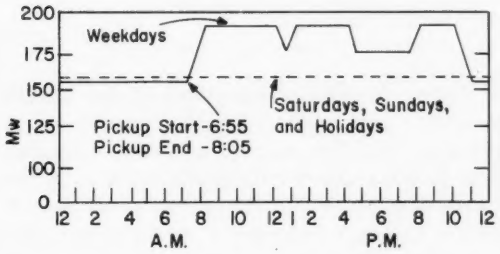


Fig. VII-2 Dresden-plant load schedule No. 4, gross generated.[3]

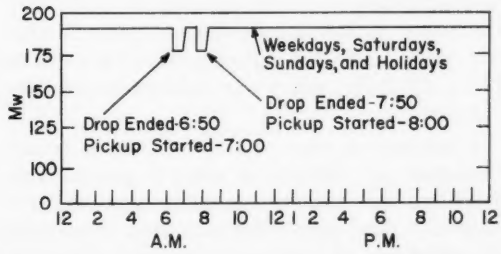


Fig. VII-3 Dresden-plant load schedule No. 5, gross generated.[3]

The treatment plant for liquid radioactive wastes processed a total of about 18 million gal of water between the start of the plant operations (October 1959) and the end of 1961. The processing, where necessary, consisted of filtration and/or ion exchange. Of the 18 million gal processed, all but about 1 million gal was reused in the plant; this remainder was, in part, disposed to the river after dilution to permissible discharge concentrations. The cost of processing is given[3] as $2.63 per 1000 gal. The schematic diagram of the waste-treatment plant is shown as Fig. VII-4.

References 4 and 5 deal largely with the experiments performed at the Dresden plant to obtain information for use in improving the reactor design and for improving the understanding of the existing plant. For example, the plant has large risers running from the reactor to the steam drum; these were extensively instrumented to ensure that no violent riser flow action was taking place. Power distributions for various core configurations and control-rod positions were calculated and were found to be in good agreement with experimentally determined data.

One method of measuring power distributions in some detail was by "gamma probing" a fuel element immediately after sustained steady-state operation of the reactor. This technique involved hoisting the fuel element to be studied to a position above the core but well below the surface of the water. A small, gamma-sensitive ion chamber was lowered into the flow channels, and gamma traverses were taken along the length of the element. A variation of this technique had previously been used on the Experimental Boiling-Water Reactor. In that case a

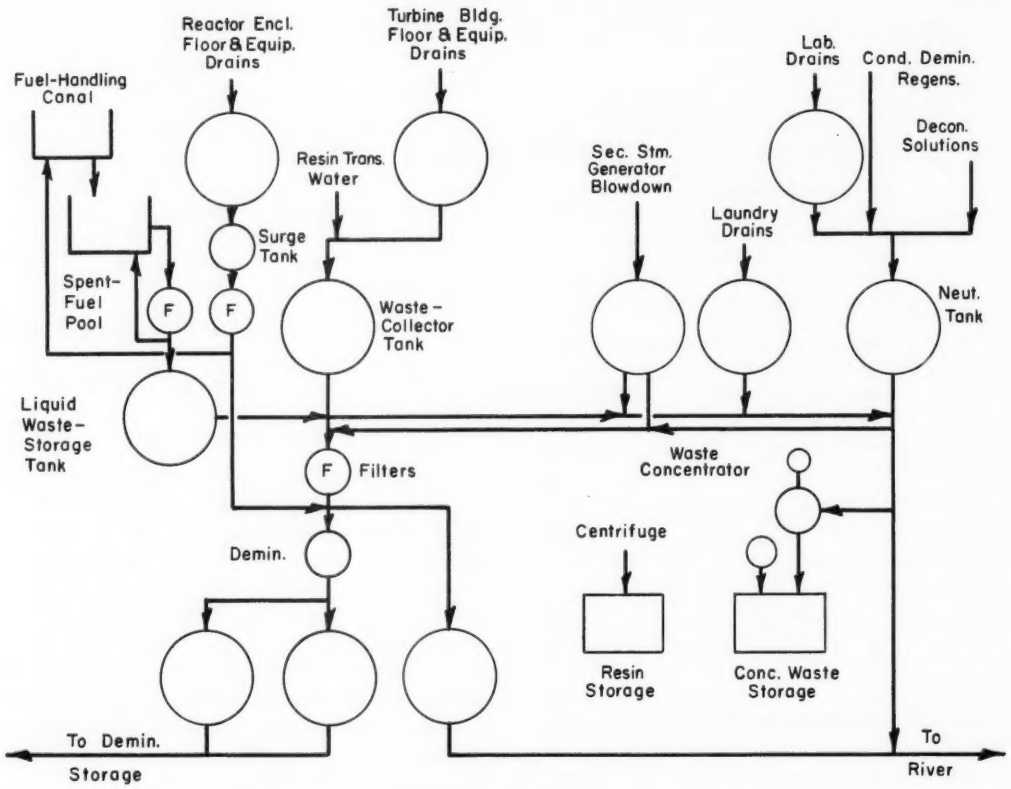


Fig. VII-4 Radioactive waste system for the Dresden plant.[3]

gamma-sensitive chemical solution ($FeSO_4$) was used as the gamma detector [reviewed in *Power Reactor Technology*, 4(3): 57-58]. Wire-activation measurements were also made in the Dresden reactor, and these substantiated the gamma probe data. A special fuel assembly was used to measure directly the corner-rod local peaking effect. This assembly was designed so that it could be disassembled under water; therefore the individual fuel rods could be surveyed with a gamma-sensitive counter. The Dresden reactor also has the capability of accommodating 64 in-core ion-chamber sensors, and these were used for power-plotting purposes during reactor operation. The locations of these sensors are given in Fig. VII-5.* Although these chambers do not give continuous spatial coverage of flux, their use enables the operator to obtain immediate indications of the effects of control-rod motions, load changes, xenon changes, etc. The in-core chambers are also used to determine whether the control rods are functioning properly, and all rods are moved weekly to check instrument response and confirm blade following.

The operating conditions for the Dresden plant are given in Table VII-2. These are the quantities as determined by measurements and tests on the actual plant, with the exception that they are based on the design value of recirculation flow ($25 \times 10^6$ lb/hr) rather than on the value of $27.1 \times 10^6$ lb/hr, which was deduced from measurements.

A number of experiments concerning measurements of dual-cycle control parameters, stability, and transient performance are reported. A band-pass filter was used to examine the spectrum of reactor noise seen by in-core and ex-core instrumentation during periods of extended steady-state operation. No evidence of

*Figures VII-5 and VII-6 and Table VII-2 are reprinted here by permission from *Proceedings of the American Power Conference*.[4]

approach to an instability threshold was noted. Transfer functions were studied by oscillating a control rod in the core, over a range of oscillation periods from 3 to 60 sec, and by noting the response of the in-core instrumentation; again, a sizable stability margin was indicated, and there was no pronounced system resonance in the frequency range studied. Data were generated by a number of transient experiments for comparison with analytical information obtained on an analog of the Dresden-plant system. Pressure-regulator set-point changes, partial load rejections, bypass-valve test openings, and various kinds of scram were studied in these tests. One of the more dramatic experiments consisted of tripping the turbine at full load and of isolating the steam flow from the main condenser by shutting the turbine bypass valve. The reactor was simultaneously scrammed. In general, the analog predicted the system performance quite well, and the authors conclude "...that the Dresden Boiling Water Reactor is indeed highly maneuverable, extremely stable, and easy to control."

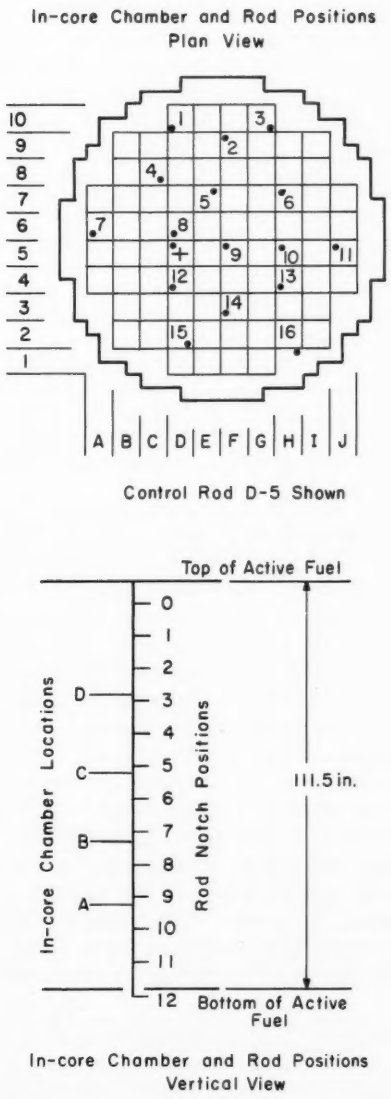


Fig. VII-5 Spatial instrumentation relations in Dresden core.[4]

Table VII-2 RATED OPERATING CONDITIONS IN THE DRESDEN REACTOR[4]

| | |
|---|---|
| Power level, Mw(t) | 630 |
| Recirculation flow, lb/hr* | $25 \times 10^6$ |
| Primary steam flow, lb/hr | $1.4 \times 10^6$ |
| Secondary steam flow, lb/hr | $1.2 \times 10^6$ |
| Inlet core subcooling, Btu/lb | 53 |
| Core average exit quality, % | 5 |
| Reactor void fractions: | |
| Percent volume of channel coolant | 17 |
| Percent volume of total moderator | 11 |
| Reactor peak heat flux (at overpower) | 350,000 |
| Minimum burnout ratio (at overpower) | 2.1 |
| Maximum void fraction at hot-channel exit (overpower), % | 65 |

*Based on a recirculation flow of $25 \times 10^6$ lb/hr instead of the $27.1 \times 10^6$ lb/hr measured in system tests.

Another interesting experiment consisted of operating the reactor at rated electrical output and of simultaneously dumping steam to the condenser through the bypass valve.[4] The purpose of the test was to investigate the ultimate capabilities of the primary steam drum. With the reactor delivering steam to both the turbine and bypass, the steam flow to the steam drum was 1.93 million lb/hr, or about 38% above the rated flow shown in Table VII-2. Although no details are given in the reference, apparently the steam drum had at least this capacity; this value is about the amount of bypassed primary steam that can be handled by the main condenser, and presumably this latter item limited the amount of steam to the 1.9 million lb/hr.

The most interesting stability experiment involved a large increase in the average steam-void content of the reactor, which was obtained by operating the reactor on only one of the four recirculation flow loops at power levels up to about 370 Mw(t). At normal rated power opera-

tion, the reactor has an average void content of about 11%; the single-loop operation raised the average voids to about 30%. Analysis of the noise spectrum indicated that the reactor was stable at 370 Mw(t), although its margin of stability was lower than at its design void fraction. This was evidenced by a low-amplitude, damped "ringing" of the reactor power following movement of a control rod. These data are shown in Fig. VII-6 for two power levels. The noise spectrum indicated a pronounced peak at a frequency of about 8 cps and a reduced peak around 1 cps. The "ringing" was in phase throughout the core, as determined from the in-core instrumentation.

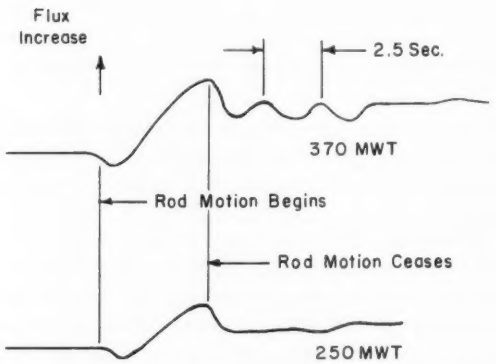


Fig. VII-6 Effects of "step" control-rod motion on Dresden reactor during high void test.[4]

Reference 6 gives details on the operation, radiation protection, and maintenance of the Dresden plant. The startup and normal operation are described, with emphasis placed on the rod programming and checks to ensure that the control rods and drives are operating properly. The maintenance has been concerned primarily with repair of system leaks. Three out of the four canned pumps have developed leaks at the joint between the canned rotor and the pump bowl; these leaks were stopped by stressing the studs to a greater extent, and, in one case, by a seal weld. Other leaks, due to check valves, valve packing, flanges, and heat-exchanger tubes, appear to be somewhat routine and of a minor nature.

# Shippingport Atomic Power Station

Information on the nuclear instrumentation system of the Shippingport Pressurized-Water Reactor (PWR) was given in *Power Reactor Technology*, 5(1): 38 and 51. The reactor protection system and the operating experience with the protection system during about two years of reactor operation are described in detail in Ref. 8. The reactor protection system contains circuits that give protection against (1) excessive power-to-coolant-flow ratio, (2) excessive nuclear level, and (3) loss of coolant flow. These circuits are shown schematically in Fig. VII-7. The systems were designed to obtain high reliability according to the following design criteria:[8]

1. Wherever possible, the use of equipment such as vacuum tubes and relays was avoided, extensive use being made of magnetic amplifiers.
2. Test equipment was installed so that the operation of this system could be checked without requiring reactor shutdown.
3. Where possible, the system was designed so that the failure of one piece of equipment will not cause complete loss of protection or result in an unnecessary shutdown. This latter consideration has led to an energize-to-shutdown type protection chain.
4. The circuitry was kept as simple as feasible, within functional requirements.

The output of the flow-to-power protection circuit results in the insertion of the control rods at normal speed to reduce the reactor power, whereas the excessive nuclear level (overpower) circuitry produces a scram if the reactor power exceeds the set point. The overall accuracy of the overpower protection system is stated to be ±10% with respect to the average power produced in the plant. This value is made up of the components shown in Table VII-3.

During the course of operation of the PWR over the seed-1 lifetime, the settings of the overpower protection system were progressively reduced, as shown in Table VII-4. The reasons for these reductions are as follows:[8]

1. As seed 1 life progressed, the core internal power shift from the seed to the blanket resulted in the maximum surface heat flux limitation of 500,000 Btu/hr-ft$^2$ in the blanket material becoming limiting and more restrictive than the limiting DNB (Departure from Nucleate Boiling) ratio criteria in the seed.

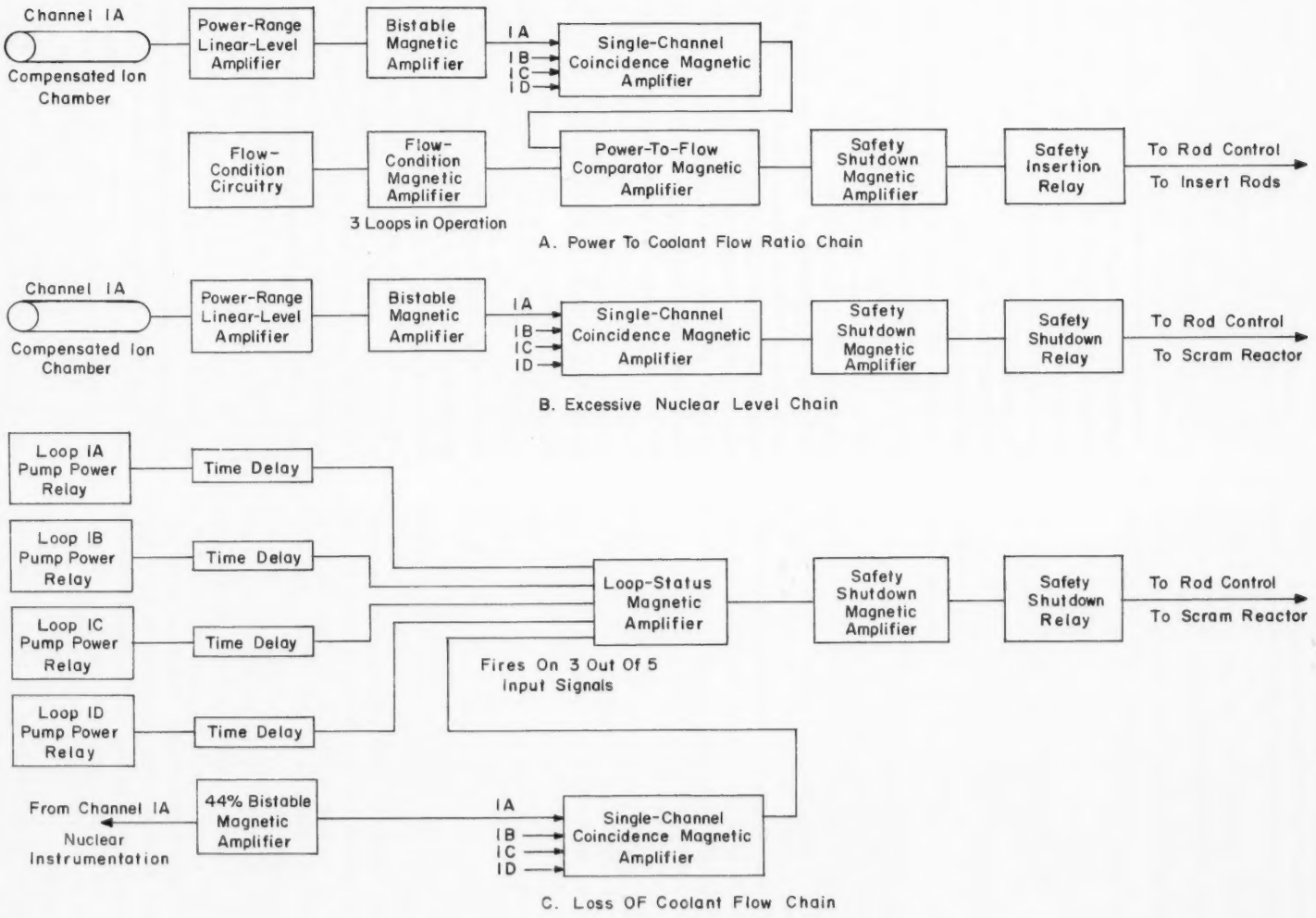


Fig. VII-7 Protection system for the Shippingport reactor.[8]

2. The calculated overshoot occurring during the worst-case rod withdrawal accident became more severe as the temperature coefficient of reactivity decreased from $-2.5 \times 10^{-4}$ δk/°F at 0 EFPH to $-1.3 \times 10^{-4}$ δk/°F at 5000 EFPH for 500°F average coolant temperature conditions. This effect results from the more rapid rate of nuclear level rise that occurs at the lower temperature coefficient of reactivity value, all other parameters in the analysis of the transient being the same.

Table VII-3 COMPONENTS OF OVERALL UNCERTAINTY IN THE OVERPOWER PROTECTION SYSTEM

| Item | Accuracy, % |
|---|---|
| Steam-plant calorimetry upon which the nuclear level calibration is based | ±3 |
| Allowable drift before correction | ±3 |
| Establishing power-range linear-level-amplifier output | ±2 |
| Trip-point setting accuracy | ±2 |
| Total | ±10 |

Table VII-4 SHUTDOWN SETTINGS[8] FOR THE SEED-1 OPERATING FLOW CONDITION

| Time in seed-1 life | Three and four pumps at fast-speed set point, % |
|---|---|
| 0 to 3000 EFPH | 138 |
| 3000 to 5000 EFPH | 117 |
| 5000 EFPH to end of seed-1 life | 109 |

During the time period from 0 to 3000 effective full-power hours (EFPH), a spurious signal initiated control-rod withdrawal while the reactor was in automatic control and at full power; the flow-to-power protection circuit was set to initiate rod insertion at 114%. This latter circuit responded to the power increase with rod insertion at normal speed and reduced the power to 105% without incident. Late in seed-1 life, when the overpower scram setting was 109%, an operator inadvertently withdrew the wrong group of control rods; the power-to-flow ratio insertion chain was cut out because of the low setting on the overpower scram. This incident caused a reactor scram. One additional scram also occurred during this time period, probably as a result of maneuvering too close to the 109% set point. The following quotation summarizes the author's comments:[8]

> Besides a decreased plant reliability that appears to be associated with a trip point of 109%, another disadvantage of the low settings is the requirement for stringent operational surveillance of the nuclear instrumentation. This can be troublesome at those times when the operating personnel's attention must be temporarily devoted to other areas.

A more recent report (Ref. 9) indicates a reduction in the number of such incidents at Shippingport during subsequent seed lives. For example, the total number of safety shutdowns decreased from 23 during seed-1 operation to 14 during seed-2 operation. This reduction was due to increased operator familiarity with plant operation and equipment.

Another major area for which protection circuitry is provided is in loss-of-flow accidents; this circuitry is also illustrated in Fig. VII-7. Scram protection is provided for two postulated incidents: (1) the complete-loss-of-flow accident, wherein power is lost to all operating main coolant pumps simultaneously, and (2) the sequential-loss-of-flow accident, wherein the loss of power occurs sequentially. For Shippingport, the sequential loss of two of the four operating pumps, followed (within 2 to 3 sec) by the loss of power to the remaining pumps, would be worse than a complete loss of flow if the reactor did not scram on the loss of the first two pumps and if the reactor power is above 70 to 80% of full power.

During the two years of operation reported in the reference, no accidents of either complete or sequential loss of flow occurred. Seven shutdowns occurred, however, during pump-switching operations; these operations were for the purpose of changing the pump speed or for transferring a pump power supply from one source to another. Pump switching was eliminated as a source of unintentional scrams, however, when the requirement was set that a pump could not be started unless the reactor was shut down. This requirement was placed on the reactor by the necessity of preventing cold-water accidents. Early in the life of the reactor the pumps were interlocked so that a pump could not be started if the coldest water in its loop was more than 20°F below the highest reactor inlet-water temperature of the other operating loops. Later in seed-1 life, however, the requirement was changed so that a pump could not be started unless the reactor was shut down.

The second refueling of Shippingport is described in Ref. 10. The first refueling of the

reactor was reviewed in *Power Reactor Technology*, 4(2): 52-58. The second refueling involved almost the same steps as the first, except for a 20-day modification to the reactor-vessel-head instrumentation supports that were made during the first refueling. The objective of the second refueling was the replacement of 32 depleted seed-2 assemblies with new assemblies. The blanket was left intact except for the replacement of two assemblies for inspection and examination. The second refueling and associated shutdown tests required 63 working days, in contrast to the 156 working days required for the first refueling. The time breakdown for the second refueling is as follows: about 10% of the time was used for replacing the 32 seed assemblies; about 50% of the time was used to remove and install the control-rod-drive mechanisms and instrumentation; and the remaining time was devoted to maintenance, checkout, and testing of the entire plant after the last seal weld on the vessel head was completed. The reference estimates that the refueling would have taken slightly more than one month if tests, calibrations, and other operations required by the experimental objectives of the plant had not been necessary.

## Postirradiation Evaluation of a Zircaloy-2 Pressure Tube

The KE reactor at Hanford is fitted with several pressure tubes that serve as parts of experimental loops capable of operation at elevated temperature and high pressure. A total of five Zircaloy-2 pressure tubes has been utilized in the test loops, and the evaluation report on the fifth tube (designated the KER-3 tube) has been issued.[11] Since the irradiation conditions are not given and since the integrated exposure is expressed in arbitrary units, the report is of limited use.

The fabrication of the pressure tube that was tested is summarized in the following quotation from Ref. 11:

> 1. Received fusion conditioned ingot melted by Allegheny Ludlum Steel Corporation from Carborundum sponge.
> 2. Forge to approximately 8-inch round.
> 3. Machine extrusion billets and jacket in steel and copper.
> 4. Extrude to 3.502-inch OD × 0.326-inch wall. Extrusion ratio 13.5/1 at 1560°F.
> 5. Dejacket, straighten, and centerless grind outside surface.
> 6. Machine ends and butt weld three extrusions for each tube in argon atmosphere using Zircaloy-2 filler wire.
> 7. Remove excess weld bead from outer and inner surface and radiograph.
> 8. Clean, pickle, and immerse in conversion-type coating solution.
> 9. Draw to NPR tube size in 3 successive drafts of 6.4%, 7.3%, and 5.9% for a total of 18.3%.
> 10. Straighten, pickle, and inspect.
> 11. Cut in half and vacuum anneal.
> 12. Tube reduce 50 percent in one pass to KER size (2.20-inch ID × 0.170-inch wall × 48 feet)
> 13. Inspect.

The pressure tube resided in the KE reactor for 28 months; 609 days of this period were power operation at temperatures ranging from 212 to 545°F. During the first 90 days, the water was adjusted to a *p*H of 4.5 with phosphoric acid, and rust-colored crud was observed on the fuel elements and spacers; the *p*H was changed to 10 for subsequent operation, and no significant corrosion products were then observed.

After discharge from the reactor, the pressure tube was cut into seven lengths and subjected to metallographic examinations, burst and tensile tests, and deflection and hardness tests. The following conclusions are quoted from Ref. 11:

> In conclusion it may be said that 28 months residence in the reactor did not have an adverse effect on the KER-3 process tube except for a slight loss of ductility. A protective film was formed by the reactor environment that appears resistant to mechanical damage and corrosion, and its formation did not perceptibly increase the hydrogen content. Strength, stiffness, and hardness were all slightly improved by irradiation. This may be associated with a precipitation of second phase constituents that also increases with irradiation. The 50 percent cold work in this material is below the threshold value necessary to cause recrystallization to begin under the KER exposure conditions.

## References

1. H. K. Hoyt, Plant Description, *Proc. Am. Power Conf.*, 24: 234-240 (1962).
2. T. Trocki, Modification and Inspection of Reactor Components, *Proc. Am. Power Conf.*, 24: 284-289 (1962).
3. G. L. Redman, Power Generation Statistics, Load

Schedules, and Performance of the Dresden Nuclear Power Station, *Proc. Am. Power Conf.*, 24: 264-272 (1962).

4. E. R. Owen, Performance Measurements of the Dresden Nuclear Power Station, *Proc. Am. Power Conf.*, 24: 240-256 (1962).
5. A. F. Veras, Reactor Performance and the Factors Affecting Economic Operation, *Proc. Am. Power Conf.*, 24: 272-283 (1962).
6. N. A. Kershaw, Operation, Radiation Protection and Maintenance, *Proc. Am. Power Conf.*, 24: 257-264 (1962).
7. A. B. Sisson, R. C. Reid, and H. W. Frazer, Operating Experience with High Flow Rate Condensate Polishing Equipment at Dresden, *Proc. Am. Power Conf.*, 23: 600-625 (1961).
8. A. I. Moss, Shippingport Reactor Protection System Experience, in Bettis Technical Review, USAEC Report WAPD-BT-21, pp. 69-77, Westinghouse Electric Corp., Bettis Atomic Power Laboratory, November 1960.
9. P. A. Fleger, I. H. Mandil, and P. N. Ross, Shippingport Atomic Power Station Operating Experience, Developments, and Future Plans, USAEC Report WAPD-T-1429, Westinghouse Electric Corp., Bettis Atomic Power Laboratory, December 1961.
10. C. E. Center, H. Feinroth, and J. E. Yingling, The Second Refueling of Core 1 of the Shippingport Atomic Power Station, USAEC Report WAPD-260, Westinghouse Electric Corp., Bettis Atomic Power Laboratory, August 1962.
11. R. C. Aungst, Postirradiation Evaluation of Zircaloy-2 Pressure Tube from KER-3, Preliminary Report, USAEC Report HW-75052, Hanford Atomic Products Operation, Sept. 25, 1962.

Section

VIII

Power Reactor Technology

# Boiling Reactors: Steam-Water Separation

The original concept of the boiling-water reactor, as exemplified, for example, in the Experimental Boiling-Water Reactor (EBWR), involves the separation of steam from the boiling water within the reactor vessel. Although the use of outside separation in external steam drums is certainly feasible, the additional piping and equipment needed for such an approach may nullify much of the simplicity and economic advantage of the direct-cycle concept. The designer, in attempting to retain the feature of internal separation as he designs for higher power densities and higher total power outputs, is confronted with two steam-water separation problems: (1) the separation of steam from the saturated coolant after it has been passed through the reactor core but before it enters the water recirculation system and (2) the separation of entrained moisture from steam being raised before the steam is admitted to a superheater or turbine. The entrained fluid under these two situations is called carryunder and carryover, respectively. One of these problems, or possibly a combination of the two, may determine the diameter of the reactor pressure vessel required for a given reactor power output. Inasmuch as present manufacturing facilities are capable of fabricating pressure vessels up to only 15 to 20 ft in diameter, the steam-water separation problem could place an upper limit on the power output attainable from a single boiling-water reactor.

Steam must be removed from the recirculated coolant in order to avoid severe pumping problems, increased pipe sizes, and reduced thermal capacity of the core. Moisture must be removed from the steam to prevent component erosion, loop radioactivity problems, and reduced plant efficiency.

The separation of moisture from steam appears to be the lesser of the two problems. Normally this separation is accomplished by a combination of gravitational and mechanical processes. The primary, or roughing, separation is accomplished by forcing the steam-moisture mixture to flow vertically upward at low velocities and by allowing the moisture droplets to "settle out" gravitationally. This procedure can normally be used to reduce the moisture content to less than 2 wt.%. Mechanical separators may then be used to reduce the moisture content further, to about $^1/_{10}$ wt.%.

A considerable amount of experimental information concerning gravitational separation is available. The Atomic Energy Division of Allis-Chalmers Mfg. Co. performed fairly extensive tests pertaining to design of the Pathfinder reactor.[1,2] These tests covered steam-water conditions between 300 and 600 psig. A relation between the height of the available separation zone and allowable steam velocities was found to exist: i.e., for reactors with deep separation zones, higher steam velocities are permissible. Where zones as deep as 3 to 4 ft are available, permissible mass velocities as high as 17,000 lb/(hr)(sq ft) (about 3.5 ft/sec) are indicated for a pressure of 600 psig.

Several plots of "breakpoint" mass velocities are included in the same reports.[1,2] These breakpoint values are velocities above which the moisture carryover increases at an unallowably rapid rate. Data taken for a separation height of 15 in. indicated that permissible mass velocities are not quite proportional to operating pressures. Since the steam density is proportional to the pressure, allowable superficial velocities will decrease as the pressure increases. At 300 psig, velocities as high as 3.5 ft/sec appear to be allowable, but, at 600 psig, velocities greater than 2.8 ft/sec should not be exceeded if the separation-zone depth is limited to 15 in. When these data are

extrapolated to 1000 psig, a maximum velocity of 1.6 ft/sec is obtained. If separation zones with heights greater than 15 in. are available, larger flow rates would be permissible. However, the variation of limiting flow rate with separation height at 600 psig indicates such a sharp increase in the necessary separation height at velocities in the 3.5 ft/sec range (which required a minimum of 28 in. for separation) that velocities greater than 4 to 5 ft/sec would appear to be borderline regardless of available height. Therefore it appears that, at pressures in the 1000-psia range, velocities greater than 2.5 ft/sec would probably produce unallowable carryover even if large separation height is available. A plot of breakpoint velocities vs. pressure is given in Fig. VIII-1.

Acceptable agreement with the extrapolation given above was obtained under a steam separation program conducted by the Nuclear Division of Combustion Engineering, Inc. (CEND).[3] These data indicated that, when superficial velocities as high as 1.9 ft/sec at 1000 psig were tested, "good quality" steam was obtained at a point 47 in. above the water-steam interface and that such velocities were "very close to theoretical limiting steam velocities."[4] CEND did not determine the limiting flow rates because the critical separation zone progressed to a point above their highest sampling station.

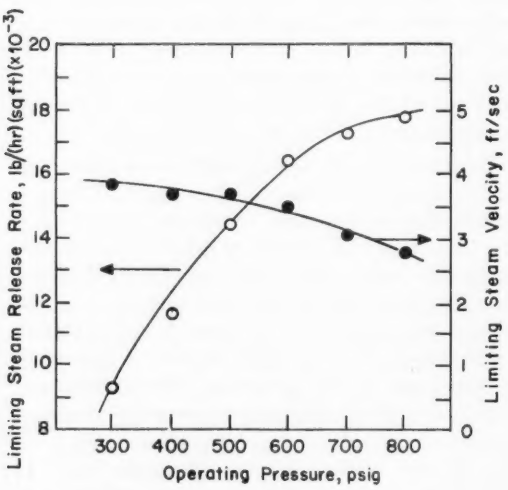


Fig. VIII-1 Limiting steam-release rates for efficient gravitational separation of entrained moisture below a height above the water-steam interface[2] of 33 in.

No high-mass-velocity data for actual reactor conditions are available. Even when the EBWR was operated at 60 Mw(t), the rising steam velocity was only about 1.1 ft/sec, with an available separation height of 6 to 8 ft.

Basically the selection of mechanical dryers for reducing steam moisture contents from 1 or 2 wt.% to about $^1/_{10}$ wt.% is not too difficult since numerous suppliers offer several varieties, each with apparently reliable specifications. However, owing to space limitations, it may be necessary for the reactor designer to modify the dryers to such an extent that testing is required to verify performance.

Most dryers can be classified as either centrifugal or impingement types. Several reactor-oriented dryer tests have been performed on such dryers during the last two or three years. Tests at pressures between 600 and 900 psig indicated that, in general, any of the several standard types may prove satisfactory. From these data it appears that the final selection should depend upon requirements other than the simple ability to reduce the moisture content of steam to a given value. Some types appear to reach "overload" or flooding conditions at relatively low flows. Other types require excessive pressure losses or occupy large volumes of valuable vessel space. Owing to these inherent properties, the final selection of a dryer type for a particular reactor design would probably depend upon the particular features or requirements of the design. In any case, the required appurtenances, such as collection trays and drain lines, should be examined carefully before a given type of dryer is selected since such components may be as voluminous and costly as the dryers proper.

A few data are available for two centrifugal dryers and three impingement types. A single-pass and a two-pass centrifugal separator[2] were tested at 300 and 600 psig. Both were generally satisfactory except that breakdown flow rates considerably lower than those specified by the supplier were found to exist. An overload flow rate of about 28,000 lb/hr was noted for the single-pass unit (size not given). The overload point appeared to be a function of the test geometry, i.e., dryer elevation, rather than an absolute value. Outlet moisture contents at lower flow rates were in the 0.1 to 0.2 wt.% range. Inasmuch as the centrifugal separators produce pressure drops as high as several pounds per square inch, their use re-

quires several feet of elevation above the steam-water interface for proper operation of water return lines.

Chevron and wire-mesh type dryers were tested in the same laboratory.[2] Both performed satisfactorily, and the wire-mesh type was later selected for use in the Pathfinder reactor. Both types indicated higher breakdown flow rates than the centrifugal separators that were tested. These flow rates, at 600 psig, were about 32,000 lb/hr for the chevron type and 29,000 lb/hr for the mesh type. The mesh type dryer was a 6-in.-thick, 5 lb/cu ft pad (openings and wire size unlisted). The dimensions of the chevron type dryer were not given.

Reference 2 does not give detailed descriptions of either the tests or the dryers, but the conclusions are, in part, as follows: All three types of dryers covered in this series of tests will provide steam of 99.9% or better quality (for an inlet moisture content of about 1%) until the overload point is reached. A reactor cross-section efficiency factor was obtained by dividing the maximum flow rate at 600 psig, which still gave 99.9% quality steam, by the dryer area (apparently the face area). The efficiency factor for the mesh type dryer is 27,600 lb/(hr)(sq ft). However, the maximum flow rate for the centrifugal dryer appeared to be limited by drain-line performance, which in turn is a function of the available dryer elevation above the reactor water level. Normally the efficiency of most centrifugal dryers increases with increasing flow rate; pressure loss is usually the load-limiting parameter. The chevron type separator, as well as several other types, requires that the entering steam be flowing in approximately a horizontal direction. Therefore they were not directly comparable on this "vessel area" basis.

Test data have been reported for an impingement type dryer that will be used in the BONUS reactor.[5] This dryer consists of vertical corrugated plates, collection trays, etc. These data indicated that between 89 and 97% of the moisture was removed when steam with moisture contents between 0.87 and 1.3 wt.%, at 875 psig, was passed horizontally between the plates at face mass velocities in the 18,000 lb/(hr)(sq ft) range.

These dryer test data indicated an increase in allowable steam mass velocity with operating pressure which was somewhat less than proportional. Thus, as in the gravity-separation process, the allowable superficial steam velocity decreases with increasing pressure, inasmuch as the steam density is almost exactly proportional to the pressure.

The separation of entrained steam from flowing water involves very complicated mechanisms, and therefore it is more difficult to

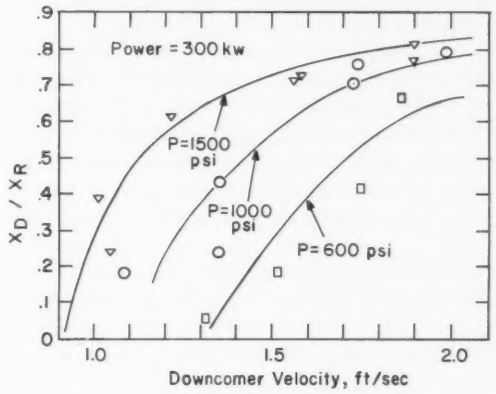


Fig. VIII-2 Effect of superficial downcomer velocity on the weight-fraction carryunder ratio.[6]

$$\frac{X_D}{X_R} = \frac{\text{quality in downcomer}}{\text{quality in riser}}$$

accomplish than separation of water droplets from steam. Further, since certain aspects of this problem have been peculiar to the nuclear power field, the available amount of pertinent information is very small. Some experimental data have been obtained for special situations, and these data may be used to set up rough guidelines.

The data and conclusions for a rather thorough experimental program and analytical study were reported recently for gravitational separation systems.[6] These data indicated that, for the usual boiling-water-reactor geometry, in which the water-steam mixture flows across the core and then downward in a downcomer region, and for pressures in the 1000-psig range, the superficial downcomer velocity cannot be much greater than 1.0 ft/sec unless large steam contents are tolerable in the downcomer water. Three plots of experimental water-steam data that were obtained under this program are shown in Fig. VIII-2. These curves show the effect of pressure, between 600 and 1500 psig, and downcomer velocity on the ratio of steam

content in the downcomer to steam content in the riser. Steam contents in the riser varied between 4 and 7 wt.%. All these data were taken in a vertical 6-in. pipe that formed the external downcomer wall. A coaxial 3-in. pipe that formed the riser also formed the internal downcomer wall. The small size of this flow system leaves room for doubt about the validity of extrapolation to predict performance in large boiling reactors.

Slip ratios were tabulated for the same experiments. Plots of these data are shown in Figs. VIII-3 and VIII-4 for water-steam mixtures at 1000 psig. Figure VIII-3 is a plot of the slip ratio as a function of the superficial downcomer velocity, whereas Fig. VIII-4 is a plot of slip ratio vs. the true downcomer liquid velocity.

An analytical expression for the downcomer slip ratio was obtained by correlation of these high-pressure data, as well as water-air data. This expression is

$$\frac{V_g}{V_L} = 0.63(\mathrm{Fr})^{0.4}\left(\frac{X}{1-X}\frac{\rho_L}{\rho_g}\right)^{0.2}$$

where $V_g/V_L$ = ratio of gas and liquid velocities
Fr = Froude number
$X$ = weight fraction of gas
$\rho_L$ = density of the liquid
$\rho_g$ = density of the gas

It was suggested that, for channel diameters greater than 3 in., the Froude number be evaluated using the 3-in. diameter. This equation agreed satisfactorily with most of the high-pressure test data obtained, as well as with some EBWR data, with only a small percentage

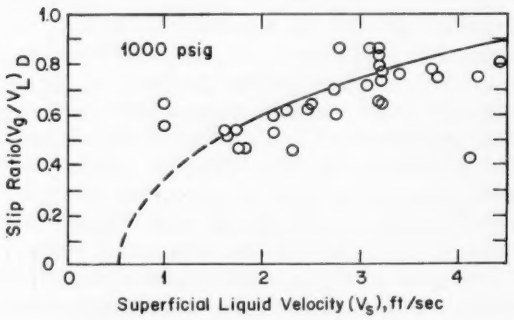


Fig. VIII-3 Slip ratio vs. superficial downcomer velocity[6] at 1000 psig.

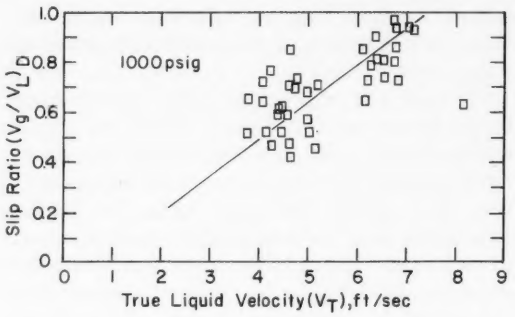


Fig. VIII-4 Slip ratio vs. true downcomer velocity[6] at 1000 psig.

of the observed ratios deviating more than ±20% from values indicated by the equation.

Instead of designing core vessels with diameters sufficiently large to allow gravitational steam separation, boiling-reactor designers have sought mechanical steam separators. Two types of mechanical steam separators have been tested sufficiently to obtain a general understanding of their performances and capacities: (1) the radial vane and (2) the downcomer. Both of these units utilize centrifugal forces, coupled with the density difference between steam and water, to obtain separation.

The radial-vane type consists of curved vanes positioned in the downcomer region between the reactor core and the vessel wall. These vanes may extend as much as several feet above and below the top of the core and have radii in the range 2 to 8 in. The water-steam mixture enters the core through a window that may be as small as 0.25 in. wide and 6 in. high and passes radially outward in the curved, expanding passages defined by the vanes. The velocities in and adjacent to the windows are quite high. Separation is accomplished by centrifugal forces acting on the fluids flowing radially between the vanes at high velocities. Figure VIII-5 is a typical simplified diagram showing the geometry of such vanes.

Data obtained by the General Electric Company indicated that, at 1000 psig, steam contents as high as 6.2 wt.% were reduced to about 0.22%, with the escaping steam containing less than 5% moisture.[7] These data were obtained in a simulated downcomer with an 8-in.-diameter annulus which was arranged coaxially about a 10-in.-diameter riser. If the vanes had not been

in place, the test for which the data were obtained would have resulted in downcomer velocities of about 1.4 ft/sec. If differences in geometry, etc., are ignored, this appears to be a worthwhile gain over the gravitational separation discussed above and typified in Fig. VIII-2. On the basis of the Argonne National Laboratory data, the gravitational separation at 1000 psig and 1.4 ft/sec downcomer velocity would have resulted in a quality ratio of about 0.42, or a steam content of about $0.42 \times 6.2 = 2.6$ wt.% in the downcomer flow. Since a velocity of about 1.1 ft/sec could not be exceeded if similar (0.22%) gravitational separation were desired, a saving in downcomer area of about 25% is indicated for these radial-vane separators.

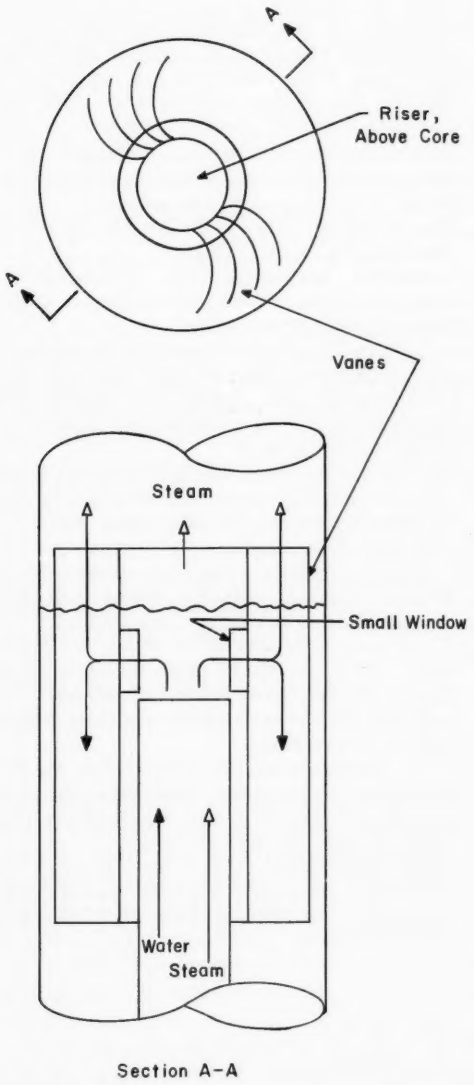


Fig. VIII-5 Simplified diagram for illustrating operation of radial-vane steam separators.

The downcomer type of steam separator also utilizes centrifugal forces to obtain separation. These separator assemblies consist of tubular flow channels that operate in a vertical position in the downcomer zone. The water-steam mixture leaving the reactor core enters the assembly through tangentially oriented windows and travels downward in a spiraling manner. A major fraction of the steam is released to the center of the tube, which is free of water, and flows upward. The water flows to a lower plenum after forming a closed vortex, which is established near the assembly outlet by a conical end fitting.

Forty-five of these 10-in. tubular separators are believed capable of handling the Pathfinder-reactor water flow rate[8] of 60,000 gal/min. Since these 45 assemblies occupy a 2-ft-wide peripheral area inside the 11-ft-diameter vessel, a downcomer area of about 56 sq ft is required. If the mechanical separators were not used, and the separation were attempted solely by gravitational means, the downcomer velocity would be about 2.4 ft/sec, about twice the permissible velocity if essentially steam-free water is required. These units are expected to be capable of meeting the Pathfinder plant requirements, which include a maximum head loss of 3.7 ft and maximum carryunder of 1 vol.% steam.

Apparently, by the use of these separators, the required Pathfinder downcomer flow area was reduced to about 50% of the area required for gravitational separation. These performance predictions were based on air-water test data. A U. S. patent on one type of downcomer separator has been subsequently issued to two persons at Allis-Chalmers.

In summary, it appears that enough data exist concerning moisture entrainment in steam to allow selection of permissible mass velocities for pressures up to 800 to 1000 psig so that moisture contents below 1 to 2 wt.% can be obtained in reactor steam domes that are at least 5 ft high. Mechanical moisture separators may then be selected, after little or no testing of several commercially available types, for a

further reduction of the moisture content to about 0.1 wt.%. However, it may be necessary to incorporate diffusers or steam spreaders in areas just above boiler fuel assemblies in order to avoid uneven steam-velocity distribution and the resultant "spouting," which increases moisture carryover.

For gravitational separation in the downcomer, a reason for maintaining downcomer velocities well below the borderline values is clearly evident in Fig. VIII-2. It can be seen that, once entrainment of steam is initiated (in the velocity range 1.0 to 1.3 ft/sec as shown in the figure), the carryunder mechanism is progressive and, as the superficial water velocity increases slightly, the carryunder increases sharply. This nonlinear increase occurs as the true water velocity also increases sharply until "overload" entrainment of steam occurs.

The possible solutions to the steam carryunder problem are (1) to include enough downcomer area in the vessel design to accommodate gravitational separation comfortably or (2) to develop a mechanical separator that meets the requirements of the specific reactor. A program is presently under way to provide the industry with basic principles and quantitative guidelines for steam separation as well as moisture separation.[9] Information of this kind is badly needed for the design of large boiling reactors, for it appears that reactors with thermal outputs of 1000 Mw or more will have crucial steam-water separation problems. Gravitational separation for one-pass boiling reactors becomes impractical for very large power outputs because much of the economic advantage inherent in large-capacity reactors is lost, and the maximum capacity is seriously limited, if the downcomer area and the steam-dome area must be increased in proportion to core area.

The important effect of steam separation problems in the downcomer on reactor vessel size is illustrated in the design of the 62-Mw(e) Pathfinder plant.[8] With a steam flow of about 616,000 lb/hr at 600 psig and a vessel diameter of 11 ft, the steam mass velocity is only approximately 6500 lb/(hr)(sq ft), about one-half of the value indicated to be permissible by experimental data. However, even at this power level, mechanical steam separators are required in the downcomer, and the required vessel diameter is set by the core area plus the area required by these steam separators rather than by considerations of steam velocity.

## References

1. J. Wilson and M. McDermott, Pathfinder Atomic Power Plant Final Report. Moisture De-Entrainment Tests in Two- and Four-Inch Diameter Test Sections, USAEC Report ACNP-5921, Allis-Chalmers Mfg. Co., Nov. 15, 1959.
2. J. F. Wilson and R. J. Grenda, Pathfinder Atomic Power Plant. Removal of Entrained Moisture from Steam Using Natural Separation and Mechanical Dryers, USAEC Report ACNP-6105, Allis-Chalmers Mfg. Co., Apr. 3, 1961.
3. Combustion Engineering, Inc., Development of Steam Separation Devices. Interim Report, USAEC Report CEND-127, April 1961.
4. R. F. Davis, The Physical Aspect of Steam Generation at High Pressures and the Problem of Steam Contamination, paper presented at a meeting of the Institution of Mechanical Engineers, London, December 1940.
5. General Nuclear Engineering Corp., BONUS-II Research and Development Program, Monthly Technical Report No. 23, May 1962, USAEC Report GNEC-236, June 15, 1962.
6. M. Petrick, A Study of Vapor Carryunder and Associated Problems, USAEC Report ANL-6581, Argonne National Laboratory, July 1962.
7. J. I. Riesland, Results of Air-Water and Steam-Water Tests on Radial Vane Steam Separator Models, USAEC Report GEAP-3787, General Electric Company, Atomic Power Equipment Department, February 1962.
8. G. C. Kutsch, D. H. Swanson, and H. W. Yant, Pathfinder Atomic Power Plant. Steam Separator Development, USAEC Report ACNP-62006, Allis-Chalmers Mfg. Co., June 15, 1962.
9. Allis-Chalmers Mfg. Co., Steam Separation Technology Quarterly Progress Report, June–September 1962, USAEC Report ACNP-62021, Oct. 10, 1962.

Section

IX

Power Reactor Technology

# Nuclear Superheat: Fuel Elements

General discussions of programs and studies for the development of integral boiling and superheating reactors have been given in *Power Reactor Technology*, 4(3): 71-85 and 5(3): 71-84. The following review is devoted to recent progress on the problem of fuel elements applicable to such reactors; this problem now appears to be the most important obstacle to the incorporation of the superheating function, in an economic way, into boiling-water reactors of the pressure-vessel type.

The most straightforward approach to the combination of boiling and superheating within a single reactor, and the one used in the two integral superheater plants currently under construction (Pathfinder and BONUS), is to provide a reactor core, composed of separate boiler and superheater sections, which will be immersed in a common body of water that will serve as coolant and moderator for the boiler section and as moderator in the superheater section. It is then necessary to provide coolant passages for the superheater elements, thermally insulated from the surrounding liquid water, wherein the saturated steam produced by the boiler section of the core may be superheated to the desired temperature. It is not usually necessary that the thermal insulation be highly effective, for any heat lost from superheated steam will serve to generate additional saturated steam; however, the insulation must be good enough to permit superheating to the desired temperature without exceeding the thermal limitations of the fuel-element materials. When speaking of superheater fuel elements for these reactors, one is usually referring to some sort of an assembly that includes the fuel itself, the superheated steam passage or passages, and the thermal insulation. A straightforward approach to the design of such an element is illustrated by the BONUS element, a cross section of which is shown in part *a* of Fig. IX-1. This consists of a simple fuel rod, composed of sintered $UO_2$ pellets in a metal jacket and surrounded by a double-walled "process tube" that provides the thermal insulation in the form of a stagnant steam space within the double wall.

In order to produce steam temperatures in the desired range (about 900 to 1050°F), the fuel cladding of superheater elements must operate at temperatures up to 1250°F or higher and in an atmosphere of superheated steam containing a rather high concentration of radiolytically decomposed oxygen (of the order 30 ppm). Under these conditions it is not possible, at least at present, to use materials of low neutron cross section. One cannot even rely upon the experience gained with the higher cross-section materials in conventional superheaters because conventional practice is to hold the oxygen content at a very low level and, of course, to employ much thicker tubes than would be permissible in a nuclear reactor. Indeed, the current evidence is that the stainless steels used in normal practice are not adequate for the nuclear superheater and that high-nickel alloys will be necessary. The effects of radiation introduce further uncertainties in the performance of possible materials for nuclear superheaters. The few measurements that have been made—most of which have been directed at the gas-cooled rather than the steam-cooled application—suggest that irradiation at high temperature may reduce seriously the stress-rupture strength and the ductility of such alloys as Inconel,[1,2] Inconel X (Ref. 3), type 304 stainless steel,[1,4] and A-286 (Ref. 3). Under these circumstances, one would prefer fuel-element designs that inherently reduce the amount of parasitic material associated with the fuel so that considerations

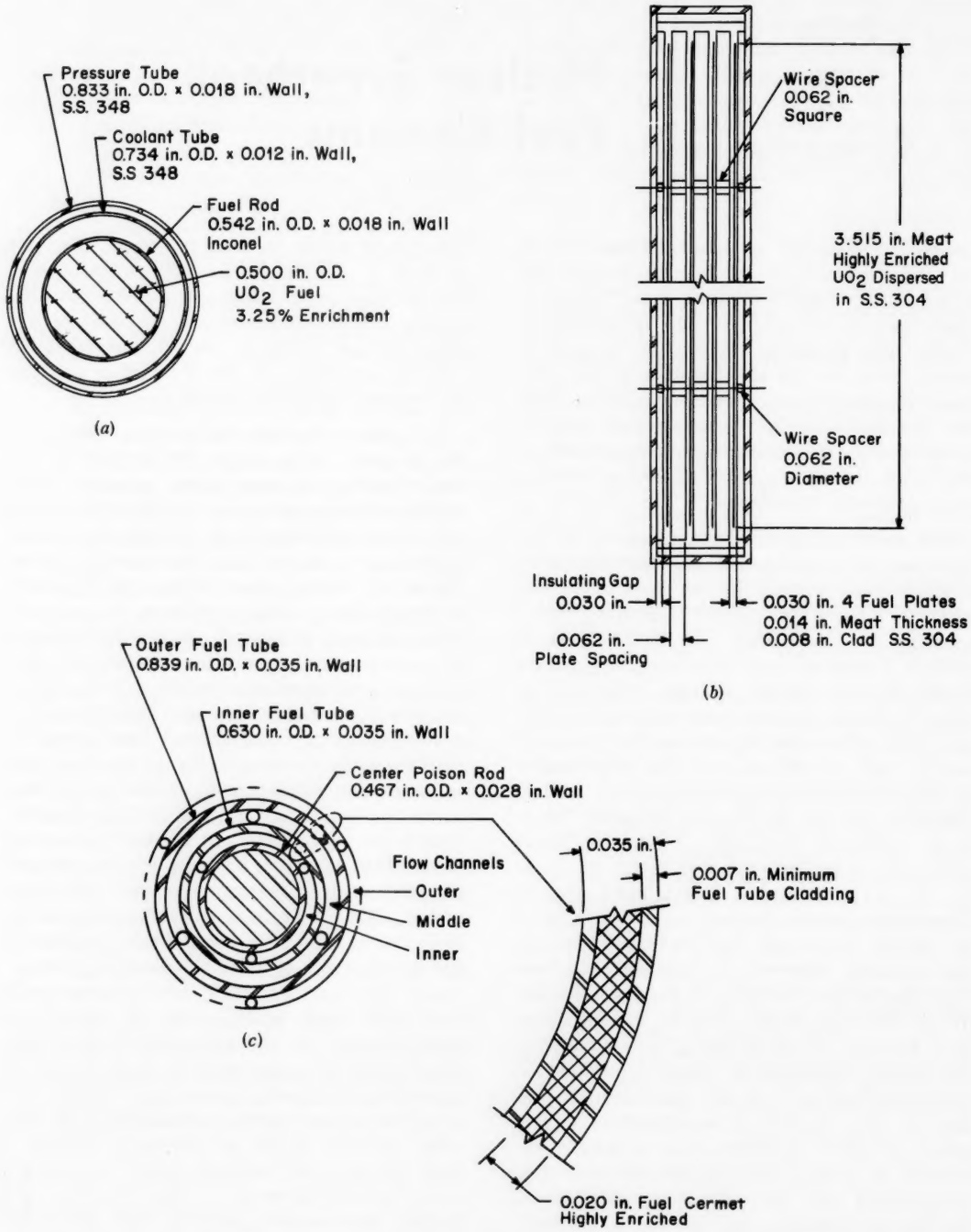


Fig. IX-1 Cross sections of various superheater elements. (*a*) BONUS. (*b*) BORAX-V. (*c*) Pathfinder.

of neutron economy will place the least possible restrictions on the compositions of the materials used and upon the thicknesses of sections.

Fuel elements that are under development for more advanced nuclear superheat applications—either in integral boiling-superheating reactors or in separate superheat reactors

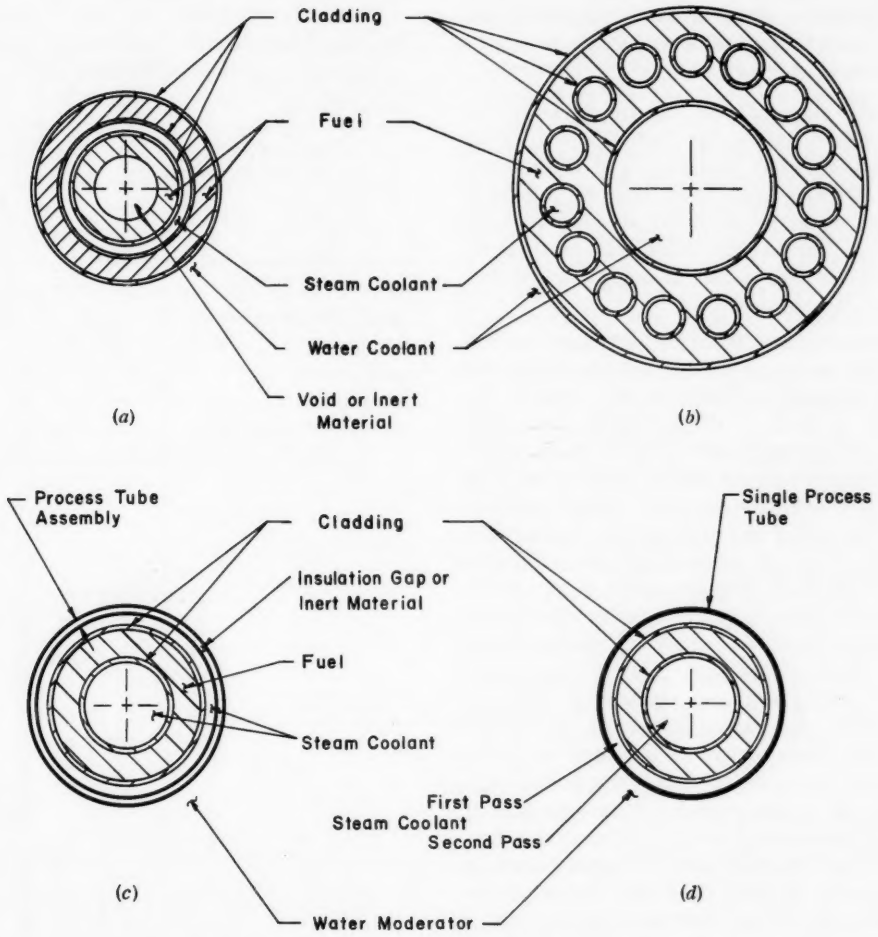


Fig. IX-2 Advanced element designs for superheating reactors.

The superheater elements planned for the three integral superheat reactors currently under construction are shown, in cross section, in Fig. IX-1. Since these reactors—the BONUS reactor[5] in Puerto Rico, the Pathfinder[6] reactor near Sioux Falls, S. Dak., and the experimental reactor[7] BORAX-V at the National Reactor Testing Station—are the first representatives of the integral superheat type, it is not surprising that their fuel elements leave something to be desired in the way of neutron economy.

employing water moderation—are shown in cross section in Fig. IX-2. The annular element surrounded by a process tube tends to use less parasitic material, for a given quantity of fuel, than the rod type elements exemplified by the BONUS element. Representatives of this annular type[8,9] are shown in parts *c* and *d* of Fig. IX-2. In the development of these elements, an attempt has also been made to reduce parasitic absorption by using thin sections. Various methods of minimizing parasitic material in the process-tube assembly have been

tested to a limited extent.[10] Included is the use of vibratory-compacted $Al_2O_3$ between tubes used as the inner and outer walls of the process tube in order to strengthen the assembly for resisting the external hydrostatic pressure due to the pressure drop in the coolant channel. Also included is the use of Zircaloy tubing with a stainless-steel liner.

The fuel element with the simplest type of process tube is shown in part *d* of Fig. IX-2. In this element the insulating gap is omitted, and a relatively high heat loss is tolerated from the steam in the outer annulus because the steam attains its final temperature by making a second pass through the central channel of the element.

Another approach to the problem involves the use of the uranium oxide fuel itself as the thermal insulation. Thus, in the element illustrated in part *a* of Fig. IX-2, the outer surface of the outer fuel annulus is in direct contact with the liquid water, and it serves as part of the surface used for steam generation.[11] The inner annulus is the passage in which the steam is superheated. An extension of this principle is shown in part *b* of Fig. IX-2, in which a rather massive annular element is used, penetrated by a number of tubular steam passages in which the superheating takes place. Both the inner and outer surfaces of the massive annulus are in contact with the liquid water, and they serve the purpose of steam generation. The elements shown in parts *a* and *b* of Fig. IX-2 both transfer about one-half of their total heat output to the boiling water. It is evident that elements such as those shown in parts *a* and *b* of Fig. IX-2 have large advantages with respect to neutron economy, particularly when it is recognized that the surfaces in contact with liquid water might be clad with low-cross-section materials such as Zircaloy, whereas the higher cross-section materials might be used only for cladding those surfaces which superheat the steam. It is equally apparent that elements of these types pose problems of differential thermal expansion and that they require the fabrication of rather complex clad-oxide fuel bodies. Experimental elements of these types have been fabricated by vibratory-compaction techniques. Owing to the favorable experience with vibratory compaction, elements of these types appear very promising. As for the differential expansion problems, the solutions will depend upon the details of the behavior of such $UO_2$-metal assemblies under the conditions of irradiation and power production, and they must be demonstrated by in-pile testing of experimental elements.

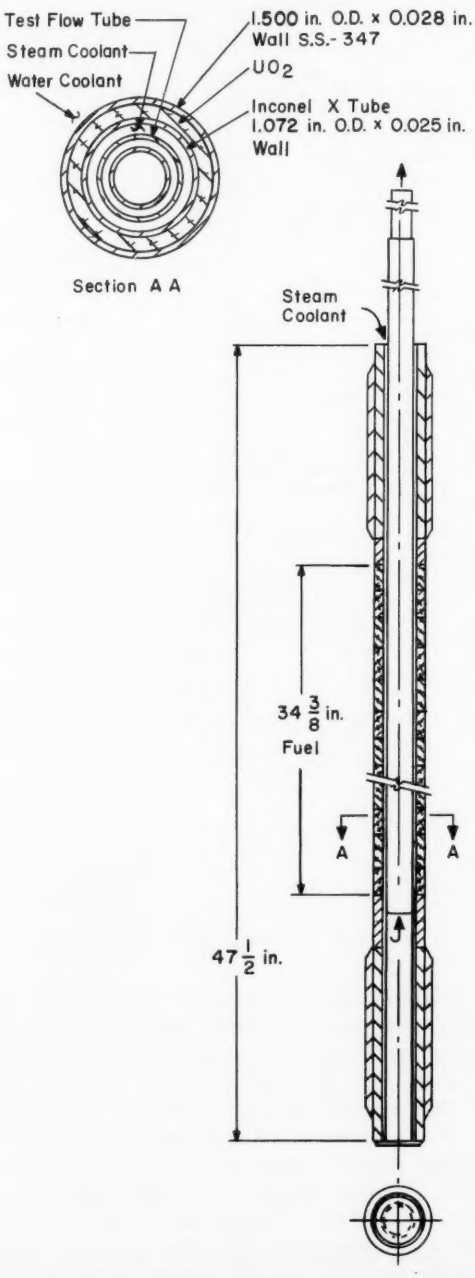


Fig. IX-3 In-pile test fuel-element assembly.

At present, only a very limited amount of test information is available to indicate the durability of any of the fuel-element types illustrated in Fig. IX-2. Seven fuel elements of the types shown in parts *c* and *d* of Fig. IX-2 have received relatively short (up to 570 Mwd/ton average burnup) in-pile tests.[9,12] Six of these elements were clad with types 304 and/or 347 stainless steel; one element was clad with Inconel. From the point of view of neutron economy, five of these seven fuel elements had cladding that was reasonably thin (0.028 in. or less); cladding failures were found in three of these five elements. No failures were found in the 0.028-in.-Inconel-clad element, and no cladding failures were found in two elements that had relatively thick stainless-steel cladding (0.049 and 0.035 in. thick). The failures have been attributed to chloride stress corrosion, but it is not clear to what extent stress per se (producing plastic strain of the irradiated material) may have contributed to the failures.

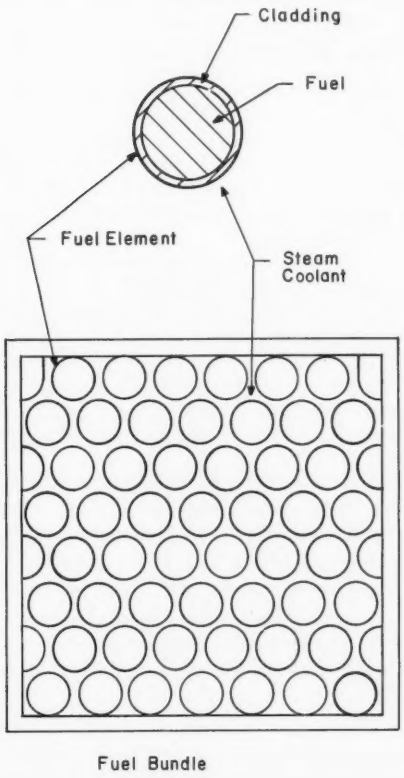


Fig. IX-4 Element for superheating a portion of a mixed-spectrum boiling and superheating reactor.

Only one fuel element of the type shown in part *a* of Fig. IX-2 has received an in-pile test.[13] The test element, which is illustrated in Fig. IX-3, consisted of the outer annulus only, and it was fabricated from sintered annular $UO_2$ pellets. It was irradiated to a maximum exposure of about 1000 Mwd/ton of uranium, and it experienced about 20 reactor scrams from significant power levels during the test period. The maximum cladding temperature on the steam passage was estimated to be at least 1275°F. No cladding failures were found.[12] Significantly, the steam-side cladding of the element was 0.025-in.-thick Inconel X; conceivably, the high nickel-alloy content was adequate to prevent chloride corrosion and the high strength of the Inconel X was adequate for the stresses involved. No in-pile tests have been run with the fuel-element type shown in part *b* of Fig. IX-2; however, some prototypes are under construction.

Another type of fuel element (shown in Fig. IX-4) is under consideration for a fast-neutron superheat core. The fast-reactor superheat core under consideration is conceived as the central region of a mixed-spectrum superheating reactor. The fast superheating region is surrounded by an annular buffer region, and this region is, in turn, surrounded by an annular, moderated (thermal-neutron), boiling-water core region. The purpose of operating the superheat region on unmoderated neutrons is to minimize the loss of neutron economy due to stainless steel or high-nickel alloys in the cladding and structural members. The characteristics of the Mixed-Spectrum Superheater Reactor are discussed in Ref. 14.

## References

1. Oak Ridge National Laboratory, Metallurgy Division Annual Progress Report for Period Ending May 31, 1961, USAEC Report ORNL-3160, Aug. 17, 1961.
2. D. S. Billington and H. H. Crawford, Jr., Solid State Division Annual Progress Report for Period Ending August 31, 1958, USAEC Report ORNL-2614, Oak Ridge National Laboratory, Nov. 20, 1958.
3. C. G. Collins, W. H. Couts, G. L. Hammons, and F. C. Robertshaw, Radiation Effects on the Stress Rupture Properties of Inconel X and A-286, USAEC Report APEX-676, General Electric Company, Flight Propulsion Laboratory Department, December 1961.

4. Oak Ridge National Laboratory, Gas-Cooled Reactor Program. Quarterly Progress Report for Period Ending June 30, 1961, USAEC Report ORNL-3166, Aug. 28, 1961.
5. General Nuclear Engineering Corp. and Puerto Rico Water Resources Authority, Boiling Nuclear Superheater (BONUS) Power Station. Final Hazards Summary Report, USAEC Report PRWRA-GNEC-5, Feb. 1, 1962.
6. Allis-Chalmers Mfg. Co., Pathfinder Atomic Power Plant. Thermal and Hydraulic Design of the Pathfinder Boiling Water Integral Nuclear Superheating Reactor, USAEC Report ACNP-62017, Aug. 29, 1962.
7. Argonne National Laboratory, Design and Hazards Summary Report, Boiling Reactor Experiment V (BORAX V), USAEC Report ANL-6302, May 1961.
8. R. T. Pennington, Nuclear Superheat Project Ninth Quarterly Progress Report, July-September 1961, USAEC Report GEAP-3877, General Electric Company, Atomic Power Equipment Department, June 1961.
9. R. T. Pennington, Nuclear Superheat Project Tenth Quarterly Progress Report, October-December 1961, USAEC Report GEAP-4024, General Electric Company, Atomic Power Equipment Department, July 1962.
10. E. L. Esch, Development of Process Tubes for Nuclear Superheat Applications, USAEC Report GEAP-3784, General Electric Company, Atomic Power Equipment Department, Nov. 15, 1961.
11. General Nuclear Engineering Corp. and Combustion Engineering, Inc., A 200-Mw(e) Direct Cycle Boiling Water Reactor with Integral Nuclear Superheat, Reference Design with Double-Annular Boiling-Superheating Fuel Elements, USAEC Report GNEC-212, Jan. 29, 1962.
12. Proceedings of the Nuclear Superheat Meeting No. 7, September 12, 13, and 14, 1962, Sioux Falls, South Dakota (to be published).
13. A. E. Mravca, Proceedings of the Nuclear Superheat Meeting, No. 6, March 7, 8, and 9, 1962, Windsor, Connecticut, USAEC Report TID-7634, Mar. 30, 1962.
14. G. V. Brynsvold, K. Hikido, A. B. Reynolds, and D. R. Riley, Conceptual Design for a 75 MWe Mixed Spectrum Superheating Reactor Power Plant, USAEC Report GEAP-4016, General Electric Company, Atomic Power Equipment Department, Feb. 25, 1962.

Section

X

Power Reactor Technology

# Sodium-Cooled Reactors: Parts for Hallam

The Hallam Nuclear Power Facility (HNPF) was described in *Power Reactor Technology*, 5(3): 39-51. Details of the engineering and construction of the HNPF reactor structure are presented in Ref. 1; the reference gives design features and criteria for this structure, and it also discusses the fabrication and field erection. The reactor structure consists of the loading-face shield, reactor vessel and internals, outer vessel, thermal shields, support structure, cavity liner, and the reactor cavity diaphragm seal.

The following quotation from Ref. 1 summarizes some of the dimensions and weights of critical components of the HNPF plant:

> (1) The reactor vessel with internals weighed 78 tons; its shipping weight without internals is 60 tons. The diameter is 19 ft held to $\pm 1/4$ in. The length is 33 ft 2 in.
>
> (2) The outer vessel weighs 50.5 tons. The diameter is 20 ft 8 in. held to $\pm 1/4$ in. The length is 35 ft 4 in.
>
> (3) The thermal shield panels were 6 ft wide by 12 ft long by $2\,3/4$ in. thick. The total weight of the shield panels is 225 tons.
>
> (4) The loading-face shield as completed in the shop without shielding concrete weighed 60 tons. The maximum diameter at the top was 21 ft. The clearances for fit into the cavity liner were held to $1/8$ in. The overall height is 5 ft 8 in.

The above components were fabricated almost entirely in the Baldwin-Lima-Hamilton Corp. shop, and critical fit-ups were made to ensure that the field erection would proceed with a minimum of difficulty. The shop fabrication ran from April 1959 to January 1961.

The field installation ran from April 1960 to October 1961. One of the major problems was the loading-face shield; the shield was delayed in fabrication by a steel strike and by welding difficulties. To allow for this delay, a change in scheduling was accomplished, and the moderator and reflector elements were installed prior to final placement of the shield; therefore the overall combined scope of work was accomplished within schedule. Since the loading-face shield was not available, the alignment of the upper cavity liner (which positions the loading-face shield) with the grid plate (which positions the fuel) could not be directly checked before installation of the upper cavity liner. The upper cavity liner was therefore positioned (using shop information) and was welded to the cavity liner. Then the concrete shield was poured. When the loading-face shield was received, minus its concrete shielding, it was positioned in the upper cavity liner and was found to be in satisfactory alignment with the grid plate. Then the loading-face shield was removed so that the concrete could be poured in the shield. When the loading-face shield was replaced in the upper cavity liner after the pouring of the concrete in the shield, it was discovered that the shield could not be rotated through a full revolution; in addition, the required ovality tolerance of the moderator removal plugs had not been held. These discrepancies were corrected by on-site grinding and boring.

Reference 2 is devoted to an interim report on the HNPF moderator-element development; it discusses the determination of structural stability and integrity and the fabrication processes for the moderator cans. The moderator element for the HNPF, illustrated in Fig. VII-2, page 41, of the above-mentioned issue of *Power Reactor Technology*, is hexagonal in cross section and has scalloped corners. It is about 17 ft long, and the distance across the flats of the hexagon is 16 in. The moderator element is composed of graphite and is clad in a stainless-steel skin with a wall thickness of 0.016 in. This shape allows stacking of the cans to form

# NUCLEAR SCIENCE ABSTRACTS

The U. S. Atomic Energy Commission, Division of Technical Information, publishes *Nuclear Science Abstracts (NSA)*, a semimonthly journal containing abstracts of the literature of nuclear science and engineering.

*NSA* covers (1) research reports of the U. S. Atomic Energy Commission and its contractors; (2) research reports of government agencies, universities, and industrial research organizations on a world-wide basis; and (3) translations, patents, books, and articles appearing in technical and scientific journals.

Complete indexes covering subject, author, source, and report number are included in each issue. These are cumulated quarterly, semiannually, and annually providing a detailed and convenient key to the literature.

## Availability of *NSA*

**SALE** *NSA* is available on subscription from the Superintendent of Documents, U. S. Government Printing Office, Washington 25, D. C., at $22.00 per year for the semimonthly abstract issues and $15.00 per year for the four cumulated-index issues. Subscriptions are postpaid within the United States, Canada, Mexico, and all Central and South American countries, except Argentina, Brazil, British and French Guiana, Surinam, and British Honduras. Subscribers in these Central and South American countries, and in all other countries throughout the world, should remit $27.50 per year for subscriptions to semimonthly abstract issues and $17.50 per year for the four cumulated-index issues.

**EXCHANGE** *NSA* is also available on an exchange basis to universities, research institutions, industrial firms, and publishers of scientific information. Inquiries should be directed to the Division of Technical Information Extension, U. S. Atomic Energy Commission, P. O. Box 62, Oak Ridge, Tennessee.

TECHNICAL PROGRESS REVIEWS may be purchased from Superintendent of Documents, U. S. Government Printing Office, Washington 25, D. C. for $2.00 per year for each subscription or for $0.55 per issue. The use of the coupon below will facilitate the handling of your order.

POSTAGE AND REMITTANCE: Postpaid within the United States, Canada, Mexico, and all Central and South American countries except as hereinafter noted. Add $0.50 per year, or $0.15 per single issue, for postage to all other countries, including Argentina, Brazil, British and French Guiana, Surinam, and British Honduras. Payment should be by check, money order, or document coupons, and MUST accompany order. Remittances from foreign countries should be made by international money order, or draft on an American bank, payable to the Superintendent of Documents, or by UNESCO book coupons.

*order form*

SUPERINTENDENT OF DOCUMENTS
U. S. GOVERNMENT PRINTING OFFICE
WASHINGTON 25, D. C.

Enclosed:
document coupons ☐ check ☐ money order ☐

Charge to Superintendent of Documents No._____

Please send a one-year subscription to

☐ REACTOR MATERIALS
☐ POWER REACTOR TECHNOLOGY
☐ NUCLEAR SAFETY
☐ REACTOR FUEL PROCESSING

(Each subscription $2.00 a year; $0.55 per issue.)

SUPERINTENDENT OF DOCUMENTS
U. S. GOVERNMENT PRINTING OFFICE
WASHINGTON 25, D. C.

(Print clearly)

Name _____

Street _____

City _____ Zone ____ State _____